LONGITUDINAL STUDIES OF *CAENORHABDITIS ELEGANS* AGING AND BEHAVIOR USING A MICROFABRICATED MULTI-WELL DEVICE

Matthew Alexander Churgin

A DISSERTATION

in

Bioengineering

Presented to the Faculties of the University of Pennsylvania in Partial Fulfillment of the Requirements for the Degree of Doctor of Philosophy

2017

Supervisor of Dissertation

_____

Christopher Fang-Yen
Assistant Professor of Bioengineering and Neuroscience

Graduate Group Chairperson

_____

Ravi Radhakrishnan
Professor of Bioengineering and Chemical and Biomolecular Engineering

Dissertation Committee

David H. Brainard (chair), RRL Professor of Psychology
F. Bradley Johnson, Associate Professor of Pathology and Medicine
John I. Murray, Associate Professor of Genetics
David M. Raizen, Associate Professor of Neurology

LONGITUDINAL STUDIES OF *CAENORHABDITIS ELEGANS* AGING AND BEHAVIOR USING A MICROFABRICATED MULTI-WELL DEVICE

ACKNOWLEDGMENTS

I would first like to thank my advisor, Professor Chris Fang-Yen, for the opportunity to work in his lab on a number of fascinating questions in engineering and biology. I'd like to thank Chris for all his advice and guidance throughout my Ph.D. Chris created an intellectually stimulating environment in which I was able to work independently and solve problems on my own, and I am grateful for all I learned during my time in his lab.

I would also like to thank my thesis committee, which was comprised of Professors David Brainard, Brad Johnson, John Murray, and David Raizen, for engaging discussions about science and life. I would like to specifically thank David Raizen and John Murray, both of whom spent a considerable amount of their time giving me advice and feedback on my work. I'm very fortunate to have been surrounded by a group of brilliant and friendly mentors during my time in graduate school.

I would also like to thank members of the HHMI program leadership, Professors James Gee, Peter Davies, Andrew Maidment, and Ann Tiao, who gave me the opportunity to attend Penn as a graduate student. I'd also like to thank members of the Penn worm community and the Penn Bioengineering department. It is to all these wonderful peers and mentors that I owe my development as a scientist.

I'd like to thank my family, especially my parents and grandparents, for their love and support, for giving me the opportunities to succeed, for giving me so many places I could

call home, and for always comforting me with Joe Leone's fresh mozzarella and roast beef sandwiches, which I cannot recommend highly enough.

Finally, I want to thank my wife, Betsy, for her endless well of kindness, support, and patience. She has the impressive ability to withstand hours of conversation pertaining to the aging process of roundworms and their behavioral responses to treatment with exogenous biogenic amines, to such an extent that might actually be unhealthy. Nevertheless, I never would have been able to make it so far without her companionship. Having the chance to spend my life with her is without a doubt the greatest joy of my life.

ABSTRACT

LONGITUDINAL STUDIES OF *CAENORHABDITIS ELEGANS* AGING AND BEHAVIOR USING A MICROFABRICATED MULTI-WELL DEVICE

Matthew Alexander Churgin

Christopher Fang-Yen

The roundworm *C. elegans* is a powerful model organism for dissecting the genetics of behavior and aging. The central genetic pathways regulating lifespan, such as insulin signaling, were first identified in worms. *C. elegans* is also the only animal for which a full map of all neural synpatic connections, or connectome, exists. However, current manual and automated methods are unable to efficiently monitor and quantify behavioral phenotypes which unfold over long time scales. Therefore, it has been difficult to study phenotypes such as long-term behavior states and behavioral changes with age in worms. To address these limitations, here I describe a novel device, called the WorMotel, to longitudinally monitor behavior in up to 240 single *C. elegans* on time scales encompassing the worm's maximum lifespan of two months. The WorMotel is fabricated from polydimethylsiloxane from a 3-D printed negative mold. Each device consists of 240 individual wells, each of which houses a single worm atop agar and bacterial food. I use custom software to quantify movement between frames to longitudinally monitor behavior for each animal. I first describe the application of the WorMotel to the automation of lifespan measurements in *C. elegans*, the characterization of intra-strain and inter-strain variability in behavioral decline, the relationship between behavior and lifespan, and the scaling of behavioral decline with increasing stress. I then describe the

application of the WorMotel to quantify locomotive behavioral states and their modulation by the presence or absence of food as well as biogenic amine neurotransmitters. Using the WorMotel in combination with genetics and pharmacology, I outline a neural circuit by which the biogenic amines serotonin and octopamine regulate locomotion state to signal animals to adopt behavior appropriate to a fed and fasting state, respectively. I include protocols for construction of custom imaging rigs and requirements for long-term imaging as an appendix. The WorMotel is a powerful tool that can facilitate discovery and understanding of the mechanisms underlying long-term phenotypes such as behavioral states and aging.

TABLE OF CONTENTS

CHAPTER 1: Introduction and Overview

Advances in science, medicine, and public health have been extraordinarily successful in improving human survival and quality of life over the past two centuries. Maximum human lifespan in developed countries has increased by an average of three months each year since 1840 (Vaupel 2010; Christensen et al. 2010) (Figure 1.1). As human populations have aged, however, previously uncommon diseases, such as cancer, heart disease, and neurodegeneration, have become more prominent (Christensen et al. 2010; Vaupel et al. 1998). These age-associated illnesses exact a significant toll on human health and productivity (Vaupel 2010; Vaupel et al. 1998; Wimo et al. 2013). While much work is dedicated to understanding the specific pathophysiology of these diseases, aging itself is the number one risk factor for many of them (Christensen et al. 2010; Lopez-Otin et al. 2013). If we could improve our understanding of aging and its pathophysiology, we might be able to learn how to mitigate a number associated with old age. Therefore, an important goal of biomedical research is to understand the determinants of lifespan and healthy aging in the hopes of ameliorating the detrimental aspects of aging.

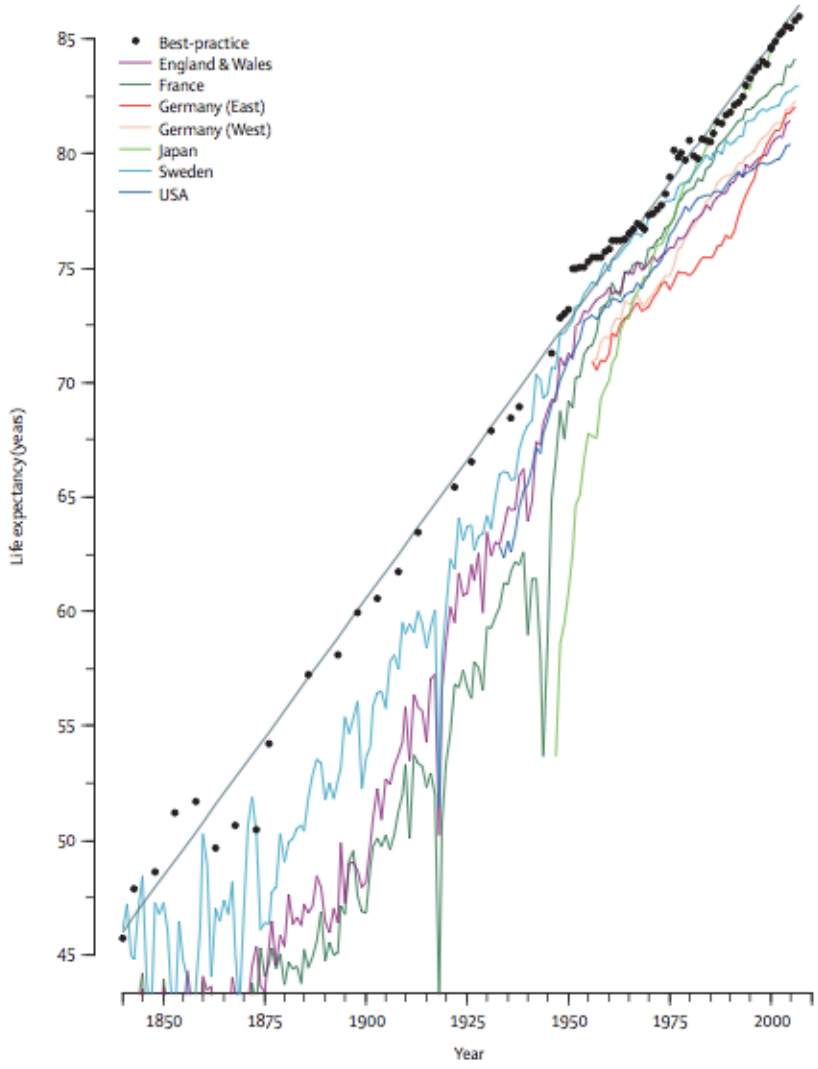

Figure 1.1 Best practice life expectancy for selected countries from 1840 to 2007. Originally published by Christensen et al. (Christensen et al. 2010)

THE BIOLOGY OF AGING

Aging can be defined as an organism's systematic loss of functional capacity that leads inexorably to death, or a permanent loss of homeostasis. Aging is a complex phenotype that includes cell-autonomous and cell-non-autonomous effects. The Hayflick limit, or the limited number of divisions a cell can undergo before entering a phase of replicative senescence, is an example of cell-autonomous aging as it is observed in isolated

individual cells (DiLoreto and Murphy 2010; Lopez-Otin et al. 2013). Altered nutrient signaling, in which age-associated changes in the response to nutrients causes organism-wide alterations in energy metabolism, is an example of cell-non-autonomous aging, as aging in a tissue that does not directly sense nutrients may be influenced by a distant tissue, such as the gut or brain (Murphy, Lee, and Kenyon 2007; Lopez-Otin et al. 2013; Barzilai et al. 2012). Many other so-called "hallmarks of aging" have been discovered, and these have greatly improved our understanding of aging biology and pathophysiology (Longo, Antebi, Bartke, Barzilai, Brown-Borg, Caruso, Curiel, de Cabo, et al. 2015; Lopez-Otin et al. 2013) (Figure 1.2). Current work in the field aims to understand how to modulate these hallmarks to mitigate the deleterious effects of aging.

Figure 1.2
Hallmarks of aging. Originally published by Lopez-Otin et al. (Lopez-Otin et al. 2013)

Great progress has been made in understanding how aging can be experimentally manipulated. In the 1980s and 90s, a role for genes was discovered in the regulation of lifespan (C. Kenyon et al. 1993; Friedman and Johnson 1988). In fact, single gene mutations were found to be able to double the lifespan of the roundworm *C. elegans* (Friedman and Johnson 1988; C. Kenyon et al. 1993) (Figure 1.3).

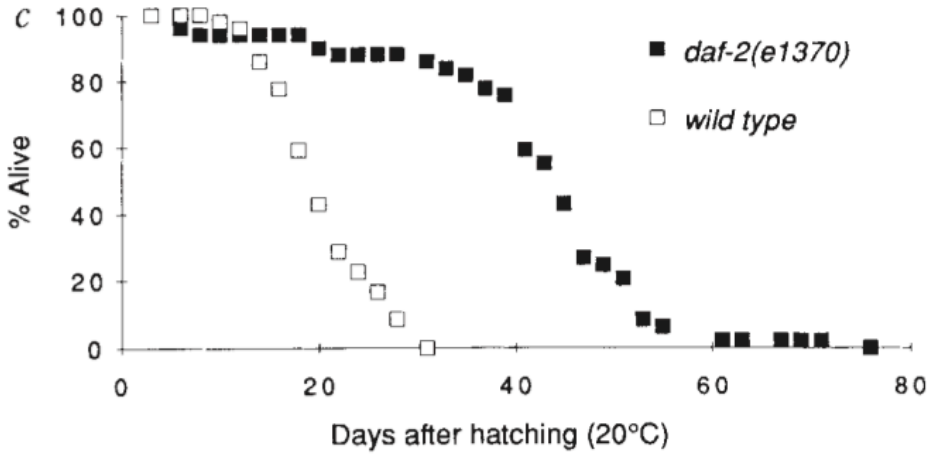

Figure 1.3 *C. elegans* lifespan curves showing that a single gene mutation can double lifespan. *daf-2* mutants harbor a loss-of-function mutation in the insulin receptor. Originally published by Kenyon et al. (C. Kenyon et al. 1993)

Since then, many more genes have been discovered that influence lifespan in roundworms, flies, and mice (C. J. Kenyon 2010). Genes that influence lifespan in these model organisms have also been found to be associated with human longevity (Lehner 2013; Deelen et al. 2013). Researchers have even identified conserved genetic signaling pathways that may be potential therapeutic targets to slow aging in humans. These targets include the mammalian target of rapamycin (mTOR), which can be targeted to slow aging in worms and mice by treatment with the drug rapamycin, and AMP-activated

protein kinase (AMPK), which can slow aging when targeted with the drug metformin (Longo, Antebi, Bartke, Barzilai, Brown-Borg, Caruso, Curiel, De Cabo, et al. 2015; Onken and Driscoll 2010; Partridge 2014).

One of the central genetic pathways regulating aging is the insulin/insulin-like signaling (IIS) pathway. This pathway, which was first discovered to exert a profound influence on lifespan in *C. elegans* (Figure 1.3), has been shown to also influence lifespan in flies, mice, and humans (Deelen et al. 2013; Metaxakis et al. 2014; Gems and Partridge 2013). The IIS pathway functions to sense nutrients in the environment and relay signals to the rest of the organism about fundamental organismal decisions regarding development and behavior, primarily by acting on the downstream transcription factor FOXO (Liang et al. 2006a; Kimura, Riddle, and Ruvkun 2011; Ogg et al. 1997) (Figure 1.4). FOXO also coordinates the cellular response to various forms of stress (Liang et al. 2006a; Driver et al. 2013; A. L. Hsu 2003). The IIS/FOXO axis is a fundamental pathway linking energy status, nutrient availability, stress, and aging in metazoans.

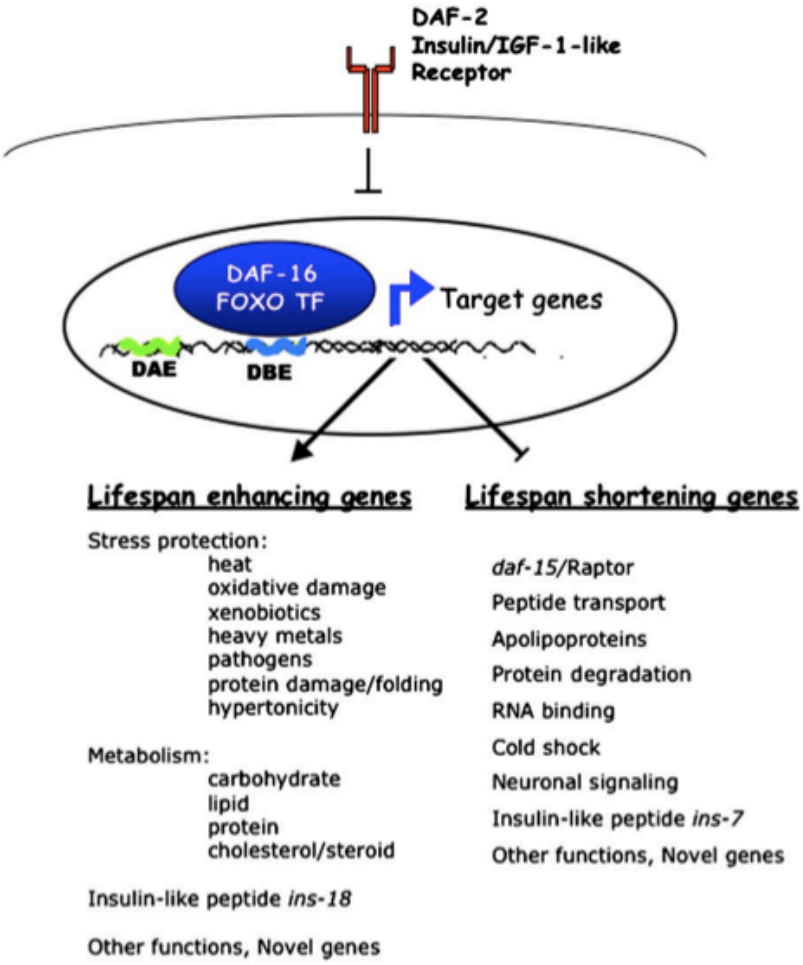

Figure 1.4 FOXO regulation of lifespan downstream of insulin signaling. Originally published by Coleen Murphy (Murphy 2006).

MEASURING AGING WITH LIFESPAN AND HEALTHSPAN

A critical question in studying aging is how to quantify aging and its effects. The most commonly recorded phenotype of aging is lifespan (Tatar 2009). Lifespan is a simple endpoint measurement that describes the amount of time an organism has survived. Therefore, it contains information about an organism's average rate of aging. However, this simple measure of aging is unable to describe the pattern of decline in health that occurs during the aging process itself (Stroustrup et al. 2013; W. B. Zhang et al. 2016).

This raises some significant issues. For example, it may be that interventions that prolong lifespan do so as the expense of health. Ideally, we would like interventions that delay aging to do so by enabling the span of health to increase to at least the same extent as the span of life.

To address this concern, recent efforts in aging research have begun to define other measurements of aging. One such category of aging measurements is an organism's healthspan, or the amount of life spent in a healthy state (Tatar 2009; Bansal et al. 2015; Iwasa et al. 2010; Hansen and Kennedy 2016). Like lifespan, healthspan is a single number that defines an aspect of aging, namely, the span of an individual's health. Healthspan is more difficult to define than lifespan, as it can take the form of a number of metrics, such as functional capacity, tissue morphology and structure, or stress resistance (Hahm et al. 2015; Pincus, Smith-Vikos, and Slack 2011; W. B. Zhang et al. 2016; Bansal et al. 2015). A current interest in the field of aging research is to identify genetic or environmental conditions that maximize not only lifespan but healthspan (Figure 1.5).

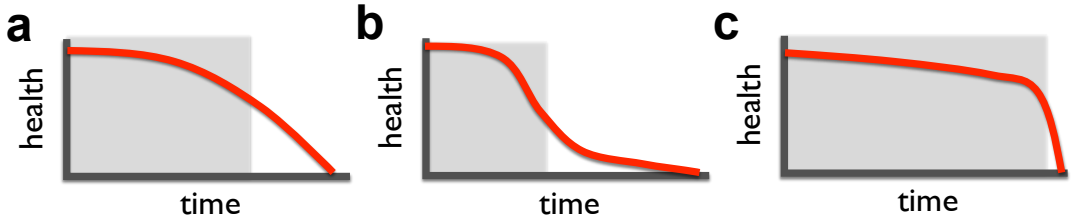

Figure 1.5 Equal lifespan does not ensure equal healthspan. Three theoretical individual animals with equal lifespans but different healthspans. Red curve indicates health trajectory over time. Gray shaded region indicates times at which each individual remains in a healthy state. a) Intermediate healthspan b) Short healthspan c) Long healthspan

The first step in improving our understanding of healthspan, however, requires the ability to measure healthspan. Unlike lifespan, which can be easily measured by counting the number of animals alive in a population over time, healthspan requires longitudinal measurements of health throughout each individual's life. Such measurements, while possible, are extremely laborious and time-consuming when performed manually. Therefore, new techniques to measure healthspan in an efficient manner are a necessity.

BIOGENIC AMINES LINK AGING, ENERGY METABOLISM, AND BEHAVIOR

Aging is an important risk factor for neurodegenerative diseases such as Alzheimer's and Parkinson's (Christensen et al. 2010), so by understanding aging we may also understand the diseases associated with it. Diseases of nervous system failure are thought to be caused by factors such as neuronal protein misfolding and aggregation (Stefani and Dobson 2003; Ross and Poirier 2004; Aguzzi and O'Connor 2010). A symptom of some neurodegenerative diseases is dysregulation of behaviors associated with energy metabolism, such as mood, aggression, feeding, and appetite (Swaab, Bao, and Lucassen 2005; Moon et al. 2011). A better understanding of the neural underpinnings of these complex behaviors is required to improve treatment for diseases that disrupt their normal function and reduce quality of life.

Biogenic amines are a conserved class of neurotransmitter signals that link energy metabolism and behavior. Biogenic amines include dopamine, serotonin, epinephrine, norepinephrine, octopamine, and tyramine (Hoffman et al. 1998; Chase and Koelle 2007;

Tecott 2007; Roeder 2005). Dysregulation of biogenic amine signaling is implicated in neuropsychiatric disorders such as anorexia, depression, Alzheimer's, and Parkinson's (Kaye et al. 1991; Haider and Haleem 2000; Finch and Cohen 1997; Curran and Chalasani 2012; Meltzer et al. 1998). For example, Parkinson's disease, a neurodegenerative disease that affects movement and cognitive function, is caused by a loss of dopamine signaling (Dauer and Przedborski 2003; Nass 2010; Kuwahara and Iwatsubo 2005). Drugs that act on norepinephrine receptors are used to treat coronary heart disease, ventricular arrhythmias, and other cardiovascular diseases associated with aging (Singewald and Philippu 1996; Bousquet, Feldman, and Schwartz 1984). Serotonin is implicated in a number of disorders, including depression, eating disorders, and insomnia, which can become more severe with age (Tecott 2007; Wilson and Argyropoulos 2005). These findings suggest that dysregulation of biogenic amine signaling is an important factor in neurodegenerative and neuropsychiatric disease. Studying biogenic amine signaling can improve our understanding of complex behaviors in humans and inform our treatment of neuropsychiatric and neurodegenerative disorders associated with aging.

C. ELEGANS IS A POWERFUL MODEL ORGANISM FOR THE STUDY OF NEUROSCIENCE AND AGING

It is difficult to study densely interconnected signaling pathways and neural circuits in complex organisms like mammals. For example, mice, whose brains contain about 1000 times fewer neurons than humans, still contain approximately 100 million neurons (Oh et al. 2014; Helmstaedter et al. 2014). Understanding how such a staggering number of cells work together to sense and process the environment and produce behavior is no

small feat. Furthermore, mammals exhibit obstacles to experimentation, such as complexities in rearing and limited access to vital organs for intervention and imaging. Therefore, researchers often look to simpler organisms that can be more easily manipulated in the lab. Results obtained by studying these simpler organisms are often transferable to other phyla such as mammals (Lehner 2013; Papatheodorou, Petrovs, and Thornton 2014; G. M. Martin 2011) (Figure 1.6).

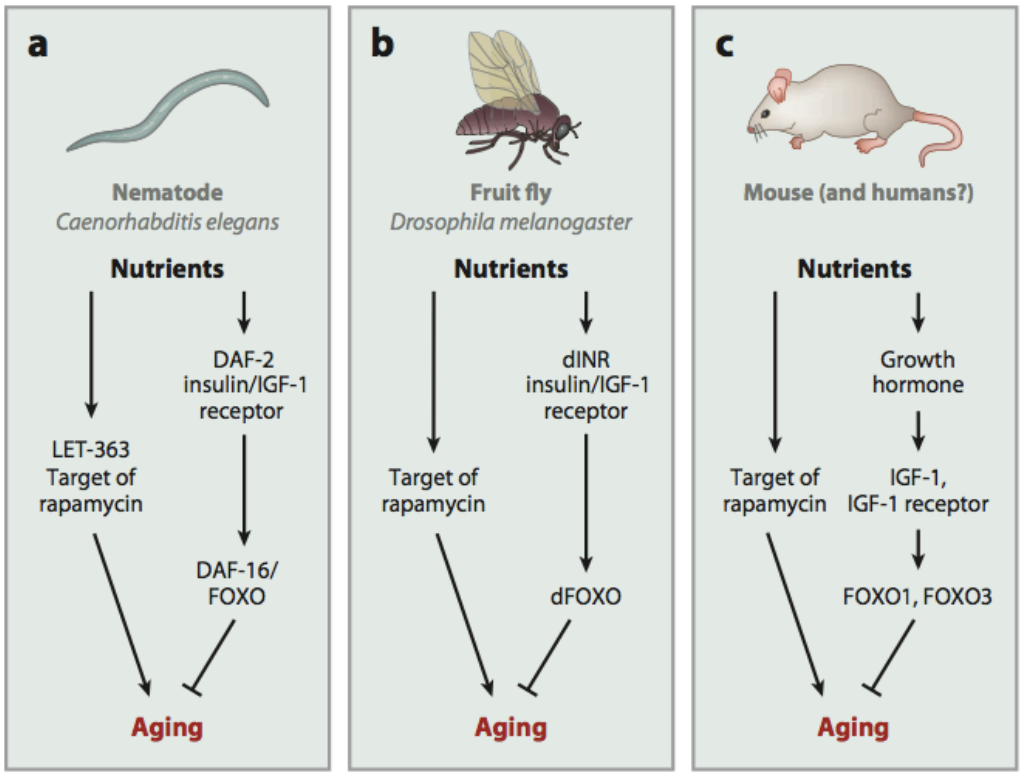

Figure 1.6 Conservation of genetic pathways regulating lifespan in organisms as diverse as a) Worms, b) Flies, and c) Mice. Originally published by Gems and Partridge (Gems and Partridge 2013).

In the 1970s, Sydney Brenner proposed the roundworm *Caenorhabditis elegans* as a model organism for genetic research (S Brenner 1974; Sydney Brenner 2003). These 1 mm-long worms (Figure 1.7) exhibit a number of features that make them attractive

candidates for biological research. The worm life cycle is about three days, making worms easy to culture in the lab. Worms exist primarily as hermaphrodites, which facilitates culturing and may reduce experimental variability. Worms are optically transparent, which facilitates imaging the tissues of live animals.

Figure 1.7 Adult *C. elegans*. Head is on the left. The adult worm is approximately 1 mm long.

Worms are grown in the lab on petri plates filled with agar, and they feed on a thin layer of *E. coli* bacteria. Individual animals can be manipulated for husbandry or experimental purposes with a platinum wire pick. The simplicity of culture and physical manipulation make *C. elegans* a convenient organism to work with in the lab.

The *C. elegans* adult hermaphrodite has a compact nervous system of only 302 neurons and 959 total cells (S Brenner 1974), making worms a highly tractable system in which to study how strings of neurons work together to produce behavior. Despite its simplicity, *C. elegans* exhibits a range of behaviors such as feeding (L. Avery 1993), locomotion (S Brenner 1974; Kawano and Zhen 2011), navigation (Gray, Hill, and Bargmann 2005; Pierce-Shimomura, Morse, and Lockery 2012), learning (Stein and Murphy 2014;

Lakhina and Murphy 2015), and mating (Liu and Sternberg 2012). Furthermore, worms are the only organism for which the entire synaptic connectivity diagram or 'connectome' (Jarrell et al. 2012; Oh et al. 2014) has been mapped (White et al. 1986). Such information facilitates the elucidation of the neural circuits that underlie behavior. Worms also enjoy a wealth of genetic tools and other technical resources (M Chalfie et al. 1994; Timmons, Court, and Fire 2001; S Brenner 1974).

The worm also exhibits numerous features that make it an attractive system in which to study the biology of aging. One such feature is the worm's short generation time, which enables rapid construction of genetic crosses and transgenic rescue strains. The worm life cycle lasts approximately three days at 20° C (Raizen et al. 2008). During this time, an embryo develops through four larval stages into a mature reproductive adult. An adult *C. elegans* hermaphrodite lays between 100 and 300 progeny (Waggoner et al. 2000; Hobson et al. 2006). In the lab, wild type *C. elegans* survive for an average of 2-3 weeks (C. Kenyon et al. 1993). The worm's short lifespan reduces the time required to perform repeated experiments on interventions that influence aging, especially in comparison with other model organisms such as flies and mice, which may live for up to four months or two years, respectively.

Finally, many *C. elegans* genes are highly homologous to those in humans, enabling study of behavior, metabolism, and aging in a simple model organism. Therefore, many results obtained in worms often yield similar results in mice and humans (C. J. Kenyon 2010). Examples of conserved genes include biogenic amine synthesis enzymes,

biogenic amine receptors, and members of nutrient sensing pathways such as the insulin receptor and the FOXO transcription factor that influence aging (Tecott 2007; Carre-Pierrat et al. 2006; C. J. Kenyon 2010) (Figure 1.4). Overall, *C. elegans* is a simple yet powerful model organism for the study of the relationship between genes, metabolism, aging, and behavior.

STUDYING AGING IN *C. ELEGANS*

Genes are a key factor that regulate various hallmarks of aging (Lopez-Otin et al. 2013; C. J. Kenyon 2010). Many genes that influence lifespan in *C. elegans* also regulate lifespan in mammals (C. J. Kenyon 2010). Therefore, genetic pathways that regulate aging are often highly conserved across evolution. Studying the genetic pathways that influence lifespan and healthspan in simple organisms can improve our understanding of aging in mammals (Longo, Antebi, Bartke, Barzilai, Brown-Borg, Caruso, Curiel, De Cabo, et al. 2015).

C. elegans is a strong candidate with which to improve our understanding of the biology of aging (C. J. Kenyon 2010; A.-L. Hsu et al. 2009; Fontana, Partridge, and Longo 2010). *C. elegans* was the first animal in which it was discovered that single gene mutations can drastically alter lifespan. For example, it was first discovered in worms that mutations in the genes *age-1* and *daf-2*, both of which are part of the insulin/insulin-like signaling pathway, can increase lifespan about two-fold (C. Kenyon et al. 1993; Friedman and Johnson 1988) (Figure 1.3-1.4). Since this discovery, many more genes and pathways have been found to influence lifespan (Murphy et al. 2003; McCormick et al. 2011; Lund

et al. 2002; Rangaraju et al. 2015; Ye et al. 2013; J Apfeld and Kenyon 1999), and many of these pathways are conserved between worms and mammals (Lopez-Otin et al. 2013).

A fundamental limitation of manual studies of aging in *C. elegans* is that these studies are almost exclusively carried out at the population level and only measure time of death. By only measuring lifespan, researchers lose all information about the aging process itself. Therefore, we do not know the impact on aging of many genes that influence lifespan. The reason this is important is that genes that increase lifespan may have deleterious effects on health, resulting in animals with longer lifespans but shorter healthspans relative to wild type (Bansal et al. 2015; W. B. Zhang et al. 2016). The relative merits of such conflicting effects are up for debate, but what is not is the need for scientists to understand the full range of effects of interventions that influence lifespan, especially as the results from simple model organisms such as worms and flies is increasingly translated to studies of mammalian (Onken and Driscoll 2010; Lakowski and Hekimi 1998; J. a Baur et al. 2006; Lee and Min 2013; Mirzaei, Suarez, and Longo 2014; Barzilai et al. 2012) and primate aging (Colman et al. 2014).

As such, a current area of great scientific and medical interest is in understanding the biology of healthspan, or the fraction of an animal's life spent in good health (Longo, Antebi, Bartke, Barzilai, Brown-Borg, Caruso, Curiel, De Cabo, et al. 2015; J. A. Baur et al. 2012; Tatar 2009). In order to measure this quantity, however, requires the ability to make life-long observations of health in individual animals over their entire lives.

VARIABILITY IN LIFESPAN AND AGING

In the lab, *C. elegans* are typically reared as clonal populations. Despite this fact, there remains significant variation in lifespan within a population (Kirkwood et al. 2005) (Figure 1.3). What is the source of such variation? One known source of variability is worms' bacterial food, which was shown to be variably pathogenic (D. H. Kim 2013; Sánchez-Blanco and Kim 2011). However, bacterial pathogenicity explains only a small fraction of lifespan variability. One possible explanation underlying the remaining variability is stochastic variability in gene expression, which may lead to variable aging in different genetic pathways or tissues (Kaern et al. 2005; Raj and van Oudenaarden 2008; Herndon and Driscoll 2002). Finer analysis of aging at the individual level may help uncover inter-individual differences in aging that can shed light on these unknown sources of variability.

A recent study measured lifespan for large populations of worms and found that the lifespan distribution scales between populations with different lifespans (Stroustrup et al. 2016) (Figure 1.8). Mutant populations with different average lifespans were found to exhibit similarly shaped lifespan curves when rescaled in time, suggesting that the causes of aging might be reduced to a single variable (Stroustrup et al. 2016). However, another recent study monitored other aging phenotypes in addition to lifespan and found that individuals with different lifespans did not exhibit a similar scaling as observed at the population level (W. B. Zhang et al. 2016). Therefore, while population lifespan curves scale, aging in individual wild type animals does not. It remains unanswered how the constellation of genetic and environmental variables are filtered through metabolic

pathways to give rise to the aging process and in what ways the aging process may vary across individuals and populations.

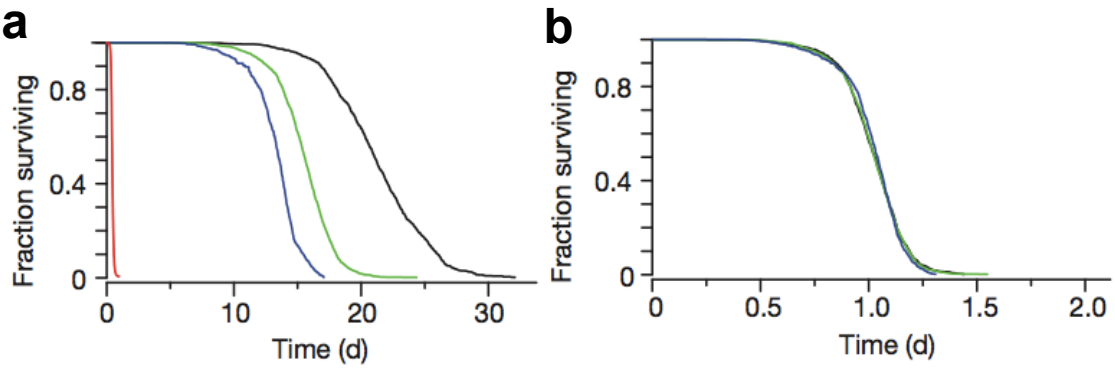

Figure 1.8 Temporal scaling of lifespan. a) Lifespan curves of worms cultivated under four different temperature conditions. Temperature conditions were 20° C (black curve), 25° C (green curve), 27° C (blue curve), and 33° C (red curve). b) Lifespan curves from panel (a) rescaled in time, indicating a conserved shape. Originally published by Stroustrup et al. (Stroustrup et al. 2016)

BIOGENIC AMINES AND BEHAVIOR

Animals must adapt their behavior to environmental conditions in order to maximize their chances of survival. Locomotion and movement patterns are a fundamental behavior that must be adjusted to the environment, and food levels are a particularly salient environmental variable that dictates how animals should behave. Food levels are a complex parameter, as the way food levels are processed by an animal are modulated by factors such as type and concentration of food (McCloskey et al. 2017), memory of past feeding or starvation (Sawin and Horvitz 2000), and the spatial arrangement of food (Calhoun et al. 2015; Calhoun and Hayden 2015).

Given the importance of the relationship between food and behavior, it should come as no surprise that an ancient system of signaling molecules regulates this relationship. Biogenic amines are conserved neuromodulators that link environment with organismal energy balance. Biogenic amines regulate behaviors dependent on energy status such as movement and feeding (Chase and Koelle 2007). Serotonin is a biogenic amine that regulates feeding and appetite in organisms as diverse as worms and humans (Tecott 2007), and it often functions as a food signal (Kaye et al. 1991; E. R. Greer et al. 2008; Srinivasan et al. 2008; Liang et al. 2006a; J Y Sze et al. 2000). Adrenaline and noradrenaline, and noradrenaline's invertebrate analog, octopamine, are "fight or flight" signals that indicate either a lack of food or a signal to cease feeding and digestion (Roeder 2005). While much is known about the basic function of biogenic amines, the precise neural circuits through which they act to sense and process the environment and in turn produce behavior are only beginning to be fully elucidated (Flavell et al. 2013a; Yang et al. 2015; Suo, Culotti, and Van Tol 2009; Suo, Kimura, and Tol 2006). As previously mentioned, biogenic amine signaling often goes awry in age-associated neurodegenerative diseases. Therefore, studying biogenic amine signaling can not only help us better understand how animals make behavioral decisions but may also improve our understanding of diseases associated with aging.

LONG-TERM BEHAVIOR IN *C. ELEGANS*

Animal behavior unfolds over time scales ranging from milliseconds up to hours, days, or longer. For example, mammals exhibit reflexive responses to auditory cues in

milliseconds (Nelken et al. 2005), but hibernate with characteristic posture and quiescent behavior for months (S. L. Martin 2008; Andrews 2007) (Figure 1.9).

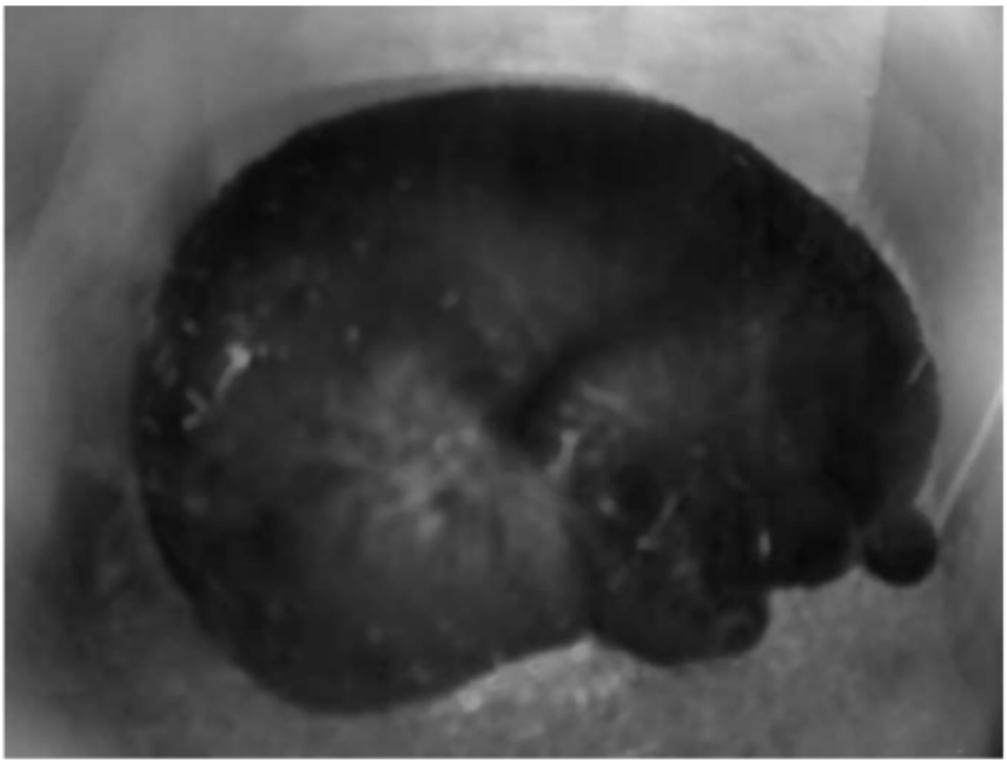

Figure 1.9 Mammalian hibernation is a long-term behavior state. A black bear is pictured during hibernation. Stereotypical posture can be observed. Hibernators also cease movement and feeding for long time periods. Originally published by Tøien et al. (Tøien et al. 2011).

A similar range of time scales are observed in worm behaviors. Short term behaviors, such as touch response (Martin Chalfie et al. 1985), acute avoidance behaviors (Edwards et al. 2008), and feeding (Nicholas F Trojanowski et al. 2014; L. Avery 1993) are more easily studied than long term ones as they are readily measured using manual methods and observation. Some longer term behaviors can be easily studied if they exhibit discrete endpoints, such as chemotaxis (P. Sengupta, Chou, and Bargmann 1996). However, in general it is more difficult to study behaviors that occur on long time scales,

such as those that unfold over hours or days, due to the difficulty of long-term manual observation. Even automated video recording methods may fail due to the inability to uniquely track individuals over time as animals in a population mix together. A related challenge in long-term monitoring is the tracking of behavioral changes with age over the entire worm lifespan.

A number of long-term behaviors have been identified in worms. These include taxis behaviors, which involve animals navigating in relation to some physical stimulus, sometimes involving memory and learning (Ramot et al. 2008; Pierce-Shimomura, Morse, and Lockery 2012; Luo et al. 2014; Garrity et al. 2010; Iino and Yoshida 2009; Bargmann and Horvitz 1991; Hedgecock and Russell 1975; Ohnishi et al. 2011; Zariwala, Faumont, and Lockery 2003).

Behavioral states are another type of long-term behavior (Gallagher, Bjorness, et al. 2013). Behavioral states are composed of multiple individual behaviors that occur coincidentally and persist over time. Sleep is an example of a behavior state. Sleep is composed of multiple discrete behaviors, namely, stereotypical posture, reduced movement, and reduced sensory responsiveness, which occur coincidentally (R. V. Lam 2006; Gerstner, Perron, and Pack 2012; Crocker and Sehgal 2010; Cirelli and Tononi 2008). Worms also exhibit behavior states. A simple example of a worm behavior state is the increase in feeding rate and slowing of locomotion that occur in tandem when animals encounter bacterial food (L. Avery 1993; Sawin and Horvitz 2000). Another long term behavior state in worms is quiescent or sleep behavior, which occurs after each

molt (Raizen et al. 2008; M D Nelson et al. 2013), where it is known as 'developmentally-timed sleep', or in response to stressors such as heat or ultraviolet radiation, where it is known as 'stress-induced sleep' (Iannacone et al. 2017; N. F. Trojanowski et al. 2015). Sleep in worms exhibits similar properties to that in mammals, such as stereotypical posture, reduced movement, reduced sensory response, and homeostasis (Raizen et al. 2008; Iwanir et al. 2013; Nagy, Raizen, and Biron 2014).

Long-term behaviors can occur on time scales ranging from hours (taxis, sleep, and other behavioral states) to months (aging). A crucial challenge is to develop methods to monitor long-term behaviors in an efficient manner, as long-term behaviors are difficult to study using manual techniques.

TECHNIQUES FOR LONG-TERM MONITORING OF *C. ELEGANS*

In order to characterize and understand behaviors that occur over long time scales, such as the locomotion behavior states and age-related decline that are the topics of this dissertation, we require methods for long-term monitoring of worm behavior. A number of approaches have been devised to study long-term phenotypes in *C. elegans*. These approaches can be classified into two groups: longitudinal and population. Longitudinal approaches aim to isolate individual animals in order to monitor each individual longitudinally over the desired time period, enabling single animal tracking, higher resolution phenotyping, and analysis of inter-individual variability. Population-based approaches aim to monitor many animals at a time, often simply by imaging a standard agar plate (Swierczek et al. 2011; Stroustrup et al. 2013). These approaches are ideal for

applications where large numbers of animals are necessary, such as subtle phenotypes. However, due to their lack of ability to track individual animals longitudinally, population-based approaches are limited to characterizing short-term behaviors.

Longitudinal imaging approaches include culturing worms in individual droplets (Belfer et al. 2013), individual wells (W. B. Zhang et al. 2016; Yu, Raizen, and Fang-Yen 2014; Bringmann 2011), microfluidic devices (Hulme et al. 2010b; Lockery et al. 2008) (Figure 1.10).

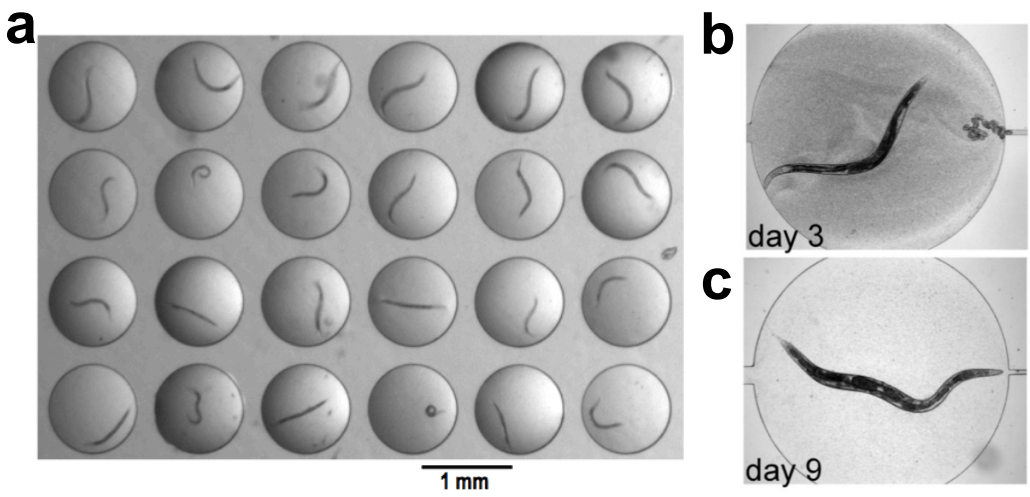

Figure 1.10 Longitudinal imaging methods. a) Worms can be monitored for their whole lives in aqueous droplets. Originally published by Belfer et al (Belfer et al. 2013). b-c) Worms can be monitored in individual wells in a microfluidic device. Originally published by Hulme et al. (Hulme et al. 2010a).

However, many of these methods are compatible with only specific worm ages, such as individual larval or adult stages, limiting their flexibility. Another approach to longitudinal imaging is to use a moving microscope stage to image a single animal on an agar plate, track the animal in real-time, and use the moving stage to keep the animal in

the field of view (Husson et al. 2012). These methods are ideal for measuring the behavior of small numbers of animals over any length scale, although longer time scales are more difficult to sustain.

Population-based imaging approaches often culture animals on a standard agar plate. They often use sophisticated image analysis software to segment individual animals and track them over short time scales (seconds to minutes). These approaches have been used to describe in detail worm response to vibration (Swierczek et al. 2011) as well as applied to measure lifespan for large populations (Stroustrup et al. 2013) (Figure 1.11).

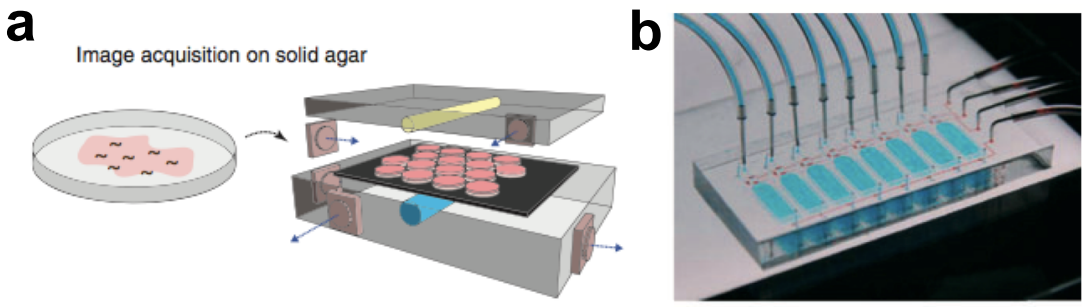

Figure 1.11 Population-based imaging methods. a) The Lifespan machine uses flat-bed scanners to image many standard agar plates at a time. Originally published by Stroustrup et al (Stroustrup et al. 2013). b) The WormFarm microfluidic device can measure populations of worms in liquid over the course of the entire lifespan. Originally published by Xian et al (Xian et al. 2013).

These methods are ideal for measuring the behavior of many animals at a time, albeit only over short-time scales.

Current methods to monitor long-term behaviors in worms can thus be broken up into approaches that are highly granular and well-suited to describing the behavior of small

number of animals, or low-resolution and better suited to describing population behaviors of hundreds or thousands of animals over short length scales. Therefore, there is a lack of methods capable of measuring individual behavior over long time scales for many animals simultaneously. Furthermore, both classes of methods previously described are not scalable either up or down, limiting their utility to specific biological questions.

OBJECTIVE

The first goal of this thesis is to develop a method for long term, longitudinal imaging of *C. elegans* behavior and lifespan. The second goal is to use a combination of genetic techniques, pharmacology, machine vision, and quantitative behavioral analysis to address questions regarding variability in behavioral decline during aging, the relationship between behavior and survival, and the neural circuits underlying food-related behavior states. In chapter 2, I will discuss the development of the longitudinal imaging device and method, called the WorMotel (Figure 1.12-1.13), and its applications to automating measurements of lifespan and behavioral aging. I also apply the method to quantifying differences in inter-individual variability in the aging process, the scaling of aging during stress, and the relationship between behavior and survival.

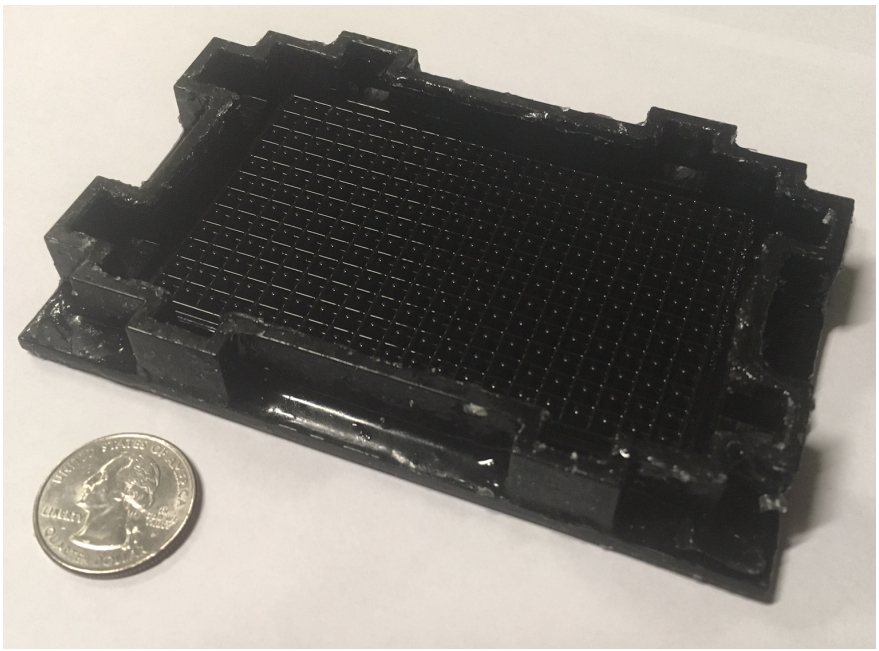

Figure 1.12 3D-printed WorMotel negative mold.

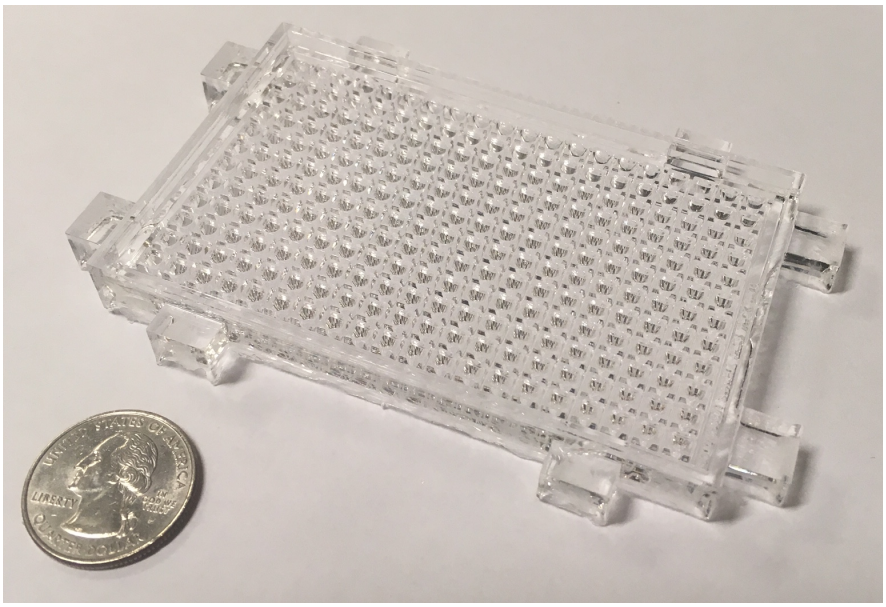

Figure 1.13 WorMotel positive cast (Silicone PDMS).

In chapter 3, I will discuss the application of my longitudinal imaging method toward quantifying locomotion behavioral states in young adult animals and their modulation by

biogenic amine neurotransmitters and food. In chapter 4, I will discuss my conclusions and future directions suggested by this work. Appendix I presents a protocol describing how to construct the imaging system used in the majority of the experiments contained in the dissertation. Appendix II and III describe characterization and construction, respectively, of a system for single cell transgene induction using a pulsed infrared laser.

CHAPTER 2: Longitudinal imaging of *Caenorhabditis elegans* in a microfabricated device reveals variation in behavioral decline during aging

Matthew A. Churgin[1], Sang-Kyu Jung[1], Chieh-Chieh (Jay) Yu[1], Xiangmei Chen[1], David M. Raizen[2], and Christopher Fang-Yen[1,3]

[1]Department of Bioengineering, School of Engineering and Applied Sciences, University of Pennsylvania, Philadelphia PA 19104. [2]Department of Neurology, Perelman School of Medicine, University of Pennsylvania, Philadelphia PA 19104. [3]Department of Neuroscience, Perelman School of Medicine, University of Pennsylvania, Philadelphia PA 19104.

This chapter is a slightly modified version of a paper published in eLife (Churgin *et al.,* 2017b). All data contained in this chapter was collected by me, except for part of Figure 2g, which was collected with the help of Xiangmei Chen, and Figure 1 Supplement 3, which was collected by Chieh-Chieh Yu. Sang-Kyu Jung helped with the writing of image processing software and contributed to the development of blue light stimulation procedure. David Raizen helped with interpreting data, drafting the manuscript, and manuscript revisions. Christopher Fang-Yen designed the WorMotel mold and associated software, helped with planning experiments, interpreting data, and drafting and revising the manuscript.

ABSTRACT

The roundworm *C. elegans* is a mainstay of aging research due to its short lifespan and easily manipulable genetics. Current, widely used methods for long-term measurement of *C. elegans* are limited by low throughput and the difficulty of performing longitudinal monitoring of aging phenotypes. Here we describe the WorMotel, a microfabricated device for long-term cultivation and automated longitudinal imaging of large numbers of *C. elegans* confined to individual wells. Using the WorMotel, we find that short-lived and long-lived strains exhibit patterns of behavioral decline that do not temporally scale between individuals or populations, but rather resemble the shortest and longest lived individuals in a wild type population. We also find that behavioral trajectories of worms subject to oxidative stress resemble trajectories observed during aging. Our method is a powerful and scalable tool for analysis of *C. elegans* behavior and aging.

INTRODUCTION

Aging consists of gradual changes in an adult organism that cause a reduction of function and an increase in mortality. Studies of model organisms such as the roundworm *C. elegans* have identified highly conserved processes and pathways which influence aging, including dietary restriction (Lakowski and Hekimi 1998; Eric L Greer and Brunet 2009), insulin/insulin-like signaling (C. Kenyon et al. 1993), and the cytoprotective DAF-16/FOXO pathway (E L Greer and Brunet 2007; Eijkelenboom and Burgering 2013; Ogg et al. 1997).

Current, widely used methods for long-term measurement of *C. elegans* aging are based on manual inspection of worm survival on agar plates. These methods are robust and technically simple, but have a number of limitations. They are labor intensive, low in throughput, and are largely focused on lifespan at the population level without access to information about health or behavior during individual life trajectories.

Previous efforts have aimed to automate *C. elegans* survival assays. One method produces high resolution survival curves by monitoring large populations of animals on standard agar plates using flatbed scanners (Stroustrup et al. 2013). However, this method monitors only lifespan and are not designed to track individual animals over their entire lifetime. Therefore, this system is limited in its ability to study aging in individual animals.

Another method (W. B. Zhang et al. 2016) used small hydrogel compartments between a glass slide and a PDMS membrane to perform long-term longitudinal monitoring of *C. elegans* aging. However, the device has a number of limitations: it is not easily scalable to large numbers of animals and does not lend itself to screening experiments. The hydrogel device requires complex image analysis software and prevents access to animals during the experiment, limiting the additional phenotypes that can be assayed in tandem. Also, the hydrogel device requires sterile mutations to be crossed into all strains tested, and all experiments must be performed at the restrictive temperature of 25° C, limiting the prospects for genetic screening.

Here we describe a device we call the WorMotel (WM), which is capable of longitudinally tracking behavior of up to 240 uniquely identified animals of any genotype per device for over 60 days. The WM consists of an array of individual wells, each of which is filled with standard agar media, bacterial food, and a single worm, enabling long term cultivation and imaging of hundreds of uniquely identified animals. By conforming to the ANSI standard microplate format, our method leverages existing scalable automation technology including worm sorters, robotic plate handlers, and chemical library screening tools. We apply our method to quantifying inter-individual and inter-strain differences in behavioral decline during aging and stress, as well as in understanding the relationship between behavior and lifespan.

RESULTS

A scalable platform for long-term imaging of worm behavior, development, and lifespan

Conventional 96-well or 384-well microplates are not well suited for worm imaging and cultivation on agar media due to three problems. First, the vertical walls of each well make it difficult to image the worms when they are close to the edge of the wells (Figure 2.1 supplement 1). Second, worms tend to crawl between the agar and well edges, again making them difficult to image clearly. Third, under humid conditions, animals can climb over the walls of the wells, mixing with other worms.

We designed the WorMotel to address these limitations. Each WorMotel consists of a transparent polydimethylsiloxane (PDMS) substrate containing a rectangular array of up

to 240 wells, produced by molding from an acrylic photopolymer 3D-printed master (Shepherd et al. 2011) (Figure 2.1, Figure 2.1 supplement 2). The well geometry is optimized for worm cultivation and imaging of a single worm per well. A rounded concave well geometry (Figure 1a) provides a clear view of the animal at all positions on the agar surface (Yu, Raizen, and Fang-Yen 2014), and also inhibits worms from burrowing under the agar (Figure 2.1 supplement 3). A network of narrow moats containing a copper sulfate solution surrounding the wells prevents animals from escaping from their wells (Figure 2.1b).

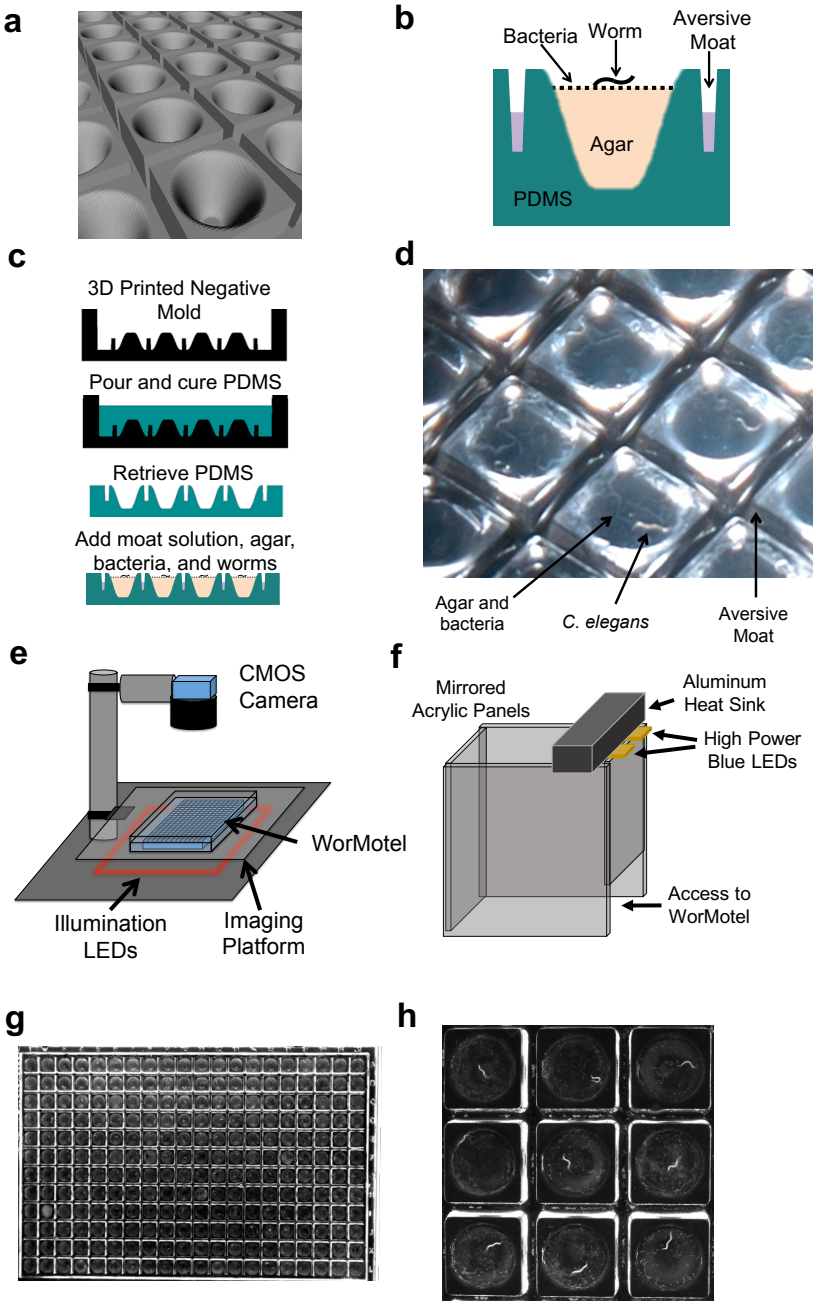

Figure 2.1 WorMotel design, fabrication, preparation, and experimental setup (a) 3D rendering of WorMotel geometry. (b) Schematic cross-section of a single well. (c) Fabrication and loading process (d) Image of WorMotel filled with agar, bacteria, and adult *C. elegans*. (e) Experimental setup (f) schematic of Blue light stimulation system. (g) Representative image of 240-well WorMotel (h) High resolution image of nine wells, each housing a single young adult N2 worm.

Each well is filled with approximately 15 μL of NGM agar, followed by a suspension of bacteria added as food. For lifespan measurements, enough bacteria is added initially to sustain worms throughout their lives, and the animals are left essentially undisturbed for the remainder of the experiment. A single worm is added manually to each well.

The WorMotel is sealed inside a polystyrene dish (Nunc Omnitray) and imaged under dark field illumination with a CMOS camera (Imaging Source) where it remains for the experiment's duration (Figure 2.1e) (Churgin and Fang-Yen 2015). If desired, however, the device may be removed periodically for manual inspection or other longitudinal assays. The pixel resolution for a field of view containing all 240 wells is 36 μm, or roughly one thirtieth the length of an adult *C. elegans* (Figure 2.1g, Video 2.1-2.3). Moving the camera closer to the WM or using a longer focal length lens reduces the field of view but enables higher resolution images to be attained (Figure 2.1h, Video 2.4).

In humans and diverse model organisms, locomotor activity has been used as a measure of health (Hausdorff et al. 1997; Grotewiel et al. 2005; Huang, Xiong, and Kornfeld 2004). It has been shown that spontaneous locomotion on food is a non-ideal measure of health since it assesses food preference in addition to locomotor ability (Hahm et al. 2015). As such, a directed behavior is preferable over spontaneous movement. We used the response to blue light illumination as a measure of locomotor ability and therefore health.

The WM can be imaged continuously or intermittently. Under intermittent imaging, the WM is automatically imaged at 0.2 frames per second for a 30 minute interval twice daily. After fifteen minutes, a blue light stimulus, which evokes an escape response in worms (Edwards et al. 2008), is applied to the entire plate for 10 s using a set of light emitting diodes (LEDs). In this manner we measure both spontaneous and evoked behavioral responses (Figure 2.1f, 2.2b-e, Video 2.1-2.3).

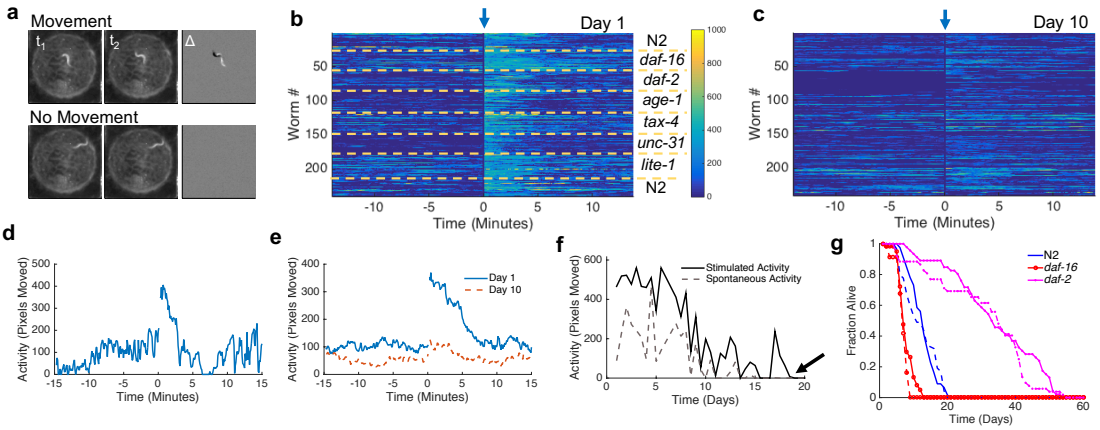

Figure 2.2 Image processing, automated lifespan calculation, and manual validation (a) Activity calculation. Delta image (right image) is calculated by pixel-by-pixel subtraction of images taken at time t_1 from images taken at time t_2. Examples are shown in which a worm moves (top) and does not move (bottom). (b) Activity, shown as a heat map, of Day 1 adult animals during a 30-minute imaging epoch. Arrow indicates 10-second blue light stimulation. (c) Activity of adult *C. elegans* on day 10. (d) Activity trace from one wild-type animal. Blue light was applied at time zero (e) Average wild-type population behavior on day 1 (solid curve) and day 10 (dashed curve) (n=30) (f) Single animal trace of maximum spontaneous (dashed) or stimulated (solid) activity across entire lifespan. Arrow indicates time of death. (g) Lifespan of animals grown on the WorMotel (solid curves) or standard plates (dashed curves)

Custom MATLAB software quantifies movement of the animal in each well. Following pixel-by-pixel subtraction of pairs of temporally adjacent frames (Raizen et al. 2008), a simple measure of behavior can be defined as the number of pixels whose intensity

changes between subsequent image frames (Figure 2.2a). Highly mobile animals yield high activity values, whereas slowly moving, older, or quiescent animals yield low activity values (Figure 2.2b-e). Activity analysis generated rich behavioral data capable of characterizing aging and development (Figure 2.2f) (M D Nelson et al. 2013; Matthew D. Nelson et al. 2014; Iannacone et al. 2017). Lifespan is determined as the the final time of nonzero movement (Figure 2.2f).

During each imaging epoch we calculate the maximum activity before and after the blue light stimulus, and we term these values the spontaneous and stimulated locomotion, respectively. We recorded the total time spent moving after the stimulus, which we term response duration. Finally, we record the response latency, defined as the delay between the end of the stimulus and the beginning of the animal's movement.

Our WorMotel method is designed to be scalable to large numbers of animals. Using standard automation tools including a plate carousel and plate handling robot (Figure 2.1 supplement 4) we have developed a system capable of intermittently imaging up to 240 plates containing 57,600 individually tracked worms.

The WorMotel enables automated lifespan and behavior measurements

We asked to what extent lifespan results from the WM agreed with those using standard manual methods. We compared the survival curves of animals reared on standard agar

plates to those in the WorMotel. We measured the lifespans of wild-type N2 alongside the short-lived strain *daf-16(mu86)* (Ogg et al. 1997) and the long-lived strain *daf-2(e1370)* (C. Kenyon et al. 1993) at 25° C (Figure 2.2g). For worms grown on standard plates, lifespan assays were carried out using standard methods (C. Kenyon et al. 1993). As expected, mean lifespan of *daf-16* mutants (WM: 7.7 ± 0.3 days, n=61; Manual: 7.0 ± 0.2 days, n=117) was shorter than that of N2 (WM: 12.3 ± 0.3 days, n=123; Manual: 12.2 ± 0.5 days, n=94) while *daf-2* mutants showed a longer lifespan (WM: 33.5 ± 1.9 days, n=46, Manual: 30.8 ± 2.0 days, n=52). We found no significant difference between survival curves acquired from worms grown on standard plates and those grown on the WorMotel. Moreover, our lifespan results agree with those previously reported for each strain (C. Kenyon et al. 1993).

We asked whether the aversive copper sulfate solution in the moat, which helps to retain animals inside their respective wells, had any effect on survival or development. We compared the duration of the L4 stage, a measurement of developmental rate, and lifespan of worms grown on a WorMotel with moats filled with NGMB to a WorMotel with moats filled with 100 mM copper sulfate (see Methods). We found no difference in developmental rate of worms grown from the L3 stage to adulthood in the presence of an NGMB (L4 Duration = 12.2 ± 0.2 hours) and copper sulfate moat (L4 Duration = 12.2 ± 0.2 hours, p=0.95). Similarly, we found no difference in the mean lifespan of N2 worms grown in the presence of an NGMB (19.2 ± 0.7 days, n=22) or copper sulfate moat (18.9 ± 1.0 days, n=23).

To test the accuracy of our automated assessment of lifespan, we manually scored the lifespan of worms grown on a WorMotel that was also imaged by camera. Manual assessments of lifespan were performed daily within two hours of a thirty-minute imaging epoch. We compared the time of death measured by our software to that measured by a human observer scoring death manually by standard methods (C. Kenyon et al. 1993). For N2 worms, the average difference between manual and automated lifespan measurement was 0.66 ± 0.6 days (n=79), indicating that automated lifespan calculation is accurate within the time resolution of standard lifespan assays. Automated lifespan was always less than or equal to manual lifespan, indicating that dead animals were never incorrectly scored as alive. Furthermore, we found no correlation between the error in automatic lifespan measurement and true lifespan (p=0.18), indicating that the error in automated lifespan score is independent of lifespan itself, i.e. absolute measurement error does not increase for worms with longer lifespan.

Together these results show that with regard to development and lifespan, results from the WorMotel are similar to those using standard methods.

Mutant strains display diverse behavioral profiles during aging

Aging in *C. elegans* is accompanied by a deterioration of many behaviors, including slowing of locomotion (Hahm et al. 2015) and feeding (Huang, Xiong, and Kornfeld 2004), and a reduced capacity for learning and memory (Stein and Murphy 2012). While

many genes have been identified that regulate aging, less is known about the effect of these genes on behavior.

To survey the relationship between lifespan and behavior, we used the WM to analyze behavioral trajectories for wild type worms and seven loss-of-function mutants for genes known to influence lifespan and/or behavior: (1) *daf-2,* which encodes the insulin/IGF receptor (C. Kenyon et al. 1993), (2) *age-1*, which encodes phosphoinositide-3-kinase, a component of the insulin/insulin-like signaling (IIS) pathway (Friedman and Johnson 1988), (3) *daf-16*, which encodes a transcription factor regulating a cytoprotective response (Ogg et al. 1997), (4) *tax-4*, which encodes a cyclic nucleotide-gated channel required for some sensory transduction (J Apfeld and Kenyon 1999), (5) *unc-31*, required for neuropeptide processing (Ailion et al. 1999), (6*) lite-1*, a gene encoding a receptor required for normal aversive response to blue light (Edwards et al. 2008), and (7) *aak-2*, a gene encoding a subunit of AMP kinase (Apfeld et al. 2004).

We assayed the activity and survival of individuals within populations of each strain (Figure 2.3a-f, Figure 2.3 supplement 1). Mean lifespans of mutant strains relative to wild type agreed with those reported in previous studies (Table 2.1). The shapes of behavior curves varied dramatically between strains.

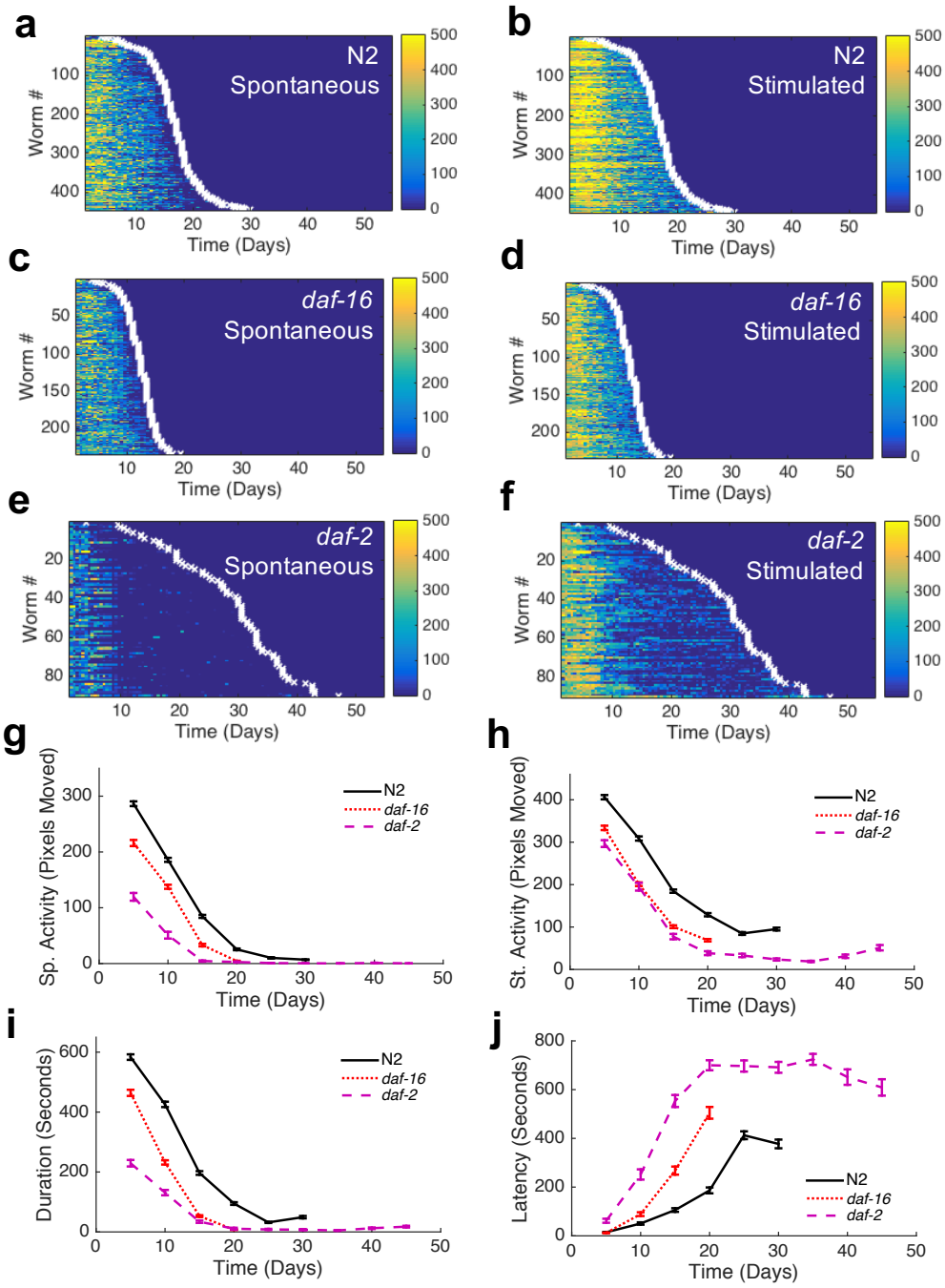

Figure 2.3 Automated quantification of behavioral changes during aging (a) Spontaneous behavior heat map for N2 (n=445). Color bar indicates the number of pixels changed over a 60-second period. (b) Stimulated behavior heat map for N2 (c) Spontaneous behavior heat map for *daf-16* (n=234) (d) Stimulated behavior heat map for *daf-16* (e) Spontaneous behavior heat map for *daf-2* (n=90) (f) Stimulated behavior heat map for *daf-2* (g) Survivor population spontaneous activity (h) Survivor population stimulated activity (i) Survivor population response duration (j) Survivor population response latency

Strain	Food Source	Lifespan (Mean ± SD) (Days)	N	P-value relative to N2 control
N2	DA837	16.8 ± 4.4	445	N/A
daf-16	DA837	12.4 ± 2.6	234	3.0×10^{-45}
daf-2	DA837	28.5 ± 9.2	90	2.1×10^{-16}
age-1	DA837	23.7 ± 8.9	119	4.3×10^{-9}
tax-4	DA837	22.0 ± 5.4	72	3.6×10^{-6}
unc-31	DA837	21.2 ± 7.2	120	3.6×10^{-4}
lite-1	DA837	19.7 ± 4.0	90	0.036
aak-2	DA837	9.6 ± 1.8	117	3.9×10^{-30}
N2	HT115 (EV RNAi)	20.9 ± 5.5	80	N/A
N2	HT115 (*daf-2* RNAi)	29.9 ± 10.3	38	1.2×10^{-6}
N2	HT115 (*odr-10* RNAi)	21.5 ± 6.5	40	0.53
daf-2	HT115 (EV RNAi)	30.0 ± 10.5	40	1.6×10^{-6}
daf-2	HT115 (*daf-2* RNAi)	34.5 ± 9.5	39	7.9×10^{-11}
daf-2	HT115 (*odr-10* RNAi)	36.9 ± 7.4	39	8.2×10^{-15}
odr-10	HT115 (EV RNAi)	21.5 ± 6.6	40	0.40
odr-10	HT115 (*daf-2* RNAi)	28.3 ± 12.5	38	4.8×10^{-4}
odr-10	HT115 (*odr-10* RNAi)	21.1 ± 7.5	40	0.49

Table 2.1 Summary of lifespan data

We included *lite-1* worms in order to determine whether these mutants, previously shown to have a reduced response to blue light (Edwards et al. 2008; Ward et al. 2008), can be assayed by our blue light illumination system for measuring stimulated activity. To our surprise, we found little difference in the responses to blue light between N2 and *lite-1* mutants, possibly because our light stimulus is higher in irradiance than that previously used, and/or our activity measurement is more sensitive to movement increases than the previously measured body bend frequency (Edwards et al. 2008). Regardless, our results for *lite-1* worms indicate that even mutants with deficits in blue light response can be assessed by our method.

Together, these results show that the WorMotel method is compatible with arbitrary strains. We used the longitudinal data generated by the WorMotel to address questions about the relationship between aging and behavior.

Mutants with short and long lifespan display patterns of late-life behavioral decline resembling those of short and long lived worms from a wild-type population

While many factors are known to modulate the mean lifespan of a population, less is known about how these factors alter the aging process on an individual level. Zhang *et al* recently showed that within a wild-type population, long-lived and short-lived animals differed in two ways (W. B. Zhang et al. 2016). First, the rate of physiological decline was slower in long-lived individuals, as might be expected. The second, however, was counter-intuitive: the additional lifespan of longer-lived individuals was primarily due to differences toward the end of the lifespan. That is, long-lived animals exhibited longer periods of low physiological function, or 'extended twilight' (W. B. Zhang et al. 2016).

A different picture was suggested by a study using automated assays of lifespan in the 'Lifespan machine' (Stroustrup et al. 2016). In this study it was reported that various genetic and environmental perturbations do not fundamentally change the shape of the survival curve, but rather only compress or dilate it in time. This result was interpreted as suggesting that the aging process in *C. elegans* is, at least at some point in its pathway, controlled by a single process describable by a single variable corresponding to the rate of aging (Stroustrup et al. 2016).

We sought to determine to what extent, 'extended twilight' and/or scaling effects apply at the behavioral level in mutants with altered aging. The concept of a universal scaling parameter in aging would suggest that the short and long-lived individuals within any strain (whether with normal, short, or long mean lifespan) would resemble their short and long-lived counterparts in the reference strain, but with a temporal scaling (Figure 2.4a). If the variations in aging rate among individuals in any isogenic strain are governed by similar factors, we would expect that long and short lived individuals would display similar late-life characteristics as their wild type counterparts. If, on the other hand, short-lived strains as a whole physiologically more closely resemble short-lived individuals of a wild type population, we might expect them to display late-life characteristics similar to these short lived individuals (Figure 2.4b). Similarly, long-lived strains might display a range of late-life decays or alternatively collectively resemble long-lived worms in the reference strain.

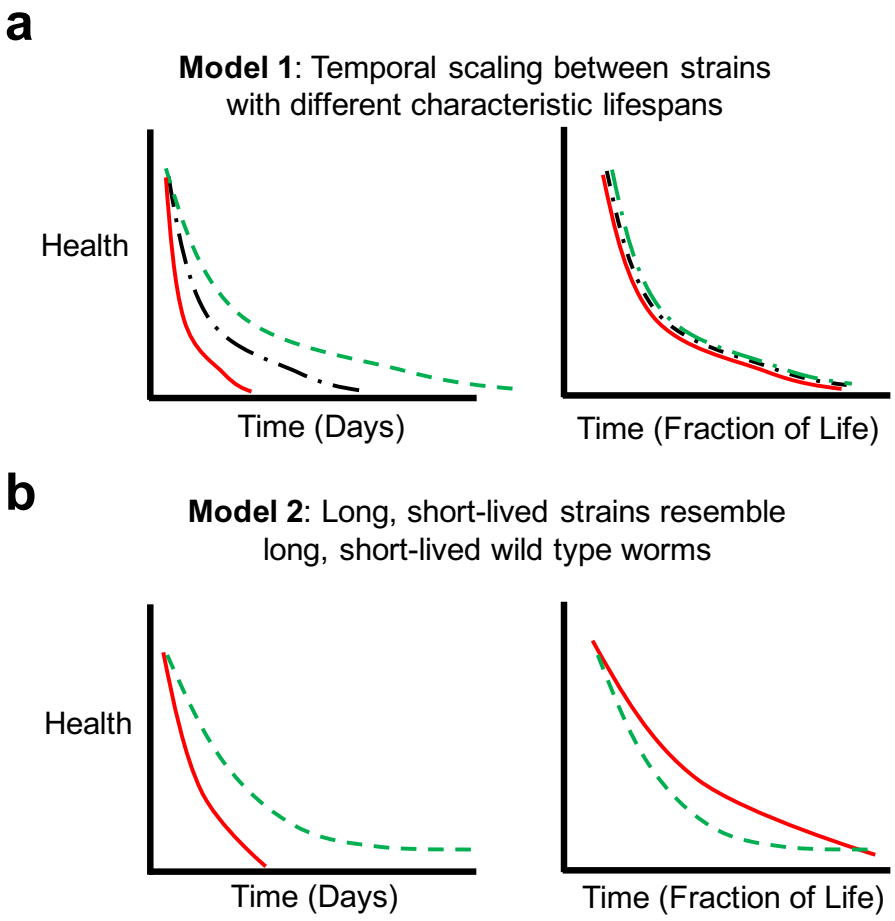

Figure 2.4 Potential aging models (a) Model 1: Temporal scaling results in identical patterns of behavioral decline when data are normalized by lifespan. Idealized decline curves for wild type (black dot-dashed), short-lived (red solid), and long-lived (green dashed) strains. Decline curves are shown as a function of chronological time (left) and fraction of life (right). (b) Model 2: Long-lived and short-lived strains resemble long-lived and short-lived wild type worms with respect to behavioral decline. Idealized decline curves for a short-lived (red solid) and long-lived (green dashed) strains. Decline curves are shown as a function of chronological time (left) and fraction of life (right).

Wild-type strain N2 worms exhibited an initial decline followed by a 'plateau' period of nearly constant spontaneous and stimulated activity and response duration and latency (Figure 2.3g-j). When we compared the behavior of the shortest-lived and longest-lived quartile of N2 worms, we found that their behavioral declines were qualitatively

different. The longest-lived animals exhibited a "decline and plateau" phenotype, in which an initial rapid decline in behavioral capacity is later replaced by a very gradual decline for the remainder of life (Figure 2.5a, h). By contrast, the shortest-lived animals showed only the rapid decline in behavior before dying (Figure 2.5a, g). The result that long-lived animals experience a long period of low behavior are consistent with the 'extended twlight' reported by Zhang et al (W. B. Zhang et al. 2016).

Short-lived *daf-16* mutants declined at a similar rate to N2, but did not exhibit any plateau phase; instead, *daf-16* worms die after their initial behavioral decline (Figure 2.3g-j, Figure 2.5c, d). A similar effect was seen in *daf-16* response duration and response latency, which do not level off but decrease or increase, respectively, at a similar rate until the time of death. Comparing the activity history of the shortest-lived N2 worms to that of *daf-16* as a whole, we found a striking correspondence between the behavioral decline of the two groups (Figure 2.5g). These results show that the behavioral decline of *daf-16* animals is not a scaled version of the wild type distribution of decline, but instead resembles the short-lived individuals in a wild-type population.

Long-lived *daf-2(e1370)* mutants, in which behavioral quiescence has been previously reported (Gems et al. 1998; Gaglia and Kenyon 2009), exhibited a decline in stimulated activity akin to that observed in N2 and *daf-16* followed by a nearly constant low level of stimulated activity and response behaviors for the remainder of life (Figure 2.3h). Spontaneous activity in *daf-2*, on the other hand, declined to near zero within 10

days of adulthood, where it remained until death. Even at very young chronological age (before day 5), *daf-2* mutants perform less well than N2 for each behavior metric scored (Figure 2.3g-j).

The "decline and plateau" phenotype of the longest-lived N2 animals was also evident in both short-lived and long-lived *daf-2* animals (Figure 2.5e, f). Long-lived strains *age-1*, *tax-4*, and *unc-31* also exhibited the "decline and plateau" phenotype (Figure 2.3 supplement 1, Figure 2.5 supplement 1). These results show that aging behavior of *daf-2* and other long-lived animals, like that of *daf-16* animals, does not resemble a scaled version of wild type. Instead, they resemble the longest-lived individuals in a wild-type population, in that they exhibit a long plateau period of low locomotory function during late life.

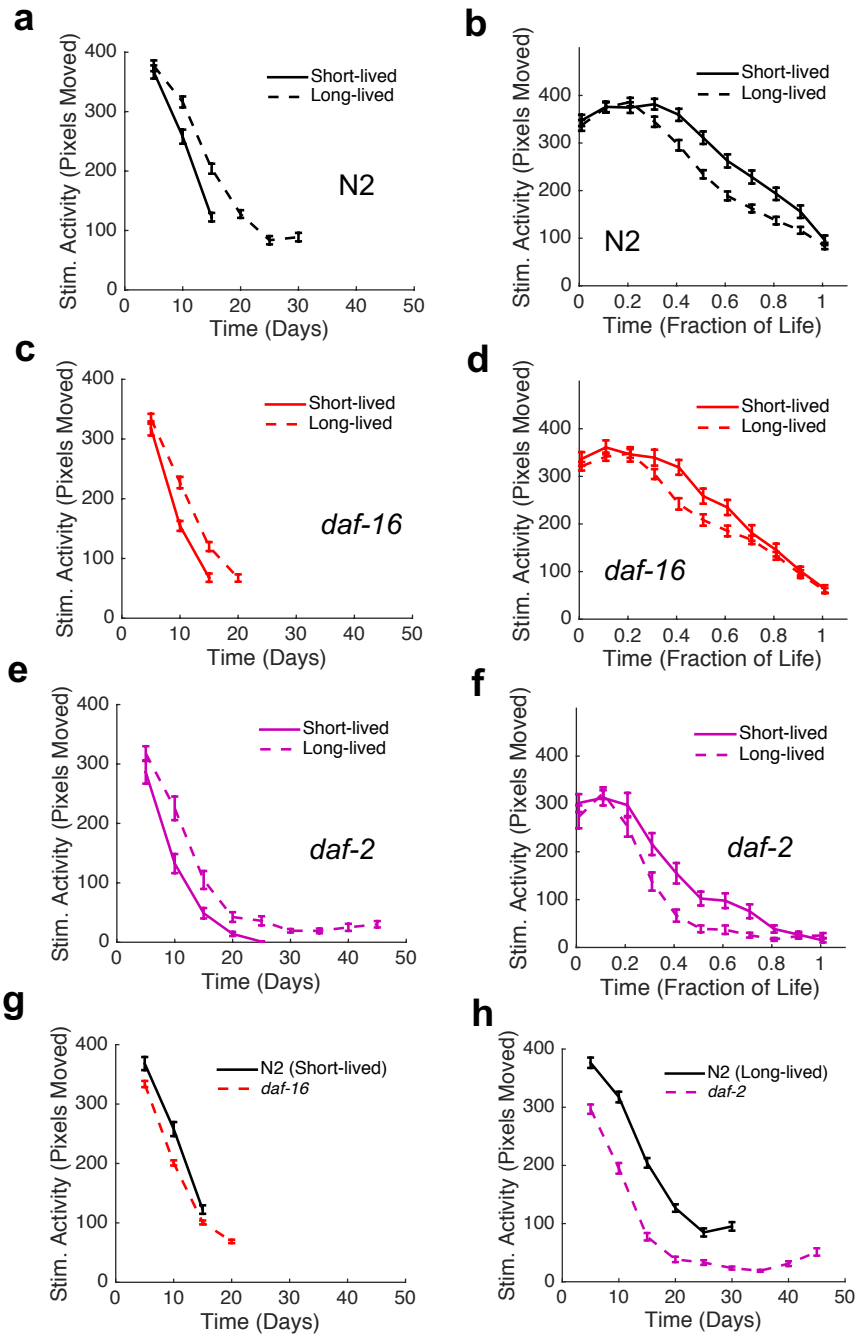

Figure 2.5 Mutants with short and long lifespan display patterns of late-life behavioral decline that resemble short and long lived worms from a wild type population (a) N2 behavior over time for the lowest quartile (solid curve) and highest quartile (dashed curve) of survivors. (b) data from panel a plotted as a fraction of each individual's life (c) *daf-16* behavior over time (d) *daf-16* behavior over fraction of life (e) *daf-2* behavior over time (f) *daf-2* behavior over fraction of life (g) Comparison of N2 lowest survivor quartile and *daf-16* (h) Comparison of N2 highest survivor quartile with *daf-2*

In order to further characterize inter-individual differences in aging, we next sought to quantify the shape of behavioral decline. We analyzed individual behavioral decline as a fraction of life and calculated early and late decline rates (Figure 2.5b, d, f, Figure 2.5 supplement 1, Figure 2.6a-c) (see Methods). We then calculated the difference in decline rates to quantify the overall shape of behavioral decline. We found that the change in decline rate negatively correlated with lifespan in all strains tested (N2: R=-0.32, p=8.0 x 10^{-12}; *daf-16*: R=-0.18, p=0.0054; *daf-2*: R=-0.25, p=0.016; *age-1*: R=-0.43, p=8.0 x 10^{-7}; *tax-4*: R=-0.41, p=4.2 x 10^{-4}; *unc-31*: R=-0.49, p=1.6 x 10^{-8}; *lite-1*: R=-0.54, p=3.9 x 10^{-8}, *aak-2*: R=-0.23, p=0.012) (Figure 2.6a-e), indicating that the shape of behavioral decline differed signficantly for individuals with differing lifespans. We observed a smooth transition between the shape of aging behavior between short-lived and long-lived individuals within each strain (Figure 2.6a-c, Figure 2.6 supplement 1). Furthermore, our results suggest that there exists a relationship between change in decline rate and lifespan that lies along a continuum across strains in addition to between individuals of the same strain (Figure 2.6e, f). Therefore, our results suggest that while behavioral decline does not temporally scale with lifespan, the stochastic sources of variability between isogenic individuals modulate the shape of aging along the same axis of variability as between short and long lived strains. For example, variability in the rate of aging may reflect a variability in the nuclear localization of DAF-16 and the activation of its targets.

Finally, we investigated the level of inter-individual variability in the rate of aging. We found that the standard deviation of decline rate change generally decreased with average

lifespan (Figure 2.6g) (R=-.70, p=0.055). That is, longer-lived strains exhibited less individual variability than shorter-lived strains. Under a temporal scaling model, both the mean decline rate change and standard deviation of decline rate change would be equal across strains with different lifespans. Therefore, our data argue against a temporal scaling model of aging.

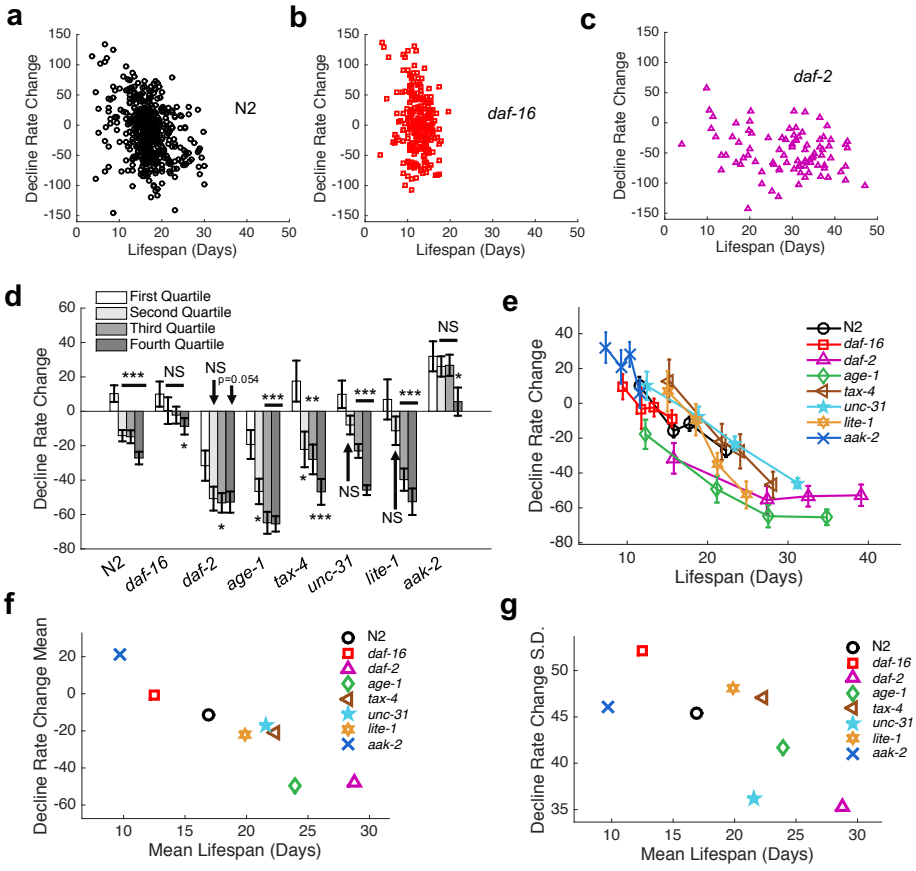

Figure 2.6 Shape of behavioral decline changes continuously with lifespan across individuals and strains (a) Change in decline rate (pixels/life fraction) versus lifespan for individual N2 animals. (b) Same data as in panel (a) presented for *daf-16* mutants (c) Same data as in panel (a) presented for *daf-2* mutants (d) Change in decline rate (pixels/life fraction) in lowest (white) to highest (dark gray) survivor quartiles. *, p<0.05; **, p<0.01; ***, p<0.001 (e) Change in decline rate (pixels/life fraction) versus lifespan for multiple strains (f) Mean decline rate change (pixels/life fraction) plotted against mean lifespan for each strain tested. Correlation coefficient r = -0.94, p = 0.0006. (g) Standard deviation of decline rate change (pixels/life fraction) plotted against mean lifespan for each strain tested. Correlation coefficient r = -0.70, p = 0.055.

Behavioral decline during acute oxidative stress resembles behavioral decline during aging

In an analysis of scaling in lifespan, Stroustrup *et al*. showed that the shape of population survival curves during thermal stress was virtually identical to that occurring during aging (Stroustrup et al. 2016). That is, the rate of population decline increases with temperature while still obeying the same fundamental kinetics. We have shown that the shape of behavioral decline is not identical for worms with different lifespans within a population. Nevertheless, we asked whether a similar scaling law holds for behavioral decline in populations during acute stress.

To test this idea, we added paraquat, which induces oxidative stress via generation of reactive oxygen species (ROS), to the WorMotel agar and monitored the animals' subsequent behavior and survival (An and Blackwell 2003). Oxidative stress, like thermal stress, greatly shortens lifespan. We found that when we added paraquat to a final concentration of 40 mM on day 1 of adulthood, wild type animals survived for 21.2 ± 8.9 hours (n=58), consistent with previous results (Figure 2.7a, Table 2.2) (An and Blackwell 2003). We compared the shape of decline for animals experiencing stress to animals experiencing normal aging (Figure 2.7b, d, f, h). We calculated the normalized mean square difference between behavior during aging and stress, and, after correcting for the average activity offset, found that the difference was 4.1% for N2, 9.7% for *daf-16*, 11.0% for *daf-2*, and 13.2% for *age-1*.

Strain	Food Source	Lifespan (Mean ± SD) (Hours)	N	P-value relative to N2 control
N2	DA837 + 40 mM Paraquat	21.2 ± 8.9	58	N/A
daf-16	DA837 + 40 mM Paraquat	16.5 ± 12.0	60	0.001
daf-2	DA837 + 40 mM Paraquat	37.4 ± 22.0	68	2.0×10^{-5}
age-1	DA837 + 40 mM Paraquat	29.7 ± 13.8	68	2.7×10^{-5}

Table 2.2 Summary of paraquat assay survival data

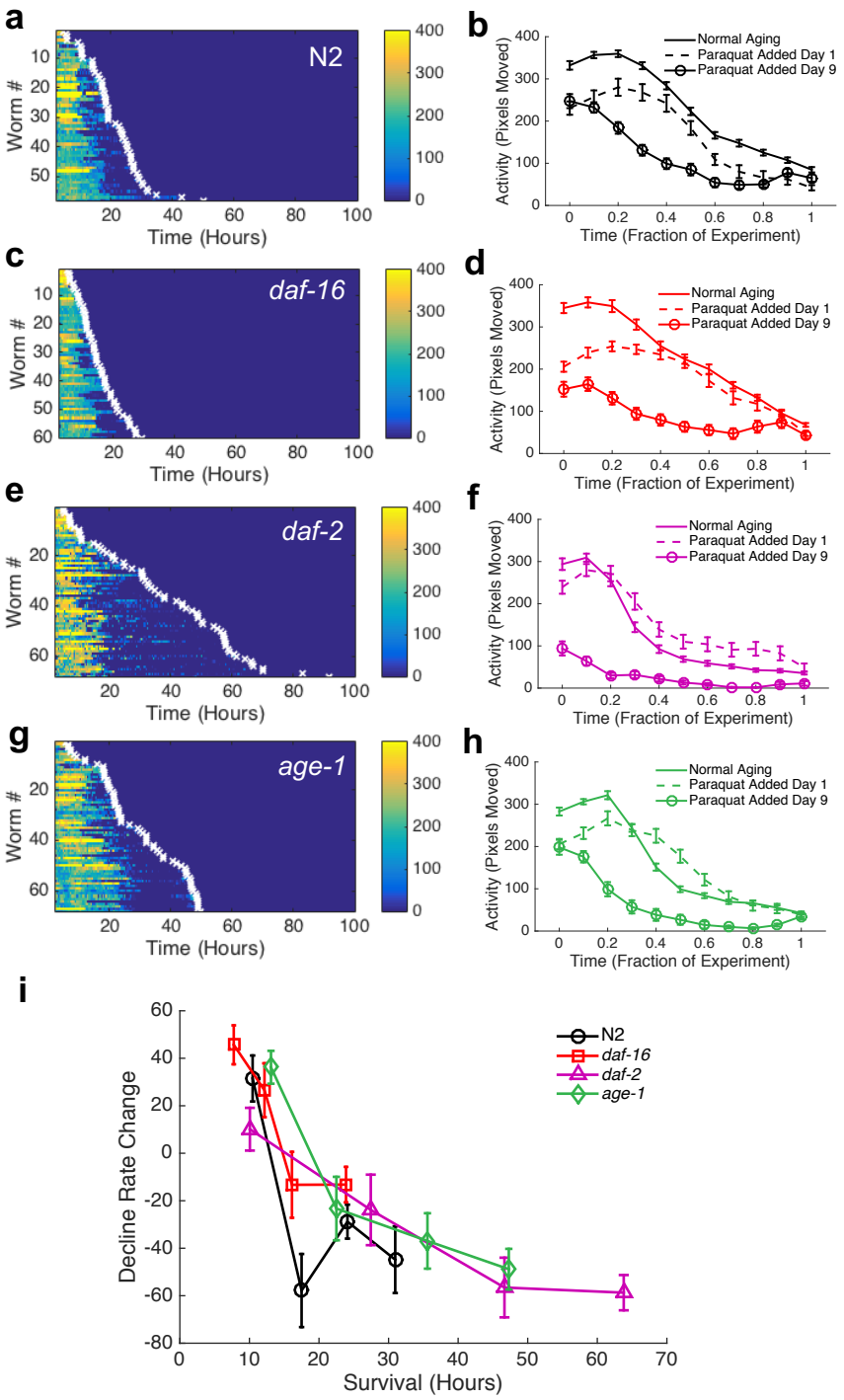

Figure 2.7 Behavioral decline during acute oxidative stress resembles behavioral decline during aging (a, c, e, g) Behavior and survival heat maps for N2 (n=58), *daf-16* (n=60), *daf-2* (n=68), and *age-1* (n=68). (b, d, f, h) Comparison of behavioral decline during normal aging (solid curve), stress with Paraquat added on day 1 of adulthood (dashed curve), and stress with Paraquat added on day 9 of adulthood (solid curve with circles) i) Change in decline rate (pixels/life fraction) for individuals versus survival on paraquat

If it is true that behavioral decline during stress beginning at day 1 of adulthood resembles a temporally scaled recapitulation of behavioral decline during normal aging, we reasoned that starting oxidative stress at mid-life should truncate the initial portion of the behavioral decline curve, as the slow decline of early aging should have already occurred naturally. To test this idea, we grew animals on the WorMotel as we did for normal aging experiments. We then added paraquat on day 9 of adulthood, and monitored worms' subsequent behavior and survival. We observed that the initial decline occurred almost immediately, indicating that, as expected, the initial portion of the aging curve was no longer present in the behavioral stress decline curve (Figure 2.7b, d, f, h). These results suggest that population-level rate of behavioral decline indeed temporally scales with increased stress.

Previously, we observed that during normal aging, the change in decline rate, a measure of the shape of functional decline, negatively correlated with lifespan. Since population behavioral decline seemed to scale between normal aging and stress, we therefore investigated the relationship between individual aging and survival during stress. We once again found a negative correlation between the change in decline rate and survival for animals grown on 40 mM paraquat (Figure 2.7i).

These results show that the shape of behavioral decline during severe oxidative stress was similar to that during and aging, despite the process of aging on oxidative stress occurring about 20 times faster. This result suggests that there exist strong parallels in the worm's behavioral responses to oxidative stress and to aging.

ODR-10 is required for elevated response threshold but not increased lifespan of daf-2 mutants

We observed that long-lived *daf-2* mutants exhibited greatly reduced locomotion amplitude and movement duration and elevated response latency to aversive blue light (Figure 2.3g-j). Previous studies have observed similar phenotypes, such as the high degree of dauer-like quiescence in *daf-2* adults (Gems et al. 1998; Gaglia and Kenyon 2009). In addition to having increased longevity, *daf-2* mutants have been shown to possess greater fat stores (Ogg et al. 1997). Reduction of insulin signaling, higher fat stores, and reduced movement are all features of hibernation in mammals, and it has been proposed that the *daf-2* mutation confers a constitutive 'hibernation-like' phenotype on these animals (Carey, Andrews, and Martin 2003; Gaglia and Kenyon 2009). Since animals deprived of fat stores or forced to move during hibernation have reduced survival (Reeder et al. 2012), we hypothesized that reduced locomotor behavior might be required for increased lifespan in *daf-2* animals.

A recent study identified ODR-10, a G-protein coupled olfactory receptor sensitive to diacetyl, as required for reduced locomotion in *daf-2* mutants (Hahm et al. 2015). ODR-10 mRNA levels are elevated in *daf-2* mutants, and *daf-2* mutants on *odr-10* RNAi show a greater maximum velocity than controls. In an effort to determine if reduced

locomotion was required for increased lifespan, we tested *daf-2* mutants with *odr-10* RNAi with the WorMotel.

We grew N2, *daf-2(e1370)*, and *odr-10(ky32)* mutants on Empty Vector (EV), *daf-2*, or *odr-10* RNAi on the WorMotel to monitor behavior and lifespan. To our surprise, we found no significant difference in spontaneous activity between either N2 or *daf-2* worms grown on EV versus *odr-10* RNAi (Figure 2.8a). These results suggest that ODR-10 does not in fact influence the reduced spontaneous movement observed in *daf-2* mutants.

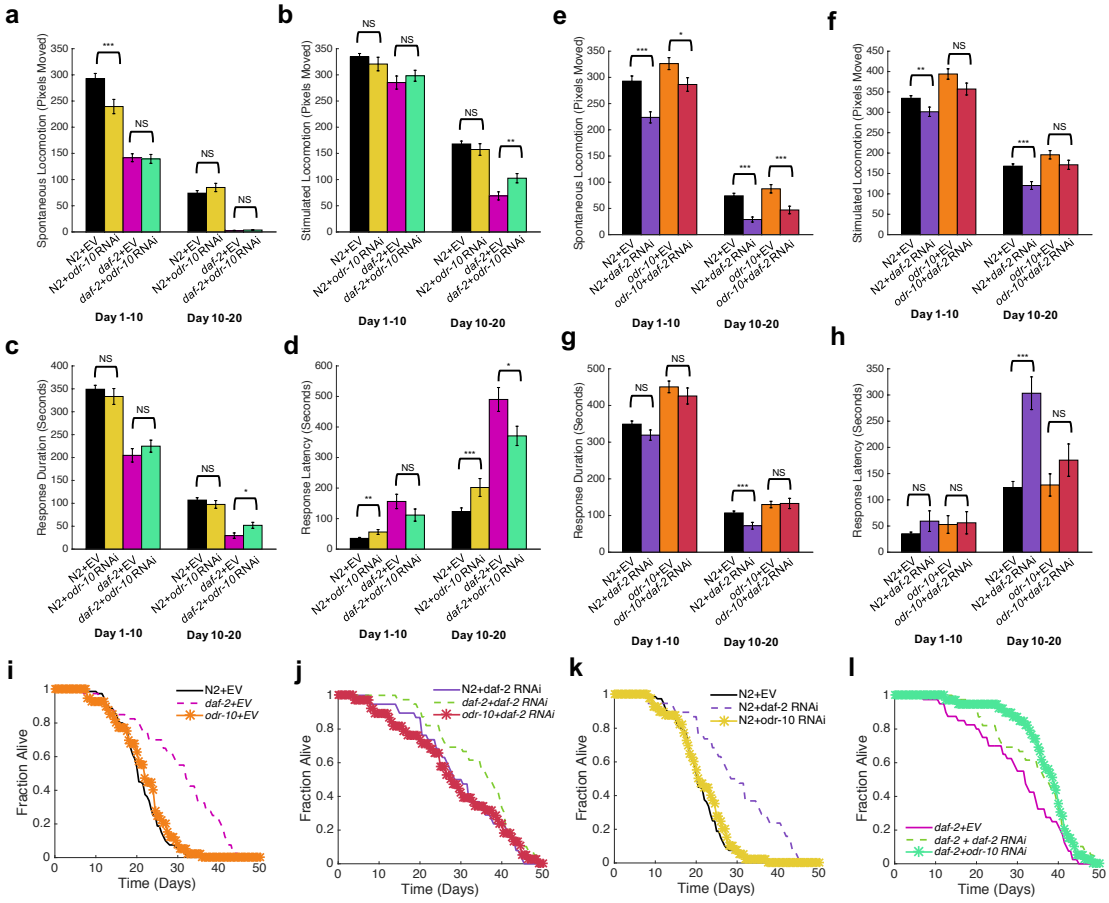

Figure 2.8 Reduced sensory response is not required for extended longevity in *daf-2* mutants (a) Spontaneous activity during days 1-10 and 10-20 of adulthood for N2 grown on Empty Vector RNAi (n=80), N2 grown on *odr-10* RNAi (n=40), *daf-2* grown on Empty Vector RNAi (n=40), and *daf-2* grown on *odr-10* RNAi (n=39). *, p<0.05; **, p<0.01; ***, p<0.001 (b) Stimulated activity for the same individuals shown in panel (a). (c) Response duration for the same individuals shown in panel (a) (d) Response latency for the same individuals shown in panel (a). (e) Spontaneous activity during days 1-10 and 10-20 of adulthood for N2 grown on Empty Vector RNAi (n=80), N2 grown on *daf-2* RNAi (n=38), *odr-10(ky32)* mutants grown on Empty Vector RNAi (n=40), and *odr-10(ky32)* mutants grown on *daf-2* RNAi (n=38). *, p<0.05; **, p<0.01; ***, p<0.001 (f) Stimulated activity for the same individuals shown in panel (e). (g) Response duration for the same individuals shown in panel (e). (h) Response latency for the same individuals shown in panel (e). (i-l) Survival curves

We examined stimulated activity in the same experiments. While we found no difference in early life stimulated activity between N2 or *daf-2* mutants grown on EV versus *odr-10* RNAi, we did find that late life stimulated activity was elevated in *daf-2* mutants grown on *odr-10* RNAi, whereas late life stimulated activity was unchanged for N2 grown on *odr-10* RNAi (Figure 2.8a, b). Furthermore, while N2 treated with *daf-2* RNAi exhibited significantly decreased stimulated activity compared to animals grown on EV RNAi, *odr-10* mutants grown on *daf-2* RNAi did not (Figure 2.8f). Similar results were observed for response duration and latency (Figure 2.8c, d, g, h). These results suggest that ODR-10 does not directly affect locomotion in *daf-2* mutants, but reduces sensitivity of *daf-2* mutants to stimuli.

Loss of function mutations in a number of genes required for sensory responses, such as such as the cyclic nucleotide channel TAX-4 and the intraflagellar transport particle homologue OSM-6, have been shown to exhibit extended longevity (Apfeld and Kenyon, 1999). Because *daf-2* mutants exhibit both reduced locomotion in addition to prolonged lifespan, it is possible that the reduced sensory responsiveness of *daf-2* mutants is a requirement for their extended longevity.

To test this idea, we compared survival curves for worms in which either *daf-2, odr-10*, or both either had loss of function mutations or were knocked down by RNAi. We found that *odr-10* mutation and *odr-10* RNAi had no effect on wild type lifespan (Figure 2.8i, k), whereas *daf-2* RNAi increased lifespan in both wild type and *odr-10* mutants to an

equal degree (Figure 2.8j, l). These results show that while ODR-10 is required for reduced sensory responses in *daf-2* mutants, it is not required for extended lifespan.

DISCUSSION

A powerful and flexible tool for assaying C. elegans *behavior*

We have used our WorMotel method to investigate inter-individual and inter-strain variability in behavioral decline and the relationship between behavior and lifespan. Large-scale automated analysis of lifespan and behavior will facilitate screening for genetic and chemical modulators of aging. This system's ability to longitudinally monitor animals throughput their lifespans may also help identify mechanisms of variability of aging between individuals in a population.

In addition to these applications in aging, we have used the WorMotel in studies of other behaviors, such as developmentally-timed quiescence (lethargus) (M D Nelson et al. 2013), stress-induced quiescence (Iannacone et al. 2017; Matthew D. Nelson et al. 2014), and adult behavior states (McCloskey et al. 2017). Therefore the WorMotel is a flexible tool for assaying *C. elegans* long-term behavior.

Functional decline follows a universal dependence on lifespan in diverse strains

We found that short-lived wild type individuals declined in a manner similar to the short-lived strain *daf-16* and that long-lived wild type individuals declined in a manner similar

to the long-lived strain *daf-2*. Furthermore, we found that the shape of decline followed a single curve with respect to lifespan (Figure 2.6e).

These results suggest that the sources of variability in lifespan in individuals also impact functional decline in a corresponding manner. For example, the N2 worm that survives 15 days due to stochastic factors will decline in a similar manner to the *daf-16* worm that survives 15 days. Furthemore, individuals with a 30-day lifespan will exhibit a different shape of functional decline, but this shape is dictated by the confluence of genetic and stochastic factors that result in the lifespan of 30 days.

One explanation for the extended longevity of insulin signaling mutants such as *daf-2* and *age-1* is via their shared transcriptional profile with dauer larvae, which can persist in harsh environments by virtue of an upregulation in stress-response and detoxification pathways (McElwee et al. 2004). Furthermore, other work has shown that at an advanced age, wild type transcriptional profiles also exhibit similarities with that of dauer larvae (Lund et al. 2002). Our finding that behavioral decline adheres to a continuum suggests that long-lived wild type worms may be physiologically and transcriptionally similar to worms with mutations in the insulin signaling pathway. Future experiments comparing gene expression in rapidly or slowly aging worms may elucidate how aging variability is manifest at the molecular level.

Extension of late-life decrepitude in long-lived worms

In addition to this and other studies (W. B. Zhang et al. 2016), a recent study (Podshivalova et al. 2017) also observed an extension of late-life behavioral quiescence in N2 and *daf-2* mutants. The authors found that intestinal bacterial colonization is a risk factor for death in *C. elegans* and that *daf-2* mutants, who exhibit a greater fraction of late-life decrepitude compared to N2, were less susceptible to this bacterial colonization. When the authors fed worms killed bacteria, they found a greater lifespan extension in N2 (40%) than *daf-2(e1368)* (16%), suggesting that bacterial colonization is a cause of premature death in N2 worms. Finally, the authors found that feeding worms dead bacteria specifically extended the period of infirmity rather than that of good health, suggesting that bacterial colonization may be a primary cause of lifespan truncation in short-lived individuals. That is, bacterial colonization may cause a reduction in late-life decrepitude in short-lived worms by causing premature death.

If bacterial colonization is a fundamental cause of the smaller fraction of late-life decrepitude observed in short-lived worms, the question remains as to why long-lived worms exhibit extended behavioral quiescence in old age. One possibility is that muscle integrity degrades with age faster than other tissues (Herndon and Driscoll 2002) such that older worms are physically able to move less well than reflected by their probability of dying. Another possibility might be related to the reduction in feeding worms exhibit with age (Huang, Xiong, and Kornfeld 2004). Feeding and locomotion are linked (McCloskey et al. 2017), so it might be that worms that have ceased feeding also tend to cease spontaneous locomotion.

Scaling of behavioral decline during acute stress

It has been hypothesized that normal aging constitutes a low-level stress that results in the slow accumulation of damage leading to senescent decline. While the accelerated aging observed during oxidative stress in our experiments is far greater than what occurs during normal physiological processes, our result that the shape of functional decline is similar during normal aging and acute oxidative stress suggests a potential underlying similarity between these two conditions. Furthermore, we show that the relationship between individual decline and survival is conserved between oxidative stress and normal aging, indicating that the processes governing the unique shape of decline for short-lived and long-lived individuals are preserved. Our results indicate that the process of functional decline can be sped up by at least a factor of twenty while still maintaining a similar average shape. Together, our results suggest that normal aging and acute oxidative stress similarly impact the process of functional decline. Future work will aim to define mechanisms for this similarity.

If functional decline were dictated only by lifespan, we expect to observe a single curve relating the shape of decline to lifespan, regardless of environmental conditions. That is, interventions that drastically shorten lifespan, such as the addition of paraquat, should all exhibit an increase in decline rate between early and late life to be continuous with the curve presented in Figure 2.6e. Instead, however, we observe a translation of the tradeoff we observe during normal aging between the shape of functional decline and lifespan.

This indicates that the shape of decline is not dictated by lifespan *per se*, but instead by the distance of an individual's lifespan relative to some standard in a given set of environmental conditions. For example, during normal aging, a lifespan of about 12 days results in neutral decline, or no change in decline rate between early and late life (Figure 2.6a, d, e), whereas during oxidative stress, a lifespan of about 12 hours results in neutral decline (Figure 2.7i). Together, these results suggest that relative to a standard lifespan in a given environment, there exists a defined shape of aging in the individuals whose lifespans differ from that standard as a result of genetic and/or stochastic factors.

ODR-10 is required for elevated response threshold but not increased lifespan of daf-2 *mutants*

We found that ODR-10 did not affect baseline locomotion of *daf-2* mutants, but did reduce the locomotory response of *daf-2* worms to an aversive stimulus. Furthmore, ODR-10 knockdown did not reduce *daf-2* lifespan, suggesting that elevated sensory response threshold is not required for increased lifespan of *daf-2* animals.

We found that ODR-10 suppressed locomotion in *daf-2* mutants only in response to stimulation, whereas Hahm et al (Hahm et al. 2015) found that ODR-10 suppressed locomotion per se in *daf-2* mutants, One simple explanation for this discrepancy is that in Hahm *et al,* locomotion assays were conducted soon after worms were manually stimulated due to picking onto the assay plate. The WorMotel allowed us to monitor worm behavior in a long-term unstimulated state in addition to after blue light

stimulation. Future experiments may shed further light on whether reduced movement is required for the extended longevity of *daf-2*. The WorMotel will be useful in quantifying behaviors that unfold over long periods of time and further exploring the relationships between behavior and lifespan.

Additional axes of variation govern the aging process

It has been reported that survival curves scale by a multiplicative constant across a diverse set of genetic and environmental perturbations (Stroustrup et al. 2016). This result was interpereted as being compatible with the sum of biological inputs being filtered through a single state variable that determines the rate of aging. Our results indicate that a single variable is unlikely to be able to account for the inter-individual variability observed in aging. We observe variability in the shape of aging between individuals (Figure 2.5a-f, 2.6a-c), indicating that the shape of aging does not scale for individuals with different lifespans. At the same time, we do observe a scaling of the relationship between the shape of aging and lifespan when the mean population rate of aging is accelerated with oxidative stress. Furthermore, we observe a difference in variability in aging decline across genotypes with differences in lifespan (Figure 2.6g). Therefore, our results indicate the likely existence of at least one additional variable across which the process of aging may vary between individuals within and across populations. Future work may uncover the full space across which the aging process may vary and mechanisms underlying variability in aging.

METHODS

Strains

The following strains were used in this study: N2, CF1038: *daf-16(mu86) I*, CB1370: *daf-2(e1370) III*, TJ1052: *age-1(hx546) II*, PR678: *tax-4(p678) III*, DA509: *unc-31(e928) IV*, KG1180: *lite-1(ce314) X*, RB754: *aak-2(ok524) X*, CX32: *odr-10(ky32) X*. All strains were maintained at 15°C under standard conditions (Stiernagle 2006). All experiments were carried out at 20°C unless otherwise stated.

WorMotel design and fabrication

To fabricate the WorMotel, we developed a 3D-printing based molding method (Shepherd et al. 2011). We designed a chip containing a rectangular array of either 48 or 240 rounded wells with 3 mm diameter, 3 mm depth, and center-to-center spacing of 4.5 mm (Figure 2.1). Each well was surrounded by a 0.5 mm wide and 3 mm deep channel, which would serve as the moat. Designs of the WorMotel masters were created using MATLAB. We printed a master corresponding to the negative of this shape with an Objet30 photopolymer 3D printer using the material VeroBlack. To mold the WM devices, we mixed Dow Corning Sylgard 184 PDMS according to the manufacturer's instructions and poured 35 g or 5 g of PDMS into the 240-well or 48-well masters, respectively. We then degassed the poured PDMS in a vacuum chamber for 1 hour or until no more bubbles were visible. Devices were cured overnight at 40°C and then removed from molds using a spatula.

WorMotel preparation

To prepare devices for experiments, the chips were first treated with oxygen plasma for 4 minutes using a plasma cleaner (PE-50, Plasma Etch Inc. or Plasmatic Systems Plasma Preen II). This treatment renders PDMS temporarily hydrophilic, which greatly facilitates the filling of wells and moats. The medium was based on standard NGM media (Stiernagle 2006) except low-gelling temperature agarose (gelling temp. 26-30°C, Research Products International) was substituted for agar to minimize solidification of the agar during filling of the wells, and streptomycin (200 ng/mL) was added to the medium to minimize bacterial contamination.

For lifespan experiments, but not for development experiments, we added 5-fluoro-2'-deoxyuridine (FUdR) to prevent growth of progeny. A frozen FUdR stock solution of 10 mg/ml in water was thawed and added to molten agar at 40°C at a concentration of 5 µL per mL just prior to filling. This yielded a final FUdR concentration of 200 µM. The moat solution consisted of 100 mM copper sulfate, which was approximately in osmotic equilibrium with the agar medium via the humidified air inside the chamber. The moat solution was added using a P200 pipette. About 15 μl of molten NGM agarose was added to each well. About 5 μl of a suspension of the *Escherichiae coli* bacterial strain DA837 (Wayne Davis et al. 1995), which is a streptomycin resistant derivative of OP50 (S Brenner 1974) was added to each well after agarose solidification. For aging

experiments, late L4 worms were added to the WorMotel manually with a platinum wire pick.

PDMS devices were placed inside either a 90 mm petri plate for 48-well WorMotels or an OmniTray (Nunc Thermo Scientific) for 240-well WorMotels. 240-well WorMotels contained alignment tabs to keep devices in alignment with respect to the OmniTray. To maintain humidity inside the dishes, we used water-absorbing polyacrylamide crystals (M2 Polymer). Sterile water was added to the crystals in a ratio of 150:1 (water:crystals) by weight. Approximately 15 g of hydrated crystals were added around the WorMotel. We placed lids on all dishes. To prevent accumulation of water condensation, lids were prepared by coating with a 30% solution of Tween 20 (Sigma-Aldrich) in water, which was allowed to dry before use. We wrapped Parafilm around the sides of the plate to reduce water loss while allowing sufficient gas exchange.

Image acquisition

Images were captured with an Imaging Source DMK 23GP031 camera (2592 x 1944 pixels) equipped with a Fujinon lens (HF12.5SA-1, 1:1.4/12.5 mm). We used Phenocapture imaging software (http://phenocapture.com/) to acquire time lapse images through a gigabit Ethernet connection. We used the time schedule option in Phenocapture to record images every 5 seconds for a 30-minute period twice daily. All experiments were carried out under dark-field illumination using four 4.7" red LED strips (Oznium) positioned approximately 2" below the WorMotel. Images were saved and

processed by a 64-bit computer with a 3.40 GHz Intel Core i3 processor and 4 GB of RAM. Images were analyzed using custom-written MATLAB software.

Different spatial resolutions can be attained by adjusting the camera's field of view and thus by modulating the number of wells viewed at once. Imaging 6 wells at once yields approximately 5 μm resolution, imaging 12 wells yields 7 μm resolution, imaging 48 wells yields 15 μm resolution, and imaging 240 wells yields 36 μm resolution.

Image processing

Temporally adjacent images were subtracted and divided by the average pixel intensity between the two images to generate normalized maps of pixel value intensity change. Depending on the task, time intervals of either 5 or 60 seconds were used to generate difference images. We refer to such difference images as 5-second or 60-second activity, respectively (see Aging Behavior Quantification). A Gaussian smoothing filter with standard deviation of one pixel was applied to the resulting difference image in order to reduce image noise. A binary threshold of 0.25 was used to minimize image noise was then applied to the filtered intensity change image in order to score whether or not movement occurred at each pixel location. All pixels in which movement occurred were summed up and the resulting value was called the 'activity' between the two frames.

Blue light stimulation, uniform illumination, and temperature monitoring

To supply the blue light illumination, we use two high power LEDs (Luminus PT-121) secured to an aluminum heat sink and connected in series. We used a relay (Schneider Electric) controlled by MATLAB through a LabJack or NIDaq interface to drive the LEDs at a current of 20 A through a power supply. To maximize the blue light irradiance and uniformity at the WorMotel, we constructed a box consisting of four acrylic mirrors with mirrored sides facing inwards and placed it around the WorMotel. We measured irradiance using a silicon power meter (Coherent). During aging experiments, blue light stimulation was applied once every twelve hours for 10 s. Temperature was continuously monitored with a temperature probe (LabJack EI1034) placed beside the sealed WorMotel.

A previous report (Edwards et al. 2008) found that continuous blue illumination at an irradiance of 2.8 mW/mm^2 kills N2 worms in 30 minutes. In our experiments, worms are subject to 20 seconds of blue light per day (10 seconds per stimulus, two stimuli per day). Therefore, it would take 90 days for worms to accrue 30 minutes of total illumination time with blue light. The irradiance of our blue light stimulus is approximately five times weaker than that used in this Edwards et al study. Assuming a linear response of blue light dosage toxicity, it would take 450 days for worms to accrue a toxic blue light dose in our experiments. Since the typical worm lifespan is between 15 and 30 days, we believe blue light toxicity in our experiments is not significant.

Copper sulfate experiments

To test whether filling moats with a copper sulfate solution had any effects on worm development or survival, we prepared two WorMotels: in the first, moats were filled with NGM Buffer (NGMB), and in the second, moats were filled with 100 mM copper sulfate. NGMB consists of the same constituents as NGM agar (Stiernagle 2006) but without peptone, cholesterol, or agar.

We manually added L3 larvae to each device and monitored the duration of the L4 stage as previously described (M D Nelson et al. 2013). When these worms reached the first day of adulthood, each animal was manually transferred to a new WorMotel, in which the agar contained FUdR, in order to assess the effect of moat solution on survival. Worms grown as larvae in the presence of a copper sulfate moat were transferred to a WorMotel whose moats were filled with copper sulfate; likewise for worms grown in the presence of an NGM moat. Lifespan was scored daily by manual methods (see below).

RNAi by feeding

We used RNAi clones for EV, *daf-2*, and *odr-10* supplied by the Ahringer RNAi Libray (Open Biosciences). Bacteria was *E. coli* strain HT115. We induced RNAi in liquid culture for two hours using 1 uM IPTG. We added 2 uM IPTG and 25 ug/mL carbenicillin to molten WorMotel agar. Liquid bacteria was added on top of solidified agar. Worms were manually added to each well with a platinum worm pick.

Lifespan determination

For manual assays, immobile worms were prodded three times with a worm pick. Those that failed to respond were scored as dead. For automated assays, the maximum activity value recorded during the fifteen minutes after each light stimulus was used to determine time of death. Time of death was defined as the time point after the last time point for which the maximum 60-second activity was nonzero.

Any worm whose activity was uniformly zero beginning on day 2 of adulthood was assumed to have left its well or was not added due to experimental error, and these wells were censored from further analysis. 15 out of 1230 worms (1.2%) were censored in this manner. *tax-4* mutants were found to escape their wells as young adults at a much higher rate than all other strains. Therefore, *tax-4* mutants found to be absent from their wells at the conclusion of each experiment were censored from analysis. 18 out of 90 worms were censored in this manner.

Aging behavior quantification

For each 30-minute imaging epoch, spontaneous and stimulated locomotion were calculated as the maximum 60-second activity before and after the blue light stimulus, respectively. Spontaneous and stimulated locomotion reflect the maximum movement of an individual before or after blue light stimulus, respectively. The response duration was

calculated as the total time during which the 5-second activity was greater than zero after the light stimulus. Response duration reflects the total time spent moving after the stimulus. The response latency was calculated as the time elapsed between the blue light stimulus and the first non-zero 5-second activity. The response latency reflects the time required for an individual to respond to an aversive blue light stimulus. Animals that did not move at all during the 15 minutes following blue light stimulation were assigned a response latency of 900 seconds.

Decline rate calculation

We first considered the stimulated activity of each individual as a fraction of life rather than chronological time. We defined early life as 20-60% of an individual's life. We defined late life as 60-100% of an individual's life. Decline rate was calculated to be the negative of the slope of the stimulated activity during either early or late life. Slope was determined with a linear fit in Matlab. For each individual, the change in decline rate was calculated as the late life decline rate minus the early life decline rate.

Paraquat treatment, imaging protocol, and data processing

300 mM paraquat stock solutions were prepared fresh each day. L4 animals were added to a WorMotel as normal. On either day 1 or day 9 of adulthood, 2 uL of paraquat stock solution were added to each well and allowed to dry. The final concentration of paraquat per well was about 40 mM, assuming uniform distribution into the agar. After addition

of paraquat to each well, excess liquid was allowed to dry (about two hours), and plates were imaged continuously at 0.2 frames per second. Blue light stimulation occurred once per hour for 10 s. Stimulated activity for each animal was determined as the maximum activity between each light stimulus. Lifespan was determined automatically as described above.

Comparison of behavioral decline during aging and stress

For a given population we calculated stimulated activity as a fraction of life during aging and stress. We then corrected the activity during stress by calculating the average difference between the two quantities. By correcting for activity amplitude we could then ask whether the shape of decline was similar during aging and stress regardless of any offset. Finally, we calculated the normalized difference between aging and stress behavior at each fractional time point of life. The average normalized difference was reported as the percentage difference between behavior during aging and stress.

Day replicates

Day replicates were defined as WorMotels prepared independently on separate days. For lifespan experiments involving DA837 bacterial food (Figure 2.3, 2.5, 2.6), at least three day replicates were performed for each strain. For lifespan experiments involving RNAi by feeding (Figure 2.8), two day replicates were performed. For survival experiments in which Paraquat was added at day 1 of adulthood (Figure 2.7), four day replicates were

performed. For survival experiments in which Paraquat was added at day 9 of adulthood (Figure 2.7b, d, f, h), two day replicates were performed.

Experimental Design and Statistical Methods

Differences in lifespan and survival distributions (Table 2.1-2.2) were compared using a Wilcoxon rank sum test. Behavioral comparisons (Figure 2.6d, Figure 2.8a-h) were performed using a two-tailed t-test.

ACKNOWLEDGEMENTS

We thank Todd Lamitina and Vivek Sharma for helpful discussions and technical assistance. Some strains were provided by the CGC, which is funded by NIH Office of Research Infrastructure Programs (P40 OD010440). C.C.Y. was supported by a University Scholars Award. C.F.Y. was supported by the Alfred P. Sloan Foundation, Ellison Medical Foundation, European Commission, and the National Institutes of Health.

FIGURE SUPPLEMENTS

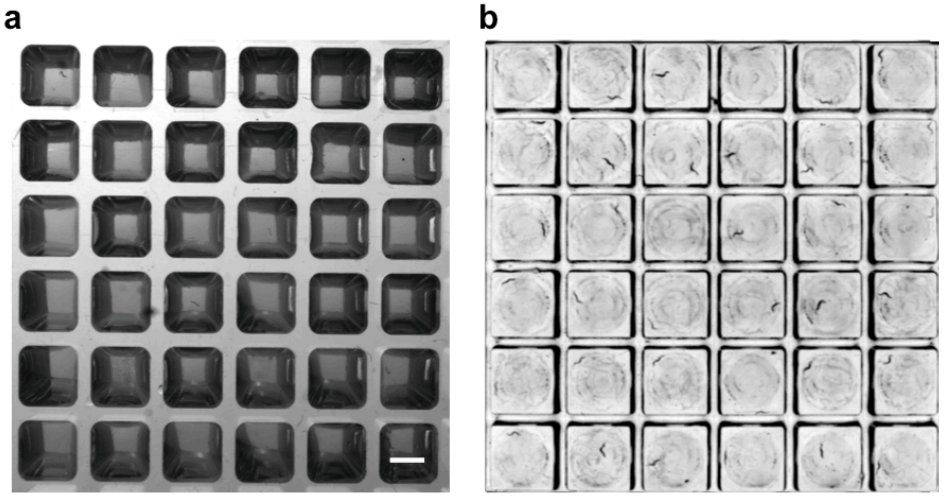

Figure 2.1 Supplement 1. Comparison of image quality with standard 384-well plate and WorMotel. (a) Image of L4 worms on agar in a standard 384-well plate. Scale bar: 2 mm. (b) Image of L4 worms on agar in a WorMotel. Individual animals are clearly visible in (b) but not in (a).

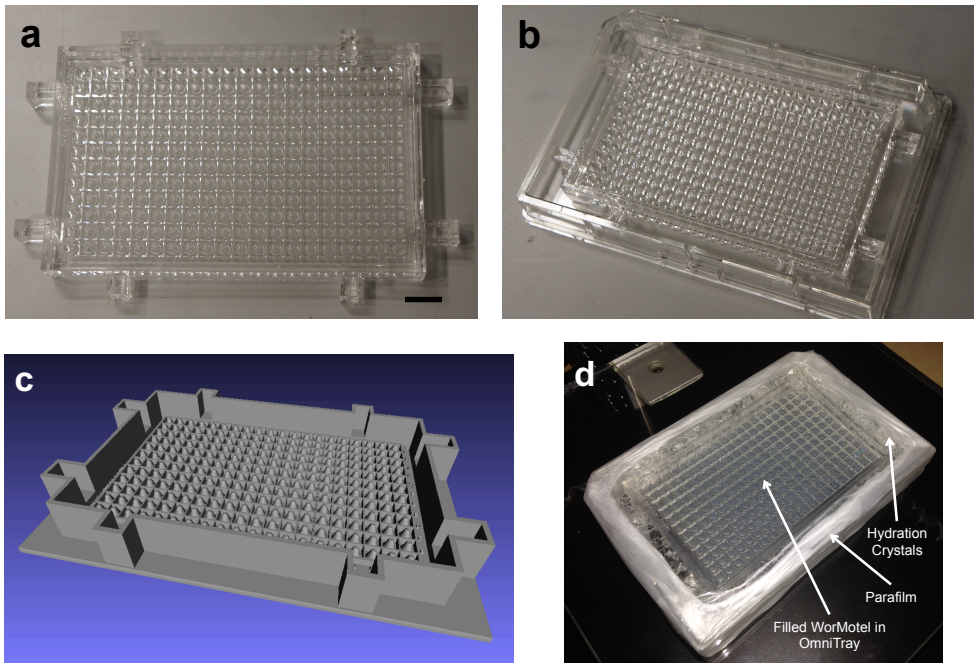

Figure 2.1 Supplement 2. 240-Well WorMotel (a) 240-well WorMotel PDMS insert. Scale Bar: 1 cm. (b) PDMS insert placed inside an OmniTray. (c) Computer rendering of the 240-well WorMotel negative master (d) Image of a WorMotel filled with agar, bacteria, and worms in an OmniTray

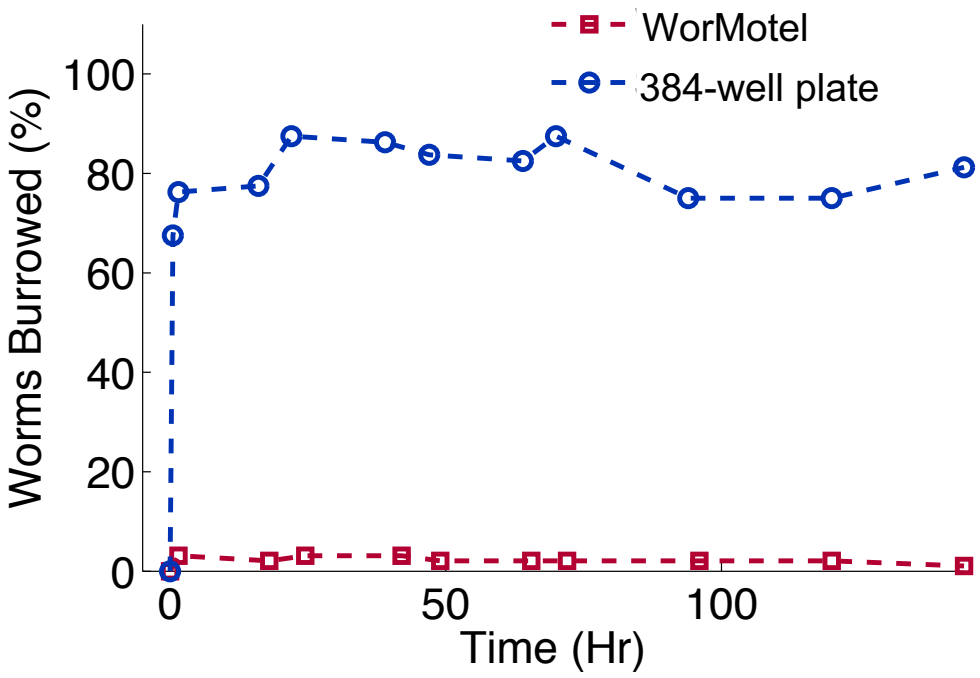

Figure 2.1 Supplement 3. WorMotel prevents burrowing. Percent of animals burrowing in the WorMotel (red squares, n=96) and in a standard 384-well microplate (blue circles, n=80).

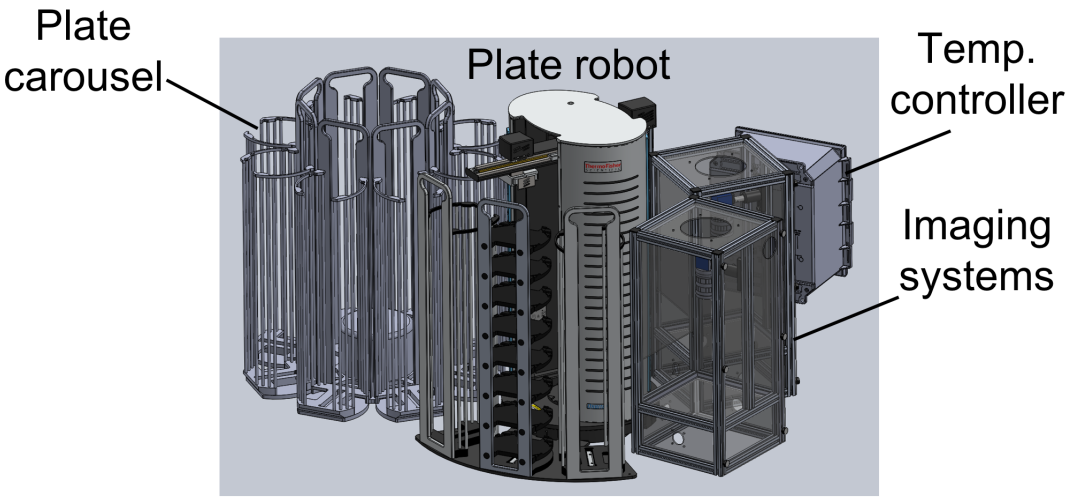

Figure 2.1 Supplement 4. Schematic of automated imaging system. An automated plate carousel (Thermo) containing 8 plate stacks holds up to 240 WorMotel plates, each containing 240 *C. elegans*. A plate handling robot (Thermo Orbitor) moves plates onto one of 3 imaging/illumination systems, where they are serially imaged. The system is contained in a light-tight enclosure and temperature is controlled to within 0.2 C by a temperature controller. All functions are controlled by custom LabView software.

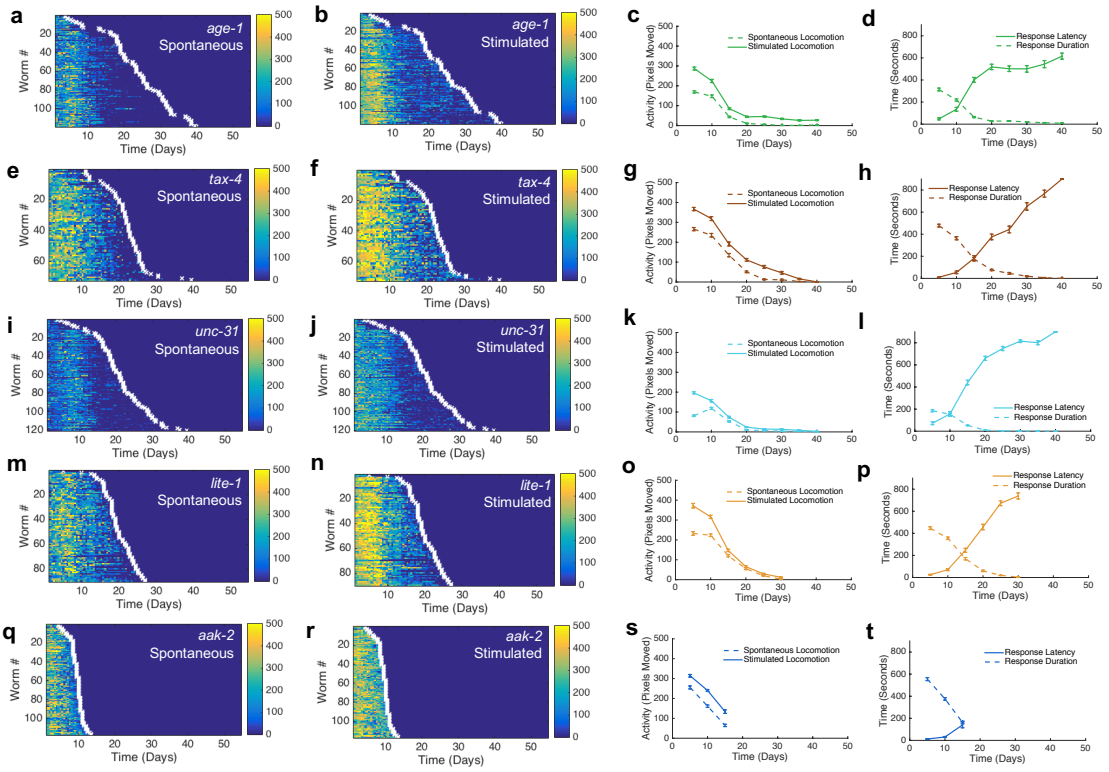

Figure 2.3 Supplement 1. Additional behavior heat maps (a) Spontaneous behavior heat map for *age-1* mutants (b) Stimulated behavior heat map for *age-1* mutants (c) Survivor spontaneous (dashed curve) and stimulated (solid curve) activity for *age-1* mutants (d) Survivor response duration (dashed curve) and latency (solid curve) for *age-1* mutants (e-h) Same data as panels a-d shown for *tax-4* mutants (i-l) Same data as panels a-d shown for *unc-31* mutants (m-p) Same data as panels a-d shown for *lite-1* mutants (q-t) Same data as panels a-d shown for *aak-2* mutants

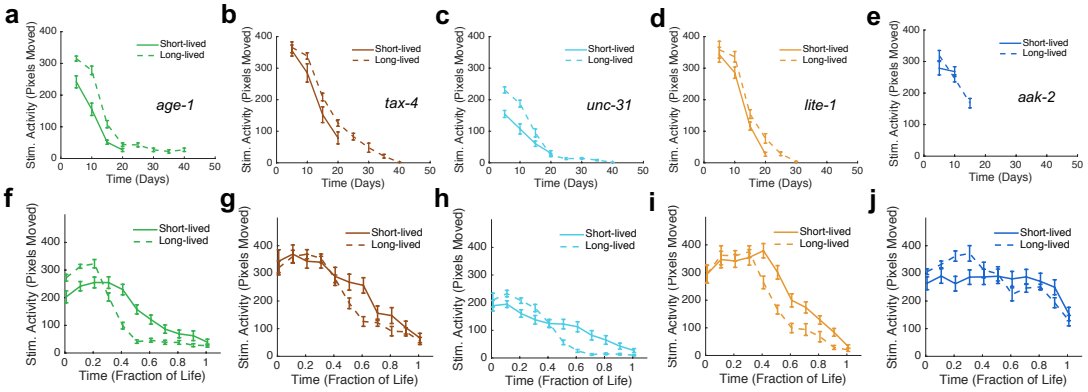

Figure 2.5 Supplement 1. Stimulated activity versus chronological time and fraction of life for long-lived individuals and short-lived individuals of the same strain (a) *age-1* mutant behavior as a function of chronological time for the lowest (solid curve) and highest (dashed curve) survivor quartiles (b) *tax-4* mutant behavior as a function of chronological time for the lowest (solid curve) and highest (dashed curve) survivor quartiles (c) *unc-31* mutant behavior as a function of chronological time for the lowest (solid curve) and highest (dashed curve) survivor quartiles (d) *lite-1* mutant behavior as a function of chronological time for the lowest (solid curve) and highest (dashed curve) survivor quartiles (e) *aak-2* mutant behavior as a function of chronological time for the lowest (solid curve) and highest (dashed curve) survivor quartiles (f-j) Same data as present in panels (a-e) presented as a function of life fraction.

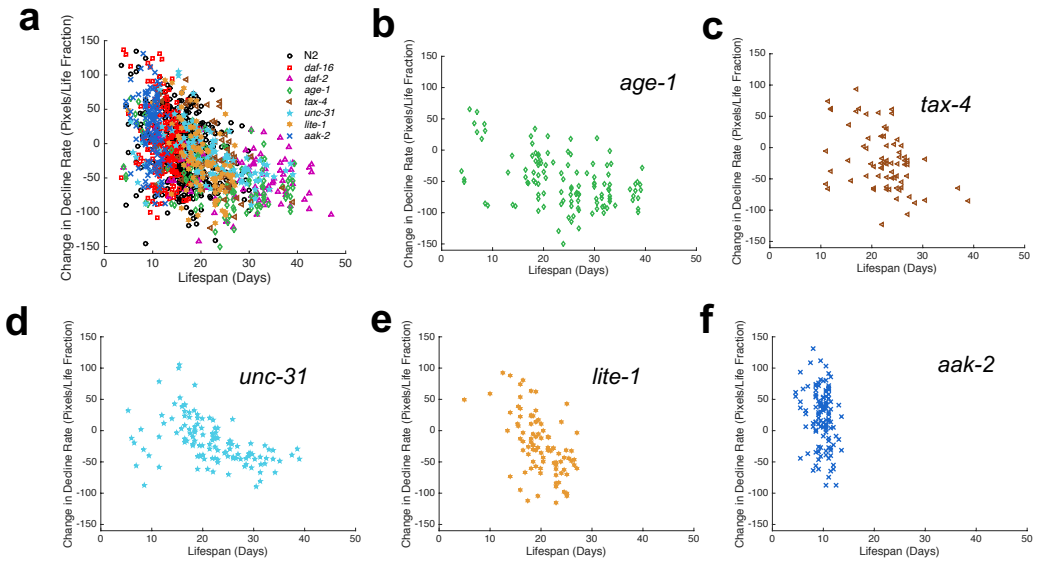

Figure 2.6 Supplement 1. Change in decline rate versus lifespan in individual animals (a) Change in decline rate versus lifespan for individuals of all strains tested (b) Change in decline rate versus lifespan for individual *age-1* mutants (c) Same data as in panel (b) presented for *tax-4* mutants (d) Same data as in panel (b) presented for *unc-31* mutants (e) Same data as in panel (b) presented for *lite-1* mutants (f) Same data as in panel (b) presented for *aak-2* mutants

VIDEOS

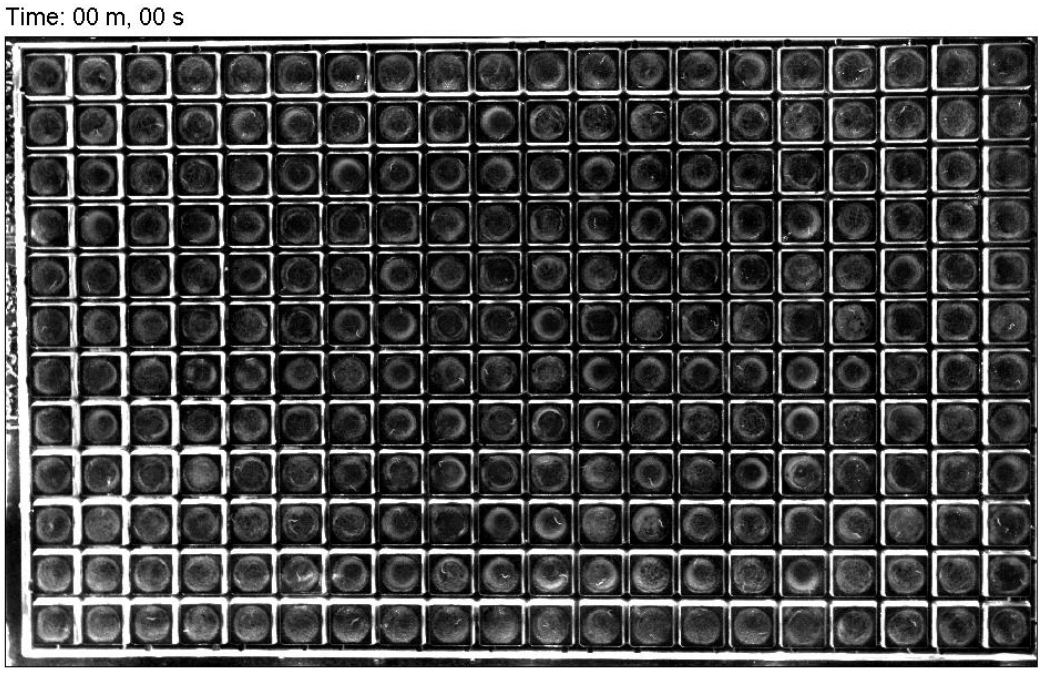

Video 2.1. Young (day 1) adults in the 240-well WorMotel. A 10 s long blue light exposure (bright flash) occurs at the 15 minute mark. FOV: 95 mm x 63 mm

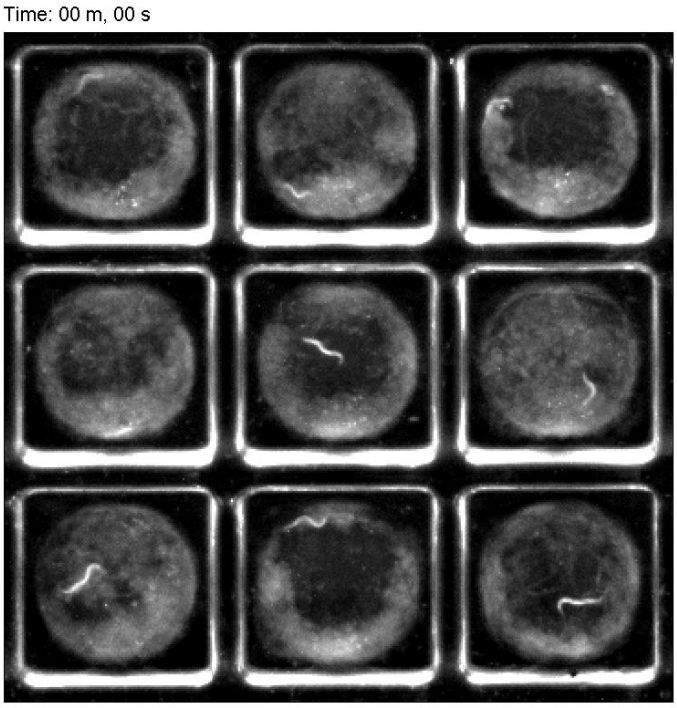

Video 2.2. Detail of 9 wells containing day 1 N2 adults. A 10 s long blue light exposure (bright flash) occurs at the 15 minute mark. FOV: 14 mm x 14 mm

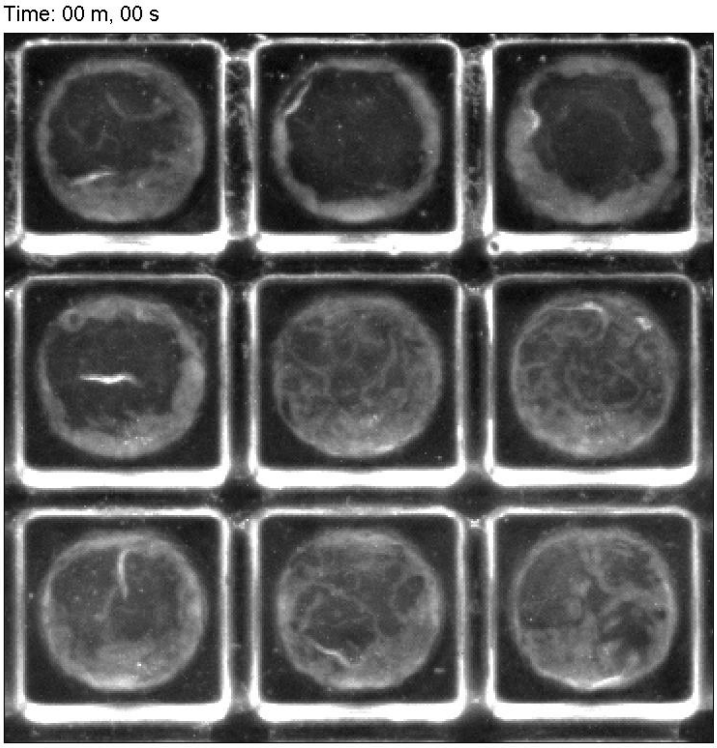

Video 2.3. Detail of 9 wells containing day 10 N2 adults. A 10 s long blue light exposure (bright flash) occurs at the 15 minute mark. FOV: 14 mm x 14 mm

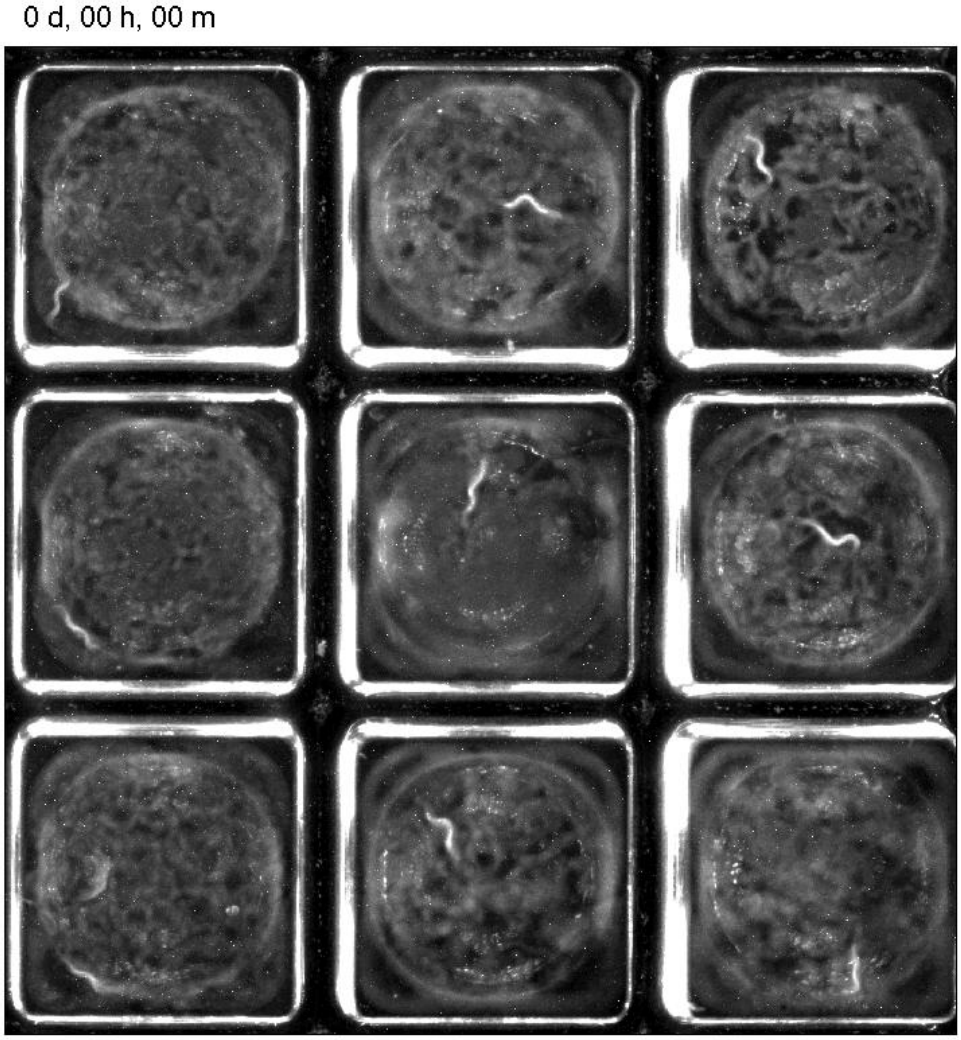

Video 2.4. High resolution video of 9 WorMotel wells containing adult animals (day 1-4). FOV: 14 mm x 14 mm

CHAPTER 3: Antagonistic serotonergic and octopaminergic neural circuits mediate food-dependent locomotory behavior in *Caenorhabditis elegans*

Matthew A. Churgin[1], Richard McCloskey[1], Emily Peters[1], and Christopher Fang-Yen[1,2]

[1]Department of Bioengineering, School of Engineering and Applied Sciences, University of Pennsylvania, Philadelphia PA 19104. [2]Department of Neuroscience, Perelman School of Medicine, University of Pennsylvania, Philadelphia PA 19104.

This chapter is a slightly modified version of a paper published in The Journal of Neuroscience (Churgin *et al.,* 2017a).

All data contained in this chapter was collected by me, except for 3 technical replicates contained in figure 7c-e, which were collected by Emily Peters. Richard McCloskey consulted on experimental procedures, data analysis, and interpretation of results. David Raizen injected *ser-5* worms with an endogenous promoter rescue construct generated by me. I performed all other *ser-5* and *ser-3* rescue injections. Christopher Fang-Yen helped with planning experiments, interpreting data, and drafting and revising the manuscript.

ABSTRACT

Biogenic amines are conserved signaling molecules that link food cues to behavior and metabolism in a wide variety of organisms. In the nematode *C. elegans*, the biogenic amines serotonin (5-HT) and octopamine regulate a number of food-related behaviors. Using a novel method for long-term quantitative behavioral imaging, we show that 5-HT and octopamine jointly influence locomotor activity and quiescence in feeding and fasting animals, and we define the neural circuits through which this modulation occurs. We show that 5-HT produced by the ADF neurons acts through the SER-5 receptor in muscles and neurons to suppress quiescent behavior and promote roaming in fasting worms, whereas 5-HT produced by the NSM neurons acts on the MOD-1 receptor in AIY neurons to promote low-amplitude locomotor behavior characteristic of well-fed animals. Octopamine, produced by the RIC neurons, acts through SER-3 and SER-6 receptors in SIA neurons to promote roaming behaviors characteristic of fasting animals. We find that 5-HT signaling is required for animals to assume food-appropriate behavior, whereas octopamine signaling is required for animals to assume fasting-appropriate behavior. The requirement for both neurotransmitters in both the feeding and fasting states enables increased behavioral adaptability. Our results define the molecular and neural pathways through which parallel biogenic amine signaling tunes behavior appropriately to nutrient conditions.

INTRODUCTION

The ability to alter behavior in response to nutritional cues is a crucial trait for organisms to adapt to changing environments. For example, many animals respond to scarcity of

food by adopting quiescent behaviors such as hibernation or diapause (Andrews 2007; Carey, Andrews, and Martin 2003; O. L. Nelson et al. 2014; van Breukelen and Martin 2015; Tu and McKnight 2006). Hibernation is a long-term behavior characterized by suppressed movement and metabolism that occurs in response to low food availability and decreased temperature (Carey, Andrews, and Martin 2003). How the nervous system initiates and sustains quiescent behavior during hibernation is poorly understood (van Breukelen and Martin 2015; Canguilhem et al. 1986; Carey, Andrews, and Martin 2003; Andrews 2007).

In many organisms, the linking of behavior and metabolism (Chase and Koelle 2007; Tecott 2007); (Roeder 2005; Roeder et al. 2003) to nutrition cues is performed in part through a widely conserved class of signaling molecules called biogenic amines. In mammals, biogenic amines regulate appetite, mood, weight, and other aspects of physiology (R. V. Lam 2006; D. Lam, Lam, and Heisler 2007)). Disorders such as anorexia, obesity, and depression, whose symptoms include altered food intake, are associated with dysregulation of the biogenic amine serotonin (5-HT) (Curran and Chalasani 2012). These disorders can be treated with drugs that increase the amount of 5-HT acting at the synapse, but how 5-HT levels relate to the complex behavioral and metabolic manifestations of these disorders is not fully understood. Thus, it is important to understand the mechanisms by which biogenic amines link environmental stimuli to behavior and metabolism.

The nematode *C. elegans* is a powerful model organism to dissect the neural circuits

linking food, behavior, and physiology owing to its compact nervous system, manipulable genetics, and a host of food-related behaviors (Piali Sengupta 2013; A. Hart 2006). Its nervous system signals in part through the biogenic amines 5-HT, dopamine, tyramine, and octopamine. Here we focus on the behavioral effects of 5-HT and octopamine in relation to food levels.

5-HT is involved in the modulation of multiple *C. elegans* behaviors in relation to food levels (Sawin and Horvitz 2000; Liang et al. 2006a; J Y Sze et al. 2000; Waggoner et al. 1998; Flavell et al. 2013a; Song et al. 2013; Ségalat, Elkes, and Kaplan 1995). During feeding, 5-HT is released and promotes locomotory slowing, thereby increasing the probability of the animal remaining on a food source (Sawin and Horvitz 2000). In addition, 5-HT increases pharyngeal pumping (feeding) and egg laying rates on food (Song et al. 2013; Waggoner et al. 1998). Mutants lacking tryptophan hydroxylase, the rate-limiting enzyme required for 5-HT synthesis, exhibit an increased propensity to developmentally arrest, indicating that lack of the positive food signal, 5-HT, discourages development into adulthood (J Y Sze et al. 2000).

While 5-HT is associated with food-related behaviors, multiple lines of evidence suggest that octopamine is associated with starvation-related behaviors. In *Drosophila melanogaster*, octopamine signaling is required for the hyperactivity observed in starved animals (Yang et al. 2015). Hyperactivity is thought to reflect the drive of starving animals to locate a food source. In *C. elegans*, octopamine inhibits egg-laying and feeding, and modulates response rate to aversive stimuli (Alkema et al. 2005; Mills et al.

2011; Wragg et al. 2007). However, octopamine's role in *C. elegans* locomotion has not been well studied, and how it acts to regulate food-dependent locomotion behavior is unknown.

Recently, our laboratory investigated the dynamics of behavioral states of worms in liquid. McCloskey *et al*. found that food, mechanical environment, insulin signals, protein kinase G signaling, and neuropeptides regulate the incidence of three behavioral states roaming, dwelling, and quiescence (McCloskey et al. 2017). While roles for acetylcholine, TGF-β, and insulin signaling have been reported in regulating these behavioral states, specific neural circuits have not been fully elucidated (Gallagher *et al*., 2013; You *et al*., 2008).

In this study, we use longitudinal imaging, pharmacology, and genetic techniques to show that the biogenic amines 5-HT and octopamine regulate behavior during feeding and fasting in *C. elegans*. We then identify the neuronal classes responsible for releasing these neurotransmitters and the receptors on which they act. We show that 5-HT and octopamine play antagonistic roles in regulating nutrient-related locomotory states.

MATERIALS AND METHODS

Strains

C. elegans were cultured as previously described (S Brenner 1974). All worms were cultured on standard agar plates with OP50 *E. coli* until just prior to experiments. N2

Bristol was used as the wild-type reference strain. The following strains were used in this study: MT15434: *tph-1(mg280) II*, DA1814: *ser-1(ok345) X*, CX12800: *ser-3(ad1774) I*, AQ866: *ser-4(ok512) III*, RB2277: *ser-5(ok3087) I*, *ser-5(tm2654) I*, *ser-5(tm2647) I*, KQ1048: *ser-6(tm2146) IV*, DA2100: *ser-7(tm1325) X*, MT9668: *mod-1(ok103) V*, MT9180: *mod-1(n3034) V*, MT9667: *mod-1(nr2043) V*, MT13113: *tdc-1(n3419) II* , MT9455: *tbh-1(n3247) X*, CX13079: *octr-1(ok371) X*, DA2289: *tph-1(mg280) II; kyEx947[pceh-2::tph-1(+)::gfp punc-122::gfp(+)],* DA2290: *tph-1(mg280) II; kyEx949[psrh-142::tph-1(+)::gfp punc-122::gfp(+)]*, SSR664: *mod-1(ok103) V; [Pmod-1::mod-1]*, SSR644: *mod-1(ok103) V; [Pttx-3::mod-1]*, SSR642: *mod-1(ok103) V; [Pgcy-36::mod-1]*, SSR665: *mod-1(ok103) V; [Pflp-1:mod-1]*, SSR662: *mod-1(ok103) V; [Pflp-8::mod-1]*, VN289: *ser-6(tm2104); tzIs3[cre::gfp, lin-15(+)]*, VN441: *ser-6(tm2104); tzIs3; vnEx142[ceh-17::ser-6, lin-44::gfp]*, YX179: *ser-5(ok3087) I; [Pser-5::ser-5, Pmyo-2::mCherry]*, YX180: *ser-5(ok3087) I; [Pmyo-3::ser-5, Pmyo-2::mCherry]*, YX181: *ser-3(ad1774) I; [Pceh-17::ser-3, Pmyo-2::mCherry]*, YX184: *ser-5(ok3087) I; [Psra-6::ser-5, Pmyo-2::mCherry]*, YX185: *ser-5(ok3087) I; [Punc-119::ser-5, Pmyo-2::mCherry].*

WorMotel Design and Fabrication

To fabricate the WorMotel, we developed a 3D-printing based molding method (Shepherd et al. 2011, Churgin et al., 2017b). We designed a chip containing a rectangular array of either 48 or 240 rounded wells with 3 mm diameter, 3 mm depth, and center-to-center spacing of 4.5 mm (Figure 3.1). Each well was surrounded by a 0.5 mm wide and 3 mm deep channel, which served as a moat. Designs of the WorMotel masters

were created using MATLAB. We printed a master corresponding to the negative of this shape with an Objet30 photopolymer 3D printer using the material VeroBlack. To mold the WM devices, we mixed Dow Corning Sylgard 184 PDMS according to the manufacturer's instructions and poured 35 g or 5 g of PDMS into the 240-well or 48-well masters, respectively. We then degassed the poured PDMS in a vacuum chamber for 1 hour. Devices were cured overnight at 40°C and then removed from molds using a spatula.

Liquid Behavioral Assays

9 μl of liquid NGM buffer (NGB), which consists of the same components as NGM but without agar or peptone (Stiernagle 2006; McCloskey et al. 2017),was added to each well of the WorMotel just prior to adding worms. Young adult animals were added manually to the liquid contained in each well of the WorMotel. Where indicated, the NGM was supplemented with either drugs or food. As a food source we used *E. coli* DA837 (Wayne Davis et al. 1995), a streptomycin resistant derivative of OP50 (S Brenner 1974). For experiments where food was added to wells, bacteria was added to NGM to a final OD of approximately 1.

For experiments with added exogenous biogenic amines, we added 5-HT hydrochloride, tyramine hydrochloride, or octopamine hydrochloride (Sigma Aldrich) in the indicated concentrations to liquid NGM prior to filling the WorMotel. Multiple genotypes or conditions were assessed on the same WorMotel. Behavioral comparisons were made only between conditions that were assayed simultaneously on the same WorMotel.

PDMS devices were placed inside a 90 mm diameter petri dish. To maintain humidity inside the dishes, we used water-absorbing polyacrylate crystals. Sterile water was added to the crystals in a ratio of 150:1 (water:crystals) by weight. Approximately 5 g of hydrated crystals were added around the WorMotel. We placed lids on all dishes. To prevent accumulation of water condensation, lids were prepared by coating with a 30% solution of Tween 20 (Sigma-Aldrich) in water, which was allowed to dry before use.

Finally, the filled WorMotel was placed upside down on the bottom of the petri plate and the lid was added. The petri plate was placed on a glass platform inside a custom imaging rig as previously described (Churgin and Fang-Yen 2015). A digital camera (see Image Acquisition) was placed beneath the glass platform and images were acquired every second until 60,000 images had been acquired, corresponding to about 16.6 hours of recording time (Churgin and Fang-Yen 2015).

Image Acquisition

Images were captured with an Imaging Source DMK 23GP031 camera (2592 x 1944 pixels) equipped with a Fujinon lens (HF12.5SA-1, focal length 12.5 mm). We used IC Capture imaging software (Imaging Source) to acquire time lapse images through a gigabit Ethernet connection. All experiments were carried out under dark-field illumination using four 4.7" red LED strips (Oznium) positioned on the glass platform surrounding the WorMotel. Images were saved and processed by a 64-bit computer with

a 3.40 GHz Intel Core i3 processor and 4 GB of RAM. Images were processed and analyzed using custom-written MATLAB software (see Image Processing).

The camera's field of view was adjusted such that 48 wells of the WorMotel were visible on the image. This field of view corresponded to a spatial resolution of approximately 15 μm.

Image Processing and data analysis

All data processing and anaylsis was carried out using MATLAB (Mathworks). Subsequent images were subtracted to generate difference images of pixel value intensity change. The difference image was normalized by average pixel intensity across the two subtracted images. A Gaussian smoothing filter with standard deviation equal to one pixel was applied to the delta image in order to reduce noise. A binary threshold of 0.35 was then applied to the filtered delta image in order to score whether or not movement occurred at each pixel location. All pixels in which movement occurred were summed up and the resulting value was called the 'activity' between the two frames.

To calculate the time spent quiescent, we first time-averaged raw activity data, with time resolution one second, with a smoothing kernel of five seconds. For each animal, we then calculated the number of frames where the activity was equal to zero. The resultant value was divided by the duration of the assay to calculate the fraction of time spent quiescent.

Histogram Fitting

We generated a histogram of the five-second time-averaged activity for each worm. We then used a non-linear least squares fitting algorithm to fit each individual worm's activity histogram to the sum of two exponential terms (with two unknown parameters each) and a Gaussian term (with three unknown parameters). We therefore fit seven parameters. The zero bin on the activity histogram, corresponding to quiescent frames, was excluded from the histogram before the fitting process as the contribution of quiescence had already been calculated.

To calculate the fraction of time spent roaming, we calculated the area under the Gaussian curve component of the fit. To calculate the fraction of time spent dwelling, we calculated the area under the two exponential curve components of the fit.

Manual Validation of Behavior

We picked at random three fasting and three feeding worms from a previously recorded experiment to manually score roaming and dwelling behavior. We examined videos recorded at 8 frames per second rather than one frame per second because we found it easier for a manual user to score behavior when data was recorded at a higher frame rate. Nevertheless, activity values were still calculated using frames captured one second apart as in all other experiments.

We examined behavior for approximately 10 minutes at each of three time points: 2 hours, 3 hours, and 4.5 hours from the start of the experiment. The purpose of using three time points was to ensure all three types of behavior were observed for each worm, not to assess temporal variations in behavior. Indeed, all three behaviors including roaming, dwelling, and quiescence were observed for each worm manually scored. A user blind to the results of the fit analysis scored behavior as roaming, dwelling, or quiescent for each worm for each frame.

Next, the activity histogram for frames the user scored as roaming and dwelling were individually generated and compared to the Gaussian or exponential components, respectively, of the full-data fit. To quantify the agreement between user-scored and computer-scored behavior, we calculated the R^2 value.

Visualizing Data in Roaming-Dwelling Space

After fitting, the roaming and dwelling fraction was calculated for each worm of a given genotype and experimental condition. For each population, the mean roaming and dwelling fraction were calculated, along with the standard deviation and orientation of principal components in roaming-dwelling space. Ellipses with dimensions corresponding to the standard error of the mean for each experimental condition were plotted with their orientation in the direction of greatest variation for that experimental condition as determined by principal component analysis.

Cloning and Transgenic Strain Construction

Rescue constructs for SER-5 were cloned using Gateway Technology (Life Technologies). The desired promoters, *ser-5* cDNA, and *unc-54 3'* UTR were acquired in entry slots 1, 2, and 3, respectively. The following plasmids in Gateway entry vectors were gifts of Zheng-Xing Wu: *sra-6p, ser-5p,* and *ser-5* cDNA (Guo et al. 2015). The LR recombination reaction was performed to produce each rescue construct. Each rescue plasmid was confirmed via sequencing. The rescue plasmid *ceh-17::ser-3* was a gift from Satoshi Suo (Yoshida et al. 2014). Transgenic strains were constructed by microinjection in the *C. elegans* germline. SER-5 rescue constructs were injected into RB2277: *ser-5(ok3087)* mutants. SER-3 rescue constructs were injected into CX12800: *ser-3(ad1774)*. For microinjections, 30 ng/µl of the desired plasmid was injected with 2 ng/µl of *myo-2::mCherry* coinjection marker and 100 ng/µl of 1 kb DNA ladder.

Statistical Methods

Differences in population behavior distributions were carried out using a two-tailed t-test. Error bars throughout the manuscript are presented as standard error of the mean, with N taken to be the number of biological replicates per condition.

RESULTS

Quantification of locomotion behavior in swimming C. elegans *with longitudinal imaging*

We first sought to better characterize *C. elegans* behavior in feeding and fasting

conditions. We monitored locomotion behavior of young adult worms using the WorMotel, a custom microplate device consisting of an array of individual wells that can be used to longitudinally image animals under solid or liquid media conditions (Churgin *et al*., 2017b). We assayed worms under liquid conditions and quantified locomotion behavior using custom machine vision software (see Methods).

We first monitored young adult N2 worms for 16 hours in liquid NGB (see Methods) grown with or without food (Figure 3.1). As previously reported, after a period of a few hours of continuous high activity, fasting worms in liquid began to cycle between high activity and behavioral quiescence (Figure 3.1) (Ghosh and Emmons 2008; McCloskey et al. 2017). The behavior of feeding and fasting worms was qualitatively very different. Fasting worms oscillated between extended high activity periods and short low activity periods, whereas feeding worms exhibited much more intermediate activity. We then plotted activity histograms for individual worms. From these histograms, we confirmed that fasting worms exhibit a more bimodal activity distribution, whereas feeding worms exhibit a mostly monotonically decreasing activity distribution.

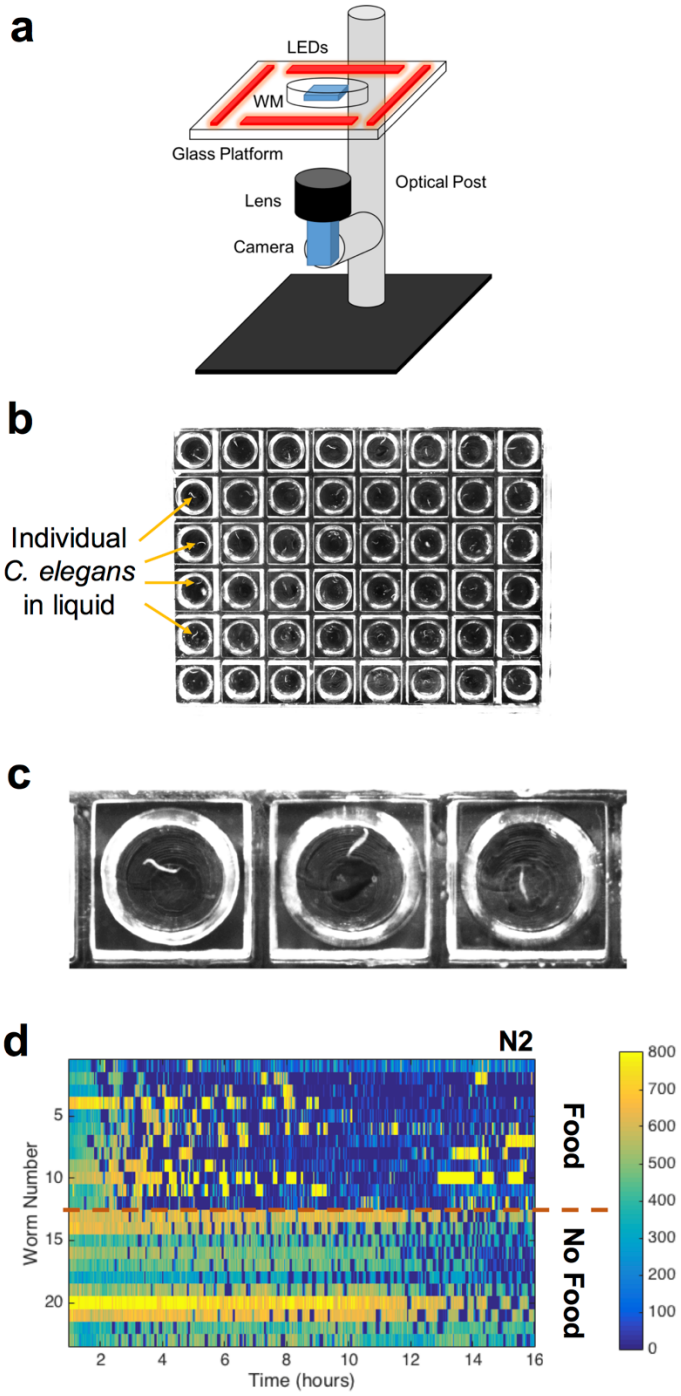

Figure 3.1 Experimental setup and data analysis

a) Experimental setup b) Example image. Individual *C. elegans* are visible in each well. c) Detail of three wells of panel b. d) Locomotion activity heat map for worms in liquid incubated with (top half) or without (bottom half) bacterial food.

To quantify behavior, we applied an empirical fit to the activity histogram on an individual worm basis (Figure 3.2a-b). We used a nonlinear least squares algorithm to fit each worm's activity histogram to a sum of two exponential terms and one Gaussian term (see Methods). Worm locomotion is usually classified into one of three behavior states: roaming, dwelling, or quiescence (McCloskey *et al.,* 2017; Flavell *et al.,* 2013). Roaming is characterized by rapid movement and propagation of body waves down the length of the worm's body. Dwelling is characterized by lower amount of movement and propagation of body waves in the anterior but not posterior of the worm's body. Quiescence is characterized by complete cessation of movement and is observed both in high food environments, where it is termed satiety, and in fasting conditions, where it is termed fasting quiescence (You et al. 2013; Gallagher, Kim, et al. 2013). We therefore wanted to classify worm activity measurements according to these commonly applied labels.

We hypothesized that the exponential and Gaussian terms of the fit corresponded to dwelling and roaming behavior, respectively. To test this idea, we performed manual assessment of behavioral states from recorded videos. We found a strong overlap between the Gaussian component of the fit with the histogram of frames in which a worm's behavior was manually scored as roaming (Figure 3.2c). Similarly, we found a strong overlap between the exponential components of the fit and the histogram of frames in which a worm's behavior was manually scored as dwelling (Figure 3.2d). Combining both frames scored as dwelling and roaming together largely matched the overall fit (Figure 3.2e, Table 3.1).

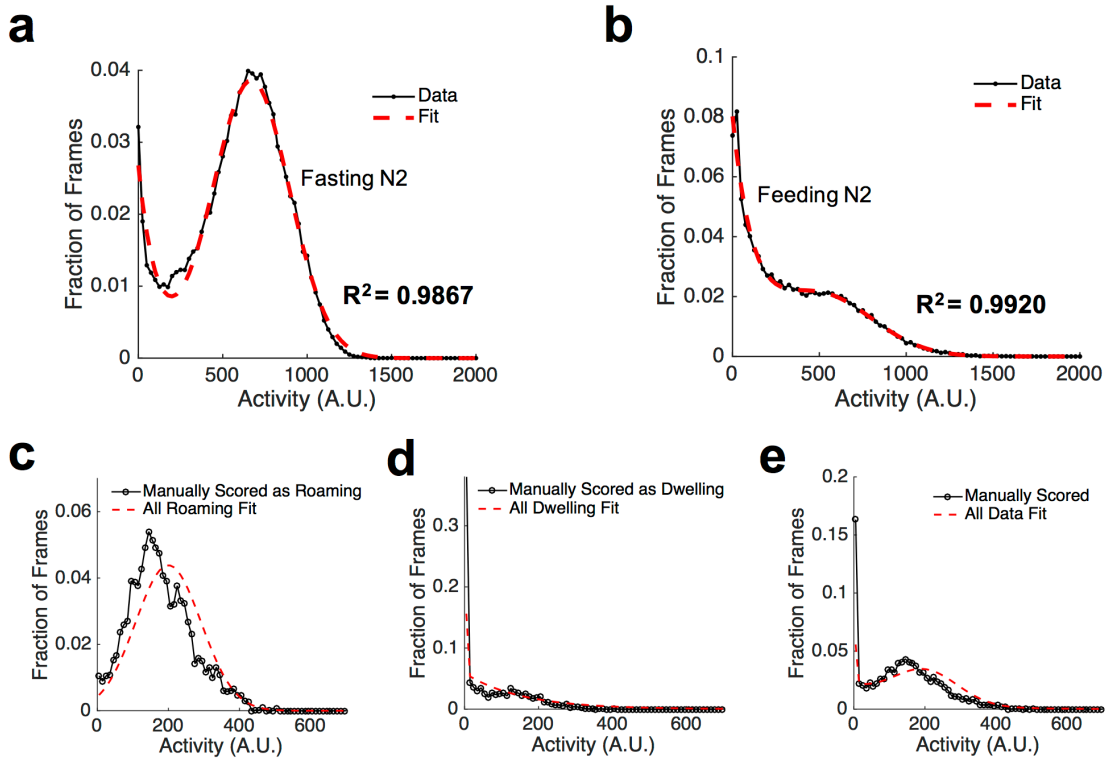

Figure 3.2 Quantitative analysis and manual validation

a) Activity histogram for a fasting worm (black curve) with fit overlaid (red dashed curve) b) Activity histogram for a feeding worm with fit overlaid c) Activity histogram for frames during which a single worm's behavior was manually scored as roaming (black curve). The Gaussian component of the fit is overlaid (red dashed curve). d) Activity histogram for frames during which the same worm's behavior as in c was manually scored as dwelling (black curve). The exponential component of the fit is overlaid (red dashed curve). e) Activity histogram for frames in the same worm's behavior as in c and d was manually scored. The full fit, consisting of both exponential and Gaussian components, is overlaid (red dashed curve).

Manual Score vs. Automatic Fit R^2 (mean ± standard deviation)	Worm #1	Worm #2	Worm #3
Feeding, Roaming R^2=0.86±0.07	R^2=0.86	R^2=0.94	R^2=0.78
Feeding, Dwelling R^2=0.77±0.13	R^2=0.62	R^2=0.85	R^2=0.84
Fasting, Roaming R^2=0.76±0.01	R^2=0.74	R^2=0.77	R^2=0.76
Fasting, Dwelling R^2=0.58±0.19	R^2=0.76	R^2=0.38	R^2=0.59

Table 3.1 Manual Behavior Score versus Automatic Fit R^2 Values

These results indicate that the exponential components of the histogram fit correspond well with frames in which worms are dwelling, and the Gaussian component corresponds with frames in which worms are roaming. Therefore, for each worm we simply summed up the area under each of these two components to calculate the fraction of time individuals spent dwelling and roaming. Quiescence was calculated as the fraction of time each worm's activity level was zero.

We found large quantitative differences in locomotion behavior between feeding and starved worms. We found that feeding caused an elevation in behavioral quiescence, a reduction in roaming, and an increase in dwelling in comparison to fasting (Figure 3.3j-n). Therefore, food status modulates multiple locomotion parameters in young adult worms.

5-HT signaling is required for worms to appropriately adapt behavior from fasting to feeding

Having established that food levels affect locomotion behaviors, we sought to determine which neurotransmitters were responsible for these changes. Since serotonin is a transmitter known to regulate behavior in response to food, we first examined the behavior of *tph-1* mutants, which lack endogenous 5-HT, in response to feeding and fasting. These mutants exhibit increased fasting quiescence, decreased feeding quiescence, and increased roaming while feeding (Figure 3.3). Therefore, endogenous 5-HT signaling is required for both wild-type fasting and feeding behavior.

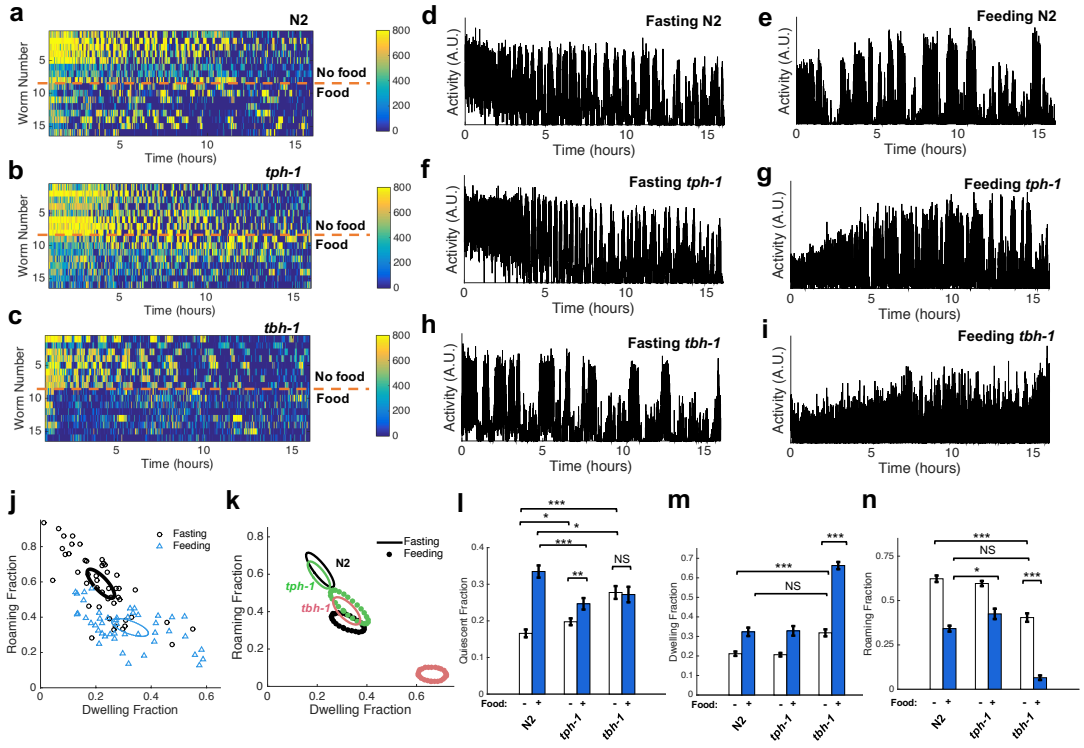

Figure 3.3 Serotonin and octopamine signaling are required for normal fasting and feeding behavior

a-c) Locomotion activity maps for N2, *tph-1*, and *tbh-1*, respectively. d) Example activity trace for a fasting N2 worm. e) Example activity trace for a feeding N2 worm. f) Example activity trace for a fasting *tph-1* worm. g) Example activity trace for a feeding *tph-1* worm. h) Example activity trace for a fasting *tbh-1* worm. i) Example activity trace for a feeding *tbh-1* worm. j) Roaming fraction versus dwelling fraction for individual fasting (black circles) or feeding (blue triangles) N2 worms. Principal component ellipses are plotted to indicate population averages and standard errors. k) Principal component ellipses illustrating fraction of time spent roaming versus dwelling for N2 (black), *tph-1* (green), and *tbh-1* (red) under fasting (solid ellipses) or feeding (dotted ellipses) conditions. Ellipse dimensions correspond to standard error of the mean. l) Quantification of fraction of time spent quiescent for N2 (n=132), *tph-1* (n=132), and *tbh-1* (n=48) worms under fasting and feeding conditions. m) Fraction of time spent dwelling. n) Fraction of time spent roaming. *, p<0.05; **, p<0.01; ***, p<0.005

We found that *tph-1* worms exhibited more roaming compared to N2 worms when assayed with food (Figure 3.3). This is consistent with previous reports that *tph-1* worms roam more on a bacterial lawn than N2 (Flavell et al. 2013b). Moreover, we found that

food treatment in *tph-1* animals had a lesser effect on the fraction of time spent quiescent. These results indicate that *tph-1* mutants are unable to fully adopt wild-type feeding behaviors in response to food. Our findings are consistent with the idea that 5-HT is released in response to food and is required for adapting locomotion behaviors to a feeding-appropriate state.

Differential effects of 5-HT produced by the ADF and NSM neurons

We asked in what neurons 5-HT is produced to regulate locomotory fasting quiescence. 5-HT is produced primarily by two neuron pairs in the head, ADFL/ADFR and NSML/NSMR, and one neuron pair near the vulva, HSNL/HSNR, as determined by expression of a *Ptph-1::GFP* transgene as well as antibody staining (Zheng et al. 2005; Ji Ying Sze et al. 2002; Liang et al. 2006b). Previous reports showed that either fasting (Cunningham et al. 2012) or *daf-2* mutation (Estevez et al. 2006) caused a reduction in *tph-1* reporter expression only in the ADF neuron, implying that 5-HT production by ADF is reduced in response to a reduction nutrient signals.

We hypothesized that 5-HT in the ADF neurons plays a role in fasting quiescence. To test this idea, we examined *tph-1* mutant worms in which wild-type TPH-1 was rescued in the ADF or NSM neurons with the cell-specific promoters *srh-142* or *ceh-2*, respectively (Song et al. 2013). As before, we noticed that *tph-1* mutants exhibit less roaming and less dwelling compared to wild type (Figure 3.4a). We found that *tph-1* rescue in ADF, but not in NSM, was sufficient to rescue roaming and dwelling to wild type levels, whereas rescue of *tph-1* in NSM caused a drastic reduction in roaming

(Figure 3.4a). Therefore, this data suggests that 5-HT produced by the ADF neuron is required for wild-type fasting behavior, whereas 5-HT produced by the NSM neuron antagonizes wild-type fasting behavior.

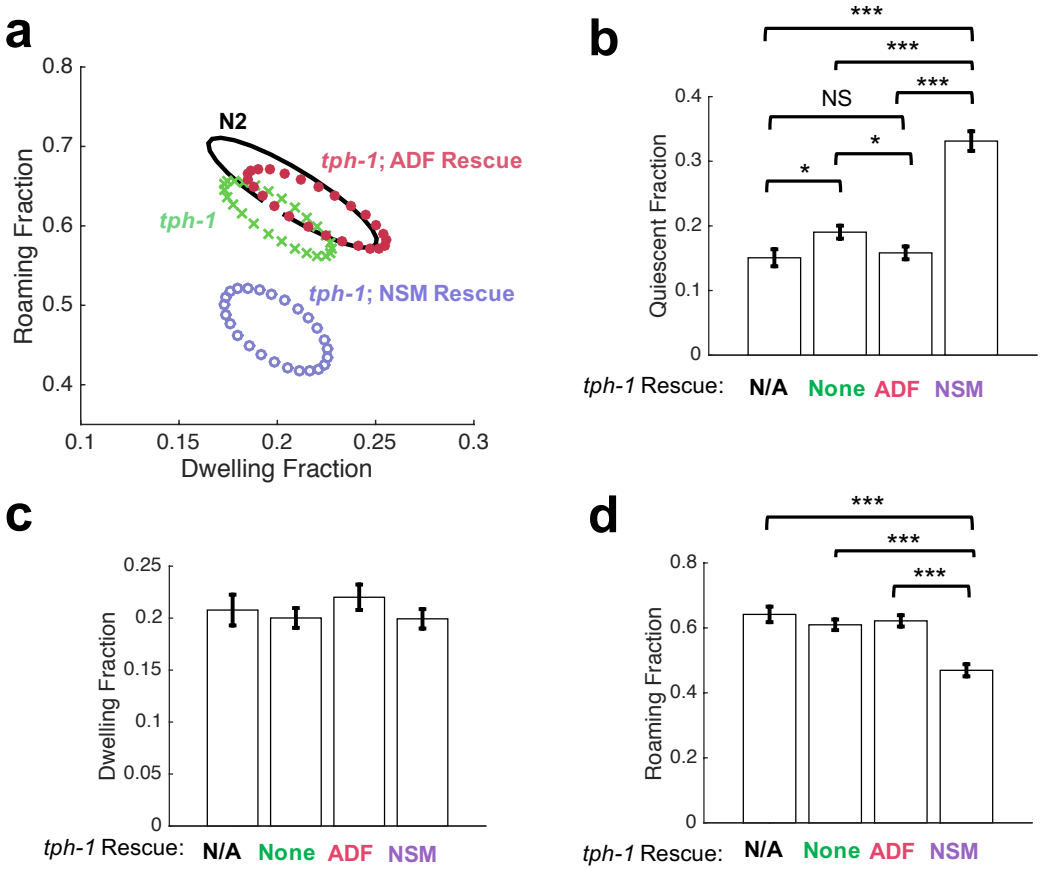

Figure 3.4 Antagonistic roles for two serotonergic neurons

a) Principal component ellipses illustrating fraction of time spent roaming versus dwelling for N2 (solid black), *tph-1* (green x's), and *tph-1* neuron-specific rescues in ADF (red dots) or NSM (purple circles). b) Fraction of time spent quiescent. c) Fraction of time spent dwelling. d) Fraction of time spent roaming. In all graphs, genotypes represented are N2 (n=84), *tph-1(mg280)* (n=84), *tph-1; Ex[Psrh-142::tph-1 (+)]* (n=84), and *tph-1; Ex[Pceh-2::tph-1 (+)]* (n=80). *, p<0.05; **, p<0.01; ***, p<0.005

As before, *tph-1* mutants exhibited slightly but significantly more quiescence than wild type, and this increase was restored to wild-type levels by rescue of TPH-1 in ADF (Figure 3.4b). By contrast, rescue of TPH-1 in NSM resulted in a large increase in fraction of time spent quiescent (Figure 3.4b). As before, fasting *tph-1* mutants exhibited an insignificant reduction in roaming, and this reduction was reversed by rescue of TPH-1 in ADF (Figure 3.4a). By contrast, rescue of TPH-1 in NSM exacerbated the reduction of roaming, suggesting that these two neurons act antagonistically to regulate the amount of roaming.

These results show that 5-HT produced by the ADF neurons is necessary and sufficient to restore wild-type fasting quiescence and behavior. Furthermore, these findings show that ADF and NSM act antagonistically with respect to roaming behavior.

Exogenous 5-HT suppresses fasting quiescence and increases dwelling

Having established that endogenous 5-HT signaling regulates fasting quiescence, we sought to determine the effect of exogenous 5-HT on the behavior of fasting worms. When we added exogenous 5-HT to the liquid media, we observed in wild-type worms an increase in dwelling and reduction in roaming (Figure 3.5a-b). Consistent with our results that *tph-1* mutants lacking 5-HT-signaling exhibit higher fasting quiescence (Figure 3.3-3.4), treatment with exogenous 5-HT suppressed wild-type fasting quiescence (Figure 3.5c).

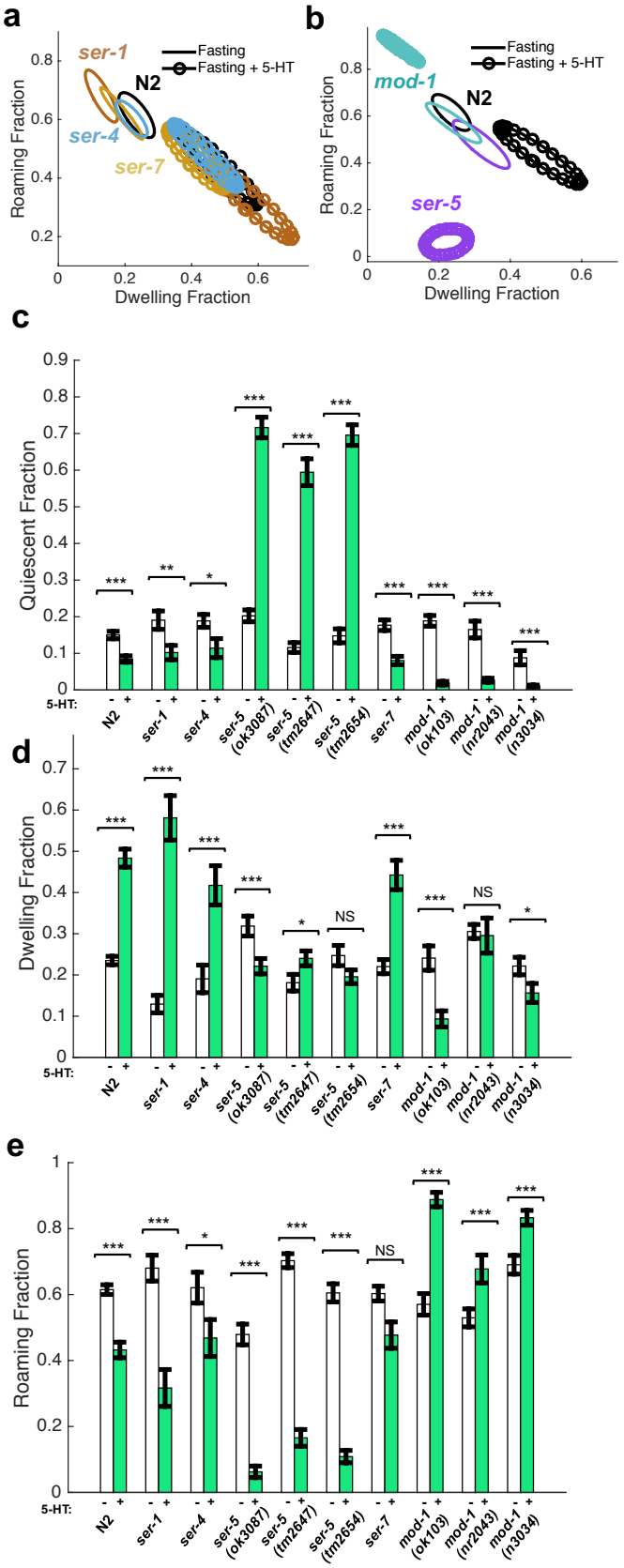

Figure 3.5 Exogenous serotonin acts through SER-5 to promote roaming and through MOD-1 to suppress roaming

a) Principal component ellipses illustrating fraction of time spent roaming versus dwelling for N2 (black), *ser-1* (brown), *ser-4* (blue), and *ser-7* (yellow) under fasting (solid ellipses) or fasting + 10 mM 5-HT (dotted ellipses) conditions. b) Principal component ellipses illustrating fraction of time spent roaming versus dwelling for N2 (black), *ser-5* (purple), and *mod-1* (cyan) under fasting or fasting + 10 mM 5-HT conditions. c) Fraction of time spent quiescent. Number of animals tested were equal for both with and without 5-HT conditions: N2 (n=124), *ser-1* (n=26), *ser-4* (n=18), *ser-5(ok3087)* (n=54), *ser-5(tm2647)* (n=24), *ser-5(tm2654)* (n=24), *ser-7* (n=38), *mod-1(ok103)* (n=28), *mod-1(nr2043)* (n=24), *mod-1(n3034)* (n=16). d) Fraction of time spent dwelling. e) Fraction of time spent roaming. *, p<0.05; **, p<0.01; ***, p<0.005

Although exogenous 5-HT suppressed quiescence, it also reduced roaming (Figure 3.5e). Therefore, exogenous 5-HT both reduces overall movement while also reducing the time spent completely immobile. Accordingly, exogenous 5-HT causes a dramatic increase in dwelling (Figure 3.5d). These results are consistent with reports that 5-HT slows locomotion (Ranganathan, Cannon, and Horvitz 2000; Flavell et al. 2013b). Therefore, exogenous 5-HT acts to promote dwelling behavior and suppress both quiescence and roaming.

5-HT promotes roaming via SER-5 and dwelling via MOD-1

We sought to determine the receptors through which exogenous 5-HT modulate locomotion. In *C. elegans*, 5-HT acts strongly through four G-protein coupled receptors and one 5-HT-gated chloride channel to regulate locomotion, feeding, fat storage, egg-laying, and other phenotypes (Ranganathan, Cannon, and Horvitz 2000; Carre-Pierrat et al. 2006; Gürel et al. 2012). To determine the receptors on which 5-HT acts, we tested the available single 5-HT receptor mutants with and without exogenous 5-HT under fasting conditions.

We found that exogenous 5-HT treatment had similar effects on quiescence, roaming, and dwelling in wild type animals as in *ser-1, ser-4,* and *ser-7* mutants (Figure 3.5a), indicating that these receptors do not contribute significantly to locomotion behavior. By contrast, exogenous 5-HT had a drastic effect on behavior of both *ser-5* and *mod-1* mutants (Figure 3.5b). We found that 5-HT suppressed quiescence in all 5-HT receptor mutants tested except for *ser-5* (Figure 3.5c). Instead of suppressing quiescence in *ser-5*

mutants, applying exogenous 5-HT resulted in greatly increased quiescence in three different alleles compared to untreated worms. Furthermore, roaming was strongly suppressed in 5-HT-treated *ser-5* mutants, indicating that SER-5 promotes movement in response to 5-HT.

Applying exogenous 5-HT to *mod-1* mutants, by contrast, resulted in quiescence suppression in three different alleles to a greater degree than for wild type worms (Figure 3.5c). Furthermore, roaming increased and dwelling decreased in 5-HT-treated *mod-1* mutants (Figure 3.5d-e), indicating that 5-HT acts through MOD-1 to suppress movement. These results are consistent with reports showing that MOD-1 promotes dwelling behavior (Ranganathan, Cannon, and Horvitz 2000; Flavell et al. 2013b). Together, our results indicate that 5-HT acts antagonistically through SER-5 to increase roaming and suppress quiescence and through MOD-1 to increase dwelling and suppress roaming (Figure 3.10).

MOD-1 acts in AIY neurons and SER-5 acts in body wall muscles and neurons to mediate behavioral effects of 5-HT

We next sought to determine in what cells or tissues the MOD-1 and SER-5 receptors act to mediate 5-HT's effects on behavior. MOD-1 is a 5-HT-gated chloride channel(Ranganathan, Cannon, and Horvitz 2000) that has been shown to act in the nervous system to mediate locomotion (Flavell et al. 2013b), learning (Y. Zhang, Lu, and Bargmann 2005), and fat levels (Noble, Stieglitz, and Srinivasan 2013). SER-5 is a G-protein coupled receptor that has been shown to act in the ASH neurons to mediate the

behavioral response to octanol and in muscles to mediate egg-laying (Harris et al. 2009; Hapiak et al. 2009). We therefore performed rescue experiments for MOD-1 and SER-5 in neurons, muscle, and specific cells to identify where these receptors act to mediate behavioral responses to 5-HT.

We first tested strains with a *mod-1* mutant background in which wild type MOD-1 was expressed under its endogenous promoter as well as under four neuron-specific promoters: *Pttx-3*, which is expressed in AIY, AIA, and AIZ neurons, *Pflp-8*, which is expressed in AUA and URX neurons, *Pflp-1*, which is expressed in RIG, AIA, and AIY neurons, and *Pgcy-36*, which is expressed in URX neurons (Noble, Stieglitz, and Srinivasan 2013). We found that rescuing MOD-1 under its endogenous promoter as well under the TTX-3 promoter resulted in partial rescue of wild type behavior when treated with 5-HT (Figure 3.6a-e). By contrast, rescuing MOD-1 under the FLP-1, FLP-8, or GCY-36 promoters did not result in behavior distinguishable from *mod-1* mutants (Figure 6a-e). The TTX-3 promoter has been previously reported to be drive expression strongly in the AIY interneurons (Flavell et al. 2013a). Therefore our results show that MOD-1 expressed in the AIY neurons is necessary and sufficient to restore wild type response to 5-HT.

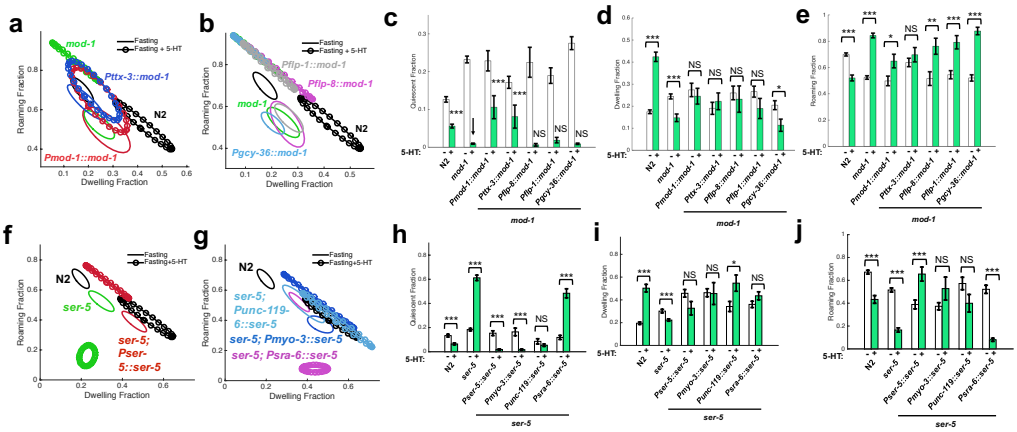

Figure 3.6 MOD-1 acts in AIY neurons and SER-5 acts in muscle and neurons to mediate 5-HT's effects on locomotor behavior

a) Principal component ellipses illustrating fraction of time spent roaming versus dwelling for N2 (black), *mod-1* (green), *mod-1;Pmod-1::mod-1* (red), and *mod-1;Pttx-3::mod-1* (blue) under fasting (solid ellipses) or fasting + 10 mM 5-HT (dotted ellipses) conditions. b) Principal component ellipses illustrating fraction of time spent roaming versus dwelling for N2 (black), *mod-1 (*green), *mod-1;Pflp-1::mod-1* (gray), *mod-1;Pflp-8::mod-1* (magenta), and *mod-1;Pgcy-36::mod-1* (blue) under fasting or fasting + 10 mM 5-HT conditions. c) Fraction of time spent quiescent. Number of animals tested were equal for both with and without 5-HT conditions: N2 (n=148), *mod-1* (n=148), *mod-1;Pmod-1::mod-1* (n=50), *mod-1;Pttx-3::mod-1* (n=38), *mod-1;Pflp-8::mod-1* (n=22), *mod-1;Pflp-1::mod-1* (n=24), *mod-1;Pgcy36::mod-1* (n=24). Significance markings are relative to *mod-1* worms treated with 5-HT (arrow). d) Fraction of time spent dwelling. e) Fraction of time spent roaming. f) Principal component ellipses illustrating fraction of time spent roaming versus dwelling for N2 (black), *ser-5* (green), *ser-5;Pser-5::ser-5* (red) under fasting (solid ellipses) or fasting + 10 mM 5-HT (dotted ellipses) conditions. g) Principal component ellipses illustrating fraction of time spent roaming versus dwelling for N2 (black), *ser-5* (green), *ser-5;Pmyo-3::ser-5* (blue), *ser-5;Punc-119::ser-5* (light blue), and *ser-5;Psra-6::ser-5* (magenta) under fasting (solid ellipses) or fasting + 10 mM 5-HT (dotted ellipses) conditions. h) Fraction of time spent quiescent. Number of animals tested were equal for both with and without 5-HT conditions: N2 (n=72), *ser-5* (n=72), *ser-5;Pser-5::ser-5* (n=16), *ser-5;Pmyo-3::ser-5* (n=16), *ser-5;Punc-119::mod-1* (n=24), *ser-5;Psra-6::mod-1* (n=16). i) Fraction of time spent dwelling. j) Fraction of time spent roaming. *, p<0.05; **, p<0.01; ***, p<0.005

Next, we generated rescue constructs for the SER-5 receptor under its endogenous promoter, a neuron-specific promoter (*Punc-119*), a body wall muscle-specific promoter (*Pmyo-3*), and an ASH-specific promoter (*Psra-6*) (see Methods), and injected them into

a *ser-5* mutant background. We found that rescuing SER-5 under its endogenous promoter fully restored the wild type response to 5-HT (Figure 3.6f-j). We found that rescuing SER-5 in either muscles or neurons rescued the behavioral response to 5-HT, whereas rescuing SER-5 in only the ASH neuron did not (Figure 3.6f-j). Therefore, SER-5 can act in both muscle or neurons to promote movement in response to 5-HT.

Octopamine and tyramine have opposite effects on locomotion

We next turned our attention toward neurotransmitters typically associated with fasting. The biogenic amines tyramine and octopamine modulate multiple behaviors and appear to signal starvation and promote starvation-related behaviors, such as suppressed pumping and egg-laying (Alkema et al. 2005; Rex and Komuniecki 2002; Rex et al. 2004; Suo, Kimura, and Tol 2006). We sought to determine the roles, if any, of these neurotransmitters in locomotion behavior mediated in relation to food.

We first tested worms defective for TDC-1, the tyrosine decarboxylase enzyme required for synthesis of tyramine and its downstream product, octopamine. We found that *tdc-1* mutants exhibited increased fasting quiescence, increased dwelling, and reduced roaming relative to wild type (Figure 3.7a). These characteristics of fasting *tdc-1* mutants largely overlap with those of feeding N2 worms (Figure 3.3j), indicating that animals lacking tyramine and octopamine behave as if feeding even in the absence of food.

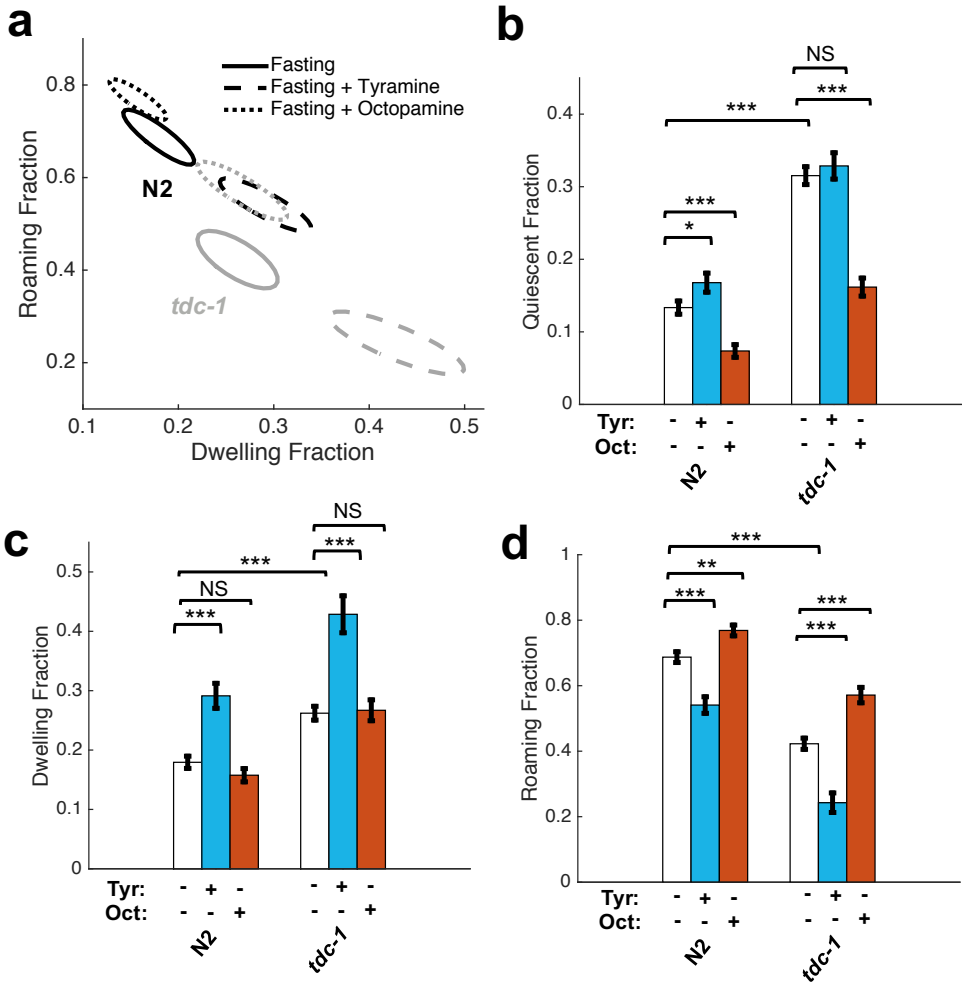

Figure 3.7 Octopamine and tyramine exert opposing effects on locomotory behavior

a) Principal component ellipses illustrating fraction of time spent roaming versus dwelling for N2 (black) and *tdc-1* (gray) under fasting (solid ellipses), fasting + 10 mM tyramine (dashed ellipses), or fasting + 10 mM octopamine (dotted ellipses) conditions b) Fraction of time spent quiescent. c) Fraction of time spent dwelling. Number of animals tested: N2 control (n=103), N2 with tyramine (n=52), N2 with octopamine (n=60), *tdc-1* control (n=104), tdc-1 with tyramine (n=52), *tdc-1* with octopamine (n=60). d) Fraction of time spent roaming. *, p<0.05; **, p<0.01; ***, p<0.005

Loss of TDC-1 abolishes the worm's ability to produce both tyramine and octopamine. To determine whether lack of tyramine or octopamine was responsible for the altered behavior in *tdc-1* mutants, we tested behavior after either exogenous tyramine or octopamine was applied. Addition of exogenous octopamine suppressed the increased

fasting quiescence in *tdc-1* mutants as well as in wild type. By contrast, exogenous tyramine slightly increased fasting quiescence in wild type, but not in *tdc-1* mutants (Figure 3.7b). These results suggest that octopamine is required for wild-type levels of fasting quiescence, and that octopamine acts to suppress quiescence.

We also found that treatment of both wild type and *tdc-1* worms with tyramine resulted in increased dwelling and reduced roaming, whereas octopamine treatment slightly reduced dwelling and slightly increased roaming (Figure 3.7c-d). These results indicate that octopamine and tyramine have largely opposing roles on locomotion, with tyramine promoting reduced locomotion typical of feeding worms and octopamine promoting increased locomotion typical of fasting worms.

Octopamine signaling is required for worms to appropriately adapt behavior to fasting

Next, we examined the behavior of *tbh-1* mutants, which lack only octopamine. We found that *tbh-1* mutants, like *tdc-1* mutants, exhibited elevated quiescence, elevated dwelling, and decreased roaming under fasting conditions in comparison to wild type animals. The defects in quiescence and roaming, but not dwelling, were reversed by exogenous treatment with octopamine (Figure 3.8a, c-e). These results show that in worms, as in flies, octopamine is responsible for the hyperactivity observed during fasting (Yang et al. 2015).

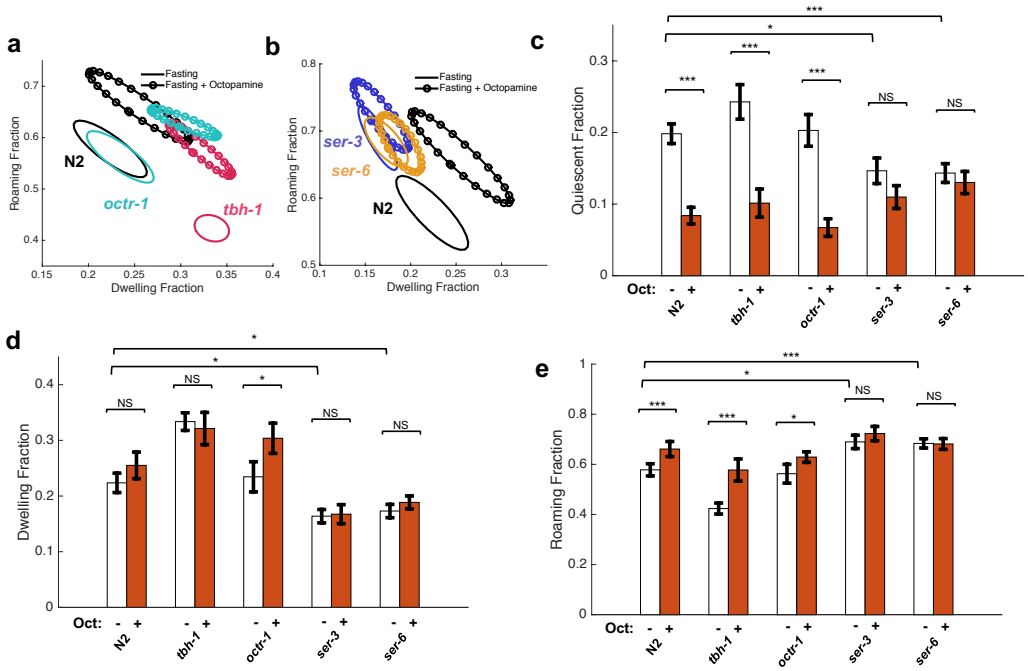

Figure 3.8 Exogenous octopamine promotes roaming and suppresses quiescence through both SER-6 and SER-3

a) Principal component ellipses illustrating fraction of time spent roaming versus dwelling for N2 (black), *tbh-1* (red), or *octr-1* (teal) under fasting (solid ellipses) or fasting + 10 mM octopamine (dotted ellipses) conditions. b) Principal component ellipses illustrating fraction of time spent roaming versus dwelling for N2 (black), *ser-3* (purple), and *ser-6* (orange) under fasting or fasting + 10 mM octopamine conditions. c) Fraction of time spent quiescent. Number of animals tested were equal for both with and without octopamine conditions: N2 (n=80), *tbh-1* (n=54), *octr-1* (n=26), *ser-3* (n=56), *ser-6* (n=72). d) Fraction of time spent dwelling. e) Fraction of time spent roaming. *, p<0.05; **, p<0.01; ***, p<0.005

The increased dwelling, decreased roaming, and increased quiescence evident in fasting *tbh-1* worms again recalls, like that of fasting *tdc-1* worms, the behavior of feeding wild type animals (Figure 3.3a, c, j, k). The finding that fasting *tbh-1* worms resemble feeding N2 worms suggests that octopamine, but not tyramine, is required for worms to adopt locomotion behaviors associated with fasting.

We next considered the behavior of *tbh-1* mutants in the presence of food. Treatment of

tbh-1 mutants with food caused a reduction in roaming and increasing in dwelling compared with fasting *tbh-1* worms. This trend is similar to that observed in wild type worms but occurred to a greater extent in *tbh-1* animals (Figure 3.3k, l-n). Feeding *tbh-1* worms exhibit greatly increased dwelling, greatly reduced roaming, and no change in quiescence compared to both fasting *tbh-1* worms. Feeding *tbh-1* worms also exhibit more dwelling and less roaming than feeding wild-type worms, suggesting that these animals overcompensate their locomotion behavior to food compared to wild type.

The finding that feeding *tbh-1* worms exhibit a large fraction of dwelling is consistent with a qualitative view of their behavior, which shows a fairly homogenous, low level of activity throughout the 16 hours of the assay, compared with the relatively more heterogeneous behavior of both feeding wild type and *tph-1* worms (Figure 3.3a-c, e, g, i). These results reinforce the notion that octopamine acts to promote movement, but also implies that this pathway acts during feeding as well as fasting.

Both SER-3 and SER-6 are required for exogenous octopamine's effects on locomotion

We next sought to determine the receptor(s) through which exogenous octopamine acts to excite roaming and suppress quiescence. We tested mutants for the three known octopamine receptors (Sun et al. 2011; R. W. Komuniecki et al. 2004; R. Komuniecki et al. 2012). We found that response to octopamine was abolished in both *ser-3* and *ser-6* mutants but remained largely intact in *octr-1* mutants (Figure 3.8a-e). Treatment with exogenous octopamine significantly increased roaming and decreased quiescence in wild type and *octr-1* mutants, but was unable to do so in either *ser-3* or *ser-6* mutants. These

results indicate that octopamine requires both SER-3 and SER-6 receptors to affect locomotion.

SER-3 and SER-6 act in the SIA neurons to mediate octopamine's effect on locomotion

We next sought to determine where the SER-3 and SER-6 receptors acted to mediate octopamine's effect on behavior. A previous report showed that SER-3 and SER-6 acted in the SIA neurons to mediate the transcription of the starvation-responsive transcription factor, CREB (Yoshida et al. 2014). We therefore tested whether rescuing SER-3 and SER-6 in the SIA neurons was sufficient to restore wild type response to octopamine.

We found that expressing SER-3 or SER-6 under the P*ceh-17* promoter, which drives expression specifically in the SIA and ALA neurons, was sufficient to restore wild type response to octopamine in SER-3 and SER-6 mutants, respectively (Figure 3.9a-e). A previous study found that octopamine modulated CREB levels in the SIA neurons, suggesting that SER-3 and SER-6 function in the SIA neurons and not ALA (Suo, Kimura, and Tol 2006; Yoshida et al. 2014). Therefore, our results suggest that SER-3 and SER-6 also function in the SIA neurons to mediate octopamine's effect on locomotion.

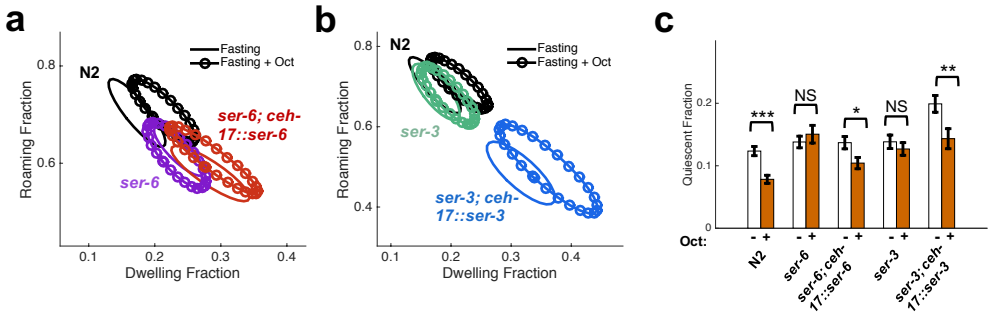

Figure 3.9 SER-6 and SER-3 function in the SIA neurons to mediate octopamine's effects on behavior

a) Principal component ellipses illustrating fraction of time spent roaming versus dwelling for N2 (black), *ser-6* (purple) and *ser-6;ceh-17::ser-6* (red) under fasting (solid ellipses) or fasting + 10 mM octopamine (dotted ellipses) conditions. b) Principal component ellipses illustrating fraction of time spent roaming versus dwelling for N2 (black), *ser-3 (*green), and *ser-3;ceh-17::ser-3* (blue) under fasting or fasting + 10 mM octopamine conditions. c) Fraction of time spent quiescent. Number of animals tested were equal for both with and without octopamine conditions: N2 (n=144), *ser-6* (n=48), *ser-6;ceh-17::ser-6* (n=48), *ser-3* (n=96), *ser-3;ceh-17::ser-3* (n=64) *, p<0.05; **, p<0.01; ***, p<0.005

DISCUSSION

Quantitative, high-throughput imaging enables characterization of complicated behavioral phenotypes

In this study, we have used the WorMotel, a novel microplate designed for long-term behavioral imaging of *C. elegans*, to elucidate the molecular and neural pathways underlying the locomotion behavioral effects of the biogenic amines 5-HT and octopamine. By acquiring high-throughput behavioral measurements, we quantified the time spent quiescent, dwelling, and roaming for up to 48 worms simultaneously over the first 16 hours of young adulthood. Automated behavioral analyses like those described here will enable quantification of complicated behavioral phenotypes and thus allow for

the dissection of how neural, genetic, and environmental variables act together to generate behavior.

As evidenced here and described elsewhere, animals utilize the same basic behaviors under different experimental conditions. In *C. elegans*, those basic behaviors are quiescence, roaming, and dwelling. However, the probability of each respective behavior is modulated as necessary to achieve an organism's goals appropriate to the current environmental state. Therefore, the ability to automatically detect and annotate different behavioral phenotypes in a quantitative way is crucial for us to understand the nuanced way the relative weights of different behavioral states are modulated in response to the environment.

Our findings support the prevailing view that 5-HT and octopamine signaling are required for appropriately adapting behavior to the presence and absence of food, respectively. We also describe the receptors and sites of action of these signalling molecules. Together, our results delineate the neural circuit and molecular mechanisms that appropriately govern locomotion behavior in relation to food levels (Figure 3.10).

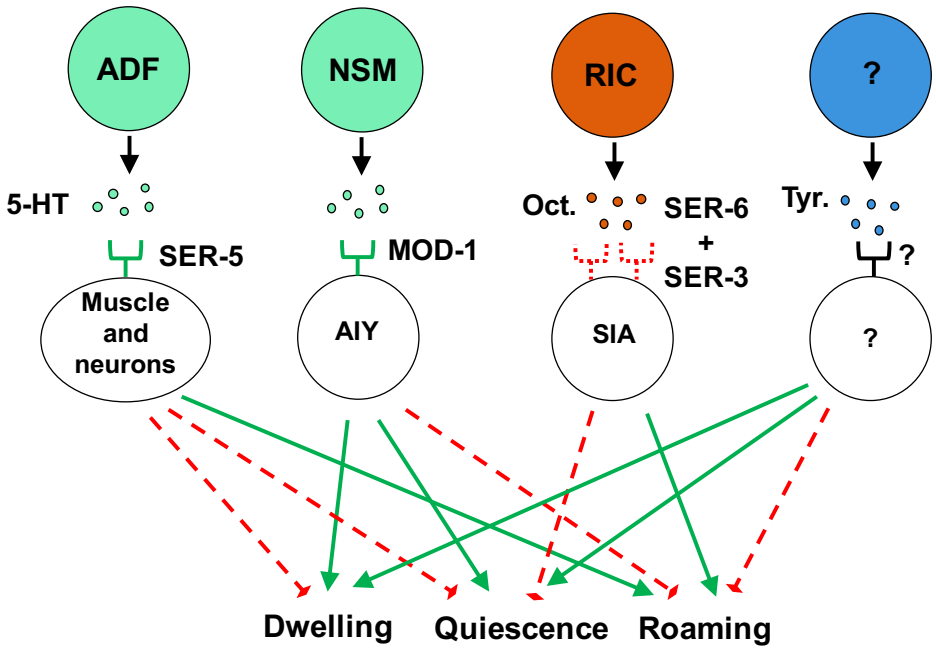

Figure 3.10 Model for biogenic amine locomotion effects

Two 5-HT-producing neurons exert opposing effects on locomotion

Our results suggest that ADF-produced 5-HT acts through SER-5 to promote roaming, whereas NSM-produced 5-HT acts through MOD-1 to promote dwelling. Therefore, serotonin acts both to increase and decrease locomotion, depending on its source. The fact that serotonin alone can both excite and suppress locomotion is supported by the fact that fasting *tbh-1* mutants, which lack the roaming-promoting signal octopamine, are able to generate periods of both dwelling and roaming (Figure 3.3c, h). This variation in behavior could be produced by the alternate release of 5-HT from ADF and NSM to produce periods of high and low locomotion, respectively.

5-HT acts antagonistically through SER-5 and MOD-1 to regulate locomotion

Previous results have shown that other 5-HT receptors act to slow locomotion in *C. elegans* (Ranganathan, Cannon, and Horvitz 2000; Carre-Pierrat et al. 2006). Our result suggests that SER-5 is the sole receptor through which 5-HT can stimulate roaming. Similarly, MOD-1 appears to be the primary receptor through which 5-HT promotes dwelling (Figure 3.5). Therefore, we confirm that 5-HT promotes dwelling via MOD-1 and show for the first time that 5-HT promotes roaming via SER-5 (Figure 3.10).

Our results suggest that ADF is an activity promoting neuron and NSM is activity-suppressing neuron. Therefore, it is plausible that ADF-produced 5-HT acts through SER-5 to regulate locomotion, as previously found in the context of copper avoidance behavior (Guo et al. 2015). Our results would then suggest that NSM-produced 5-HT therefore acts through MOD-1 to suppress locomotion.

MOD-1 acts in the AIY neurons and SER-5 acts in muscles and neurons to regulate locomotion

We found that rescuing MOD-1 under either its endogenous promoter or the TTX-3 promoter restored wild type response to 5-HT. Previous reports have also found that expressing MOD-1 under the TTX-3 promoter, which is strongly expressed in the AIY neurons, is required to promote dwelling in feeding wild type worms (Flavell et al. 2013a; Hapiak et al. 2009; Harris et al. 2009). We confirm this role for promotion of dwelling by MOD-1 in the AIY neurons. Given that MOD-1 is a 5-HT-gated chloride channel (Ranganathan, Cannon, and Horvitz 2000) and optogenetic activation of AIY

promotes roaming (Flavell et al. 2013b), it is likely that MOD-1 acts to silence AIY in response to 5-HT. Therefore, MOD-1 likely acts to suppress activity in the AIY neurons in order to promote dwelling in response to 5-HT.

We found that SER-5 could act in either muscle or neurons to promote movement in response to 5-HT. A previous study found that SER-5 acted in vulval muscle to regulate serotonergic stimulation of egg-laying (Hapiak et al. 2009). However, this study did not describe a role for SER-5 in regulating movement. Another study found that SER-5 acts in the nervous system specifically in the ASH neurons to mediate response times to octanol (Harris et al. 2009). Therefore, SER-5 occupies multiple tissue sites of action to mediate diverse behaviors. Egg-laying is associated with a transient increase in movement (McCloskey et al. 2017; Waggoner et al. 2000) Therefore, it is possible that SER-5 acts in the muscle to increase egg-laying rate, which secondarily acts to increase movement. An alternate possibility is that SER-5 acts directly on body wall muscles to promote movement. We can, however, rule out a role for the ASH neuron in regulating locomotion behavior in response to 5-HT (Figure 3.6f-j). More work is required to identify whether SER-5 acts endogenously in neurons, muscles, or both to regulate locomotion behavior.

Octopamine promotes roaming behavior via SER-3 and SER-6 in the SIA neurons

Both fasting and treatment with exogenous octopamine excite activity the cAMP response element-binding protein (CREB) transcription factor in the SIA neurons (Yoshida et al. 2014; Suo, Kimura, and Tol 2006). This effect requires the presence of

both SER-3 and SER-6. Therefore, it has been hypothesized that these receptors act non-redundantly in the SIA neurons to mediate octopamine's effects in response to starvation, perhaps via a threshold effect or dimerization.

We found that SER-3 and SER-6 also mediate octopamine's effect on behavior, and that both receptors function in SIA to mediate this effect. Therefore, our results further support the notion that both SER-3 and SER-6 are required for octopamine's effect on the response to fasting by modulating quiescent behavior (Figure 3.8-3.9). Our results suggest that the CREB transcription factor may play important roles in regulating fasting locomotion behavior.

5-HT and octopamine promote behaviors associated with feeding and fasting, respectively

Our results suggest that food initiates release of 5-HT, but that in wild type animals a reserve of octopamine signaling antagonizes this food-induced 5-HT release to antagonize the effects of 5-HT on behavior and promote roaming even when food is present. This explains why the behavior of feeding N2 worms is different from N2 worms treated with exogenous 5-HT. The dose of exogenous 5-HT permeating the cuticle in these experiments may be much larger than that released endogenously, so exogenously supplied 5-HT dominates the endogenous octopamine signal that normally counteracts 5-HT's effect. By contrast, no octopamine is present to counteract the 5-HT released in *tbh-1* mutants supplied with food, so the behavior of these animals resembles that observed in wild type treated with exogenous 5-HT (cf. Figures 3.3k and 3.7a-b).

Despite the finding that 5-HT treatment primarily promotes feeding-associated locomotion phenotypes and octopamine treatment primarily promotes fasting-associated phenotypes, we find that both transmitters are required for wild type behavior under both feeding and fasting conditions. We find that although well-fed wild type animals mostly make small movements, they also exhibit periods of high locomotion activity. This is consistent with previously published reports showing that on food, worms spend time primarily in dwelling state but also exhibit short-lived roaming states (Flavell et al. 2013b).

Our results suggest that by continuing to release lower levels of the non-dominant biogenic amine—octopamine under feeding conditions and 5-HT under fasting conditions—worms continue to maintain access to a variety of behaviors, some of which are normally associated with an environmental state they do not currently find themselves in. By reducing, but not completely eliminating, behaviors associated with environmental conditions not currently being experienced, animals maintain a high degree of adaptability.

Conserved roles of 5-HT and octopamine

5-HT and octopamine have conserved roles over diverse phyla. 5-HT is found in the protozoan Tetrahymena as an intracellular regulator of the cyclic AMP (cAMP) pathway (Turlejski 1996), a known regulator of behavior. The majority of vertebrate 5-HT receptor families also modulate cAMP levels through their effects on adenylate cyclase, indicating a remarkable degree of conservation of the molecular role of this signaling

molecule over two billion years of evolution (Turlejski 1996). The evolutionary conservation of these receptors' downstream signaling pathways suggests that understanding the molecular roles of these receptors in model organisms may contribute to our understanding of these receptors' roles in mammals.

Octopamine is found primarily in invertebrates, but also in trace amounts in mammals, and is structurally similar to the fight-or-flight hormones adrenaline and noradrenaline. Here we find that octopamine's role in worms is similar to that in flies, where it induces hyperactivity upon fasting as well wake-promotion (Crocker and Sehgal 2008). However, it was not previously known which receptors octopamine acted through to induce hyperactivity in *Drosophila*. The conservation of behavioral effects of biogenic amines suggests that roles for specific receptors may also be preserved.

Understanding the role of these signals in invertebrates may inform our understanding of the molecular bases for more complex manifestations of heightened activity based on these signals in mammals, such as aggression and anxiety.

ACKNOWLEDGMENTS

Some of the strains used in this study were provided by the by the CGC, which is funded by NIH Office of Research Infrastructure Programs (P40 OD010440). We thank H. Robert Horvitz, Ji Ying Sze, Supriya Srinivasan, Zheng-Xing Wu, and Satoshi Suo for sharing strains and plasmid reagents. We thank David M. Raizen for helpful discussions, technical assistance, and sharing of laboratory resources. C. F.-Y. was supported by the National Institutes of Health (R01-NS-084835), Ellison Medical Foundation, and the Alfred P. Sloan Research Foundation. M. C. was supported by the National Institutes of Health (R01-NS-084835). R. J. M. was supported by the National Institutes of Health (T32 HL-007712-23).

CHAPTER 4: Conclusions and Future Directions

The goal of this work was to develop a simple, scalable, and flexible method for long-term longitudinal imaging of *C. elegans*. I developed a device, called the WorMotel, to achieve this goal by using 3-D printing techniques. I then applied this device toward two areas of interest: aging and locomotion behavior states. I first developed a long-term cultivation protocol and an image analysis and processing pipeline to automatically measure lifespan and aging behavior for up to 240 worms simultaneously using the WorMotel. Using this approach, I found that despite previous reports of temporal scaling of aging across mutant populations (Stroustrup et al. 2016), the pattern of behavioral decline does not scale between short-lived and long-lived animals within or across populations. I did find, however, that behavioral decline does scale between normal aging and stressful aging. Together, these results demonstrate that aging may scale under some, but not all, conditions, and that more work is required to determine how else the aging process may vary.

I also applied the WorMotel device toward measuring changes in locomotion behavior in response to feeding or fasting. Using a combination of quantitative behavioral analysis, genetics, and pharmacology, I described a neural circuit involving the biogenic amines serotonin and octopamine that modulates the fraction of time animals spend in different behavior states. I identified the receptors through which serotonin and octopamine act to exert their behavioral effects as well as their cellular sites of action.

During the course of this work, I have developed a suite of image and data analysis software and hardware protocols designed to be simple to use and applicable to a variety of scientific questions. My software and hardware designs have been adopted by multiple other labs and researchers to answer questions regarding sleep behavior in worms (Matthew D. Nelson et al. 2014; M D Nelson et al. 2013; Iannacone et al. 2017), locomotion in free-living (McCloskey et al. 2017) and parasitic (Bais et al. 2015) worms, and sleep behavior in *Drosophila* larvae. In summary, I developed a novel device and associated software and hardware to quantify behavior longitudinally over long-time periods in microscopic model organisms and demonstrated its utility over a range of time scales and scientific areas of interest.

VARIATION IN BEHAVIORAL DECLINE DURING AGING

I found that behavioral decline during aging does not scale with lifespan within or across strains. The shape of behavioral decline differs between short-lived and long-lived individuals, with short-lived individuals exhibiting an increased rate of decline with age and long-lived individuals exhibiting a decreased rate of decline with age. Furthermore, short-lived individuals die prematurely compared with long-lived individuals in that they die on average at a level of locomotor capacity at which long-lived individuals would not. These results complicate the notion that lifespan temporally scales between genotypes and builds on work on inter-individual variability in wild type populations (Stroustrup et al. 2016; W. B. Zhang et al. 2016).

Interestingly, the shape of behavioral decline correlates with lifespan in a seemingly continuous curve across different genetic backgrounds. I initially observed that short-lived N2 mutants exhibited a pattern of behavioral decline that strongly overlapped with short-lived *daf-16* mutants. Similarly, long-lived N2 mutant decline resembled that of long-lived *daf-2* mutants. By quantifying the shape of behavioral decline and plotting this parameter versus lifespan for each individual, I confirmed the notion that the shape of behavioral decline was dictated by absolute lifespan rather than genetic background. This result suggests that individuals with similar lifespans but different genotypes might experience similar pathophysiologies underlying aging and demise. The difference in the shape of aging between individuals with different lifespasn suggests that the underling pathophysiology for differently aged animals might be unique. Two recent studies have provided evidence that individuals with different lifespans exhibit diferent causes of death. Specifically, shorter-lived individuals tend to die more from infectious causes, whereas longer-lived individuals do not (Podshivalova et al. 2017; Zhao et al. 2017). Still, more work needs to be carried out to identify the tissue-specific patterns of decline and how these can vary between individuals, as well as the potentially unique causes of death for differently aged animals.

One possible mechanistic explanation for this finding is that short-lived individuals in a wild type population might be transcriptionally similar to *daf-16* mutants, whereas long-lived individuals in a wild type population might be transcriptionally similar to *daf-2* mutants. To test this idea, future work may compare the transcriptional profiles of wild type animals with different lifespan projections. Multiple biomarkers for lifespan have

been described in *C. elegans* which are able to predict lifespan (Huang, Xiong, and Kornfeld 2004; W. B. Zhang et al. 2016). These biomarkers may be used to classify age-matched animals into bins based on projected lifespan. Then, RNA-sequencing may be performed on the two groups to determine the differences in transcriptional profile and to ascertain whether differences in gene expression underlie variability in aging. Furthermore, RNA-sequencing may be performed on *daf-16* or *daf-2* mutants in parallel to better compare differential transcriptomes between these groups.

Despite existing primarily as isogenic populations, there remains a large degree of variability in *C. elegans* lifespan. The fact that the pattern of behavioral decline correlates strongly with absolute lifespan in a continuous manner across multiple distinct genetic populations suggests that stochastic differences in gene expression may underlie lifespan variability between individuals.

BEHAVIORAL DECLINE DURING STRESS

Although I observed that behavioral decline between individuals or populations did not scale with lifespan, I observed that behavioral decline during stress did scale. I measured aging and survival for worms grown on paraquat, an oxidative-stress inducing compound (Tullet et al. 2008). At the concentration tested, paraquat reduced lifespan by approximately twenty times. The similarity in behavioral decline between normal aging and stressful aging suggests that stress simply accelerates natural processes that unfold during normal aging.

In addition, a relationship between the shape of behavioral decline and survival on paraquat similar to that observed during normal aging provides further evidence of the similarity between normal and stressful aging. Similar to observations during normal aging, short-lived individuals exhibit an increasing rate of decline with age, whereas long-lived individuals a decreasing rate of decline with age. Therefore, the pattern of aging and survival variability is preserved between normal aging and stressful aging. Therefore, aging itself may constitute a low-level stress.

Strangely, the pattern of behavioral decline during stressful aging is not continuous with the curves for normal aging. If the shape of aging were dictated solely by lifespan, I would expect to observe a continuous relationship between the shape of decline and lifespan spanning across stressful and normal aging, where lifespans range from a few hours to about two months. The apparent breakdown of this relationship indicates that the aging process may vary in ways other than absolute lifespan. Future work should aim to describe the full space across which the aging process can vary and why different genetic and environmental conditions result in different relationships between behavioral decline and survival.

RELATIONSHIP BETWEEN BEHAVIOR AND LIFESPAN

I observed that long-lived mutants exhibited reductions in movement. This behavior has been observed before, primarily in the context of reduced insulin signaling (Gems et al. 1998; Gaglia and Kenyon 2009). Because reductions in movement were associated with long-lived mutants, I hypothesized that reduced movement might be required for

extended lifespan. Therefore, I set out to genetically decouple reduced movement from longevity in *daf-2* mutants.

It has previously been shown that mutations that disrupt sensory processing can extend lifespan, suggesting that nervous system excitability may influence lifespan (J Apfeld and Kenyon 1999). In Chapter 2, I found that the G protein-coupled receptor ODR-10 is required for the suppressed sensory response observed in *daf-2* mutants. However, ODR-10 had no effect on lifespan of either wild type or *daf-2*. Therefore, reduced sensory response to the extent observed in *odr-10* mutants is not required for extended lifespan.

A previous study found that ODR-10 suppressed the reduced movement of *daf-2* mutants (Hahm et al. 2015). However, this study observed animal movement after manually transferring animals to a new plate. In my experiments, ODR-10 had no effect on baseline locomotion in wild type or *daf-2* mutants, suggesting that ODR-10 influences sensory responses to aversive stimuli but not spontaneous locomotion itself. This clarifying result highlights that long-term observation can disambiguate between behaviors that occur spontaneously versus those that are evoked. The vast majority of behavior studies involve some sort of acute experimenter intervention, such as plate movement (which induces vibrations in the agar substrate on which worms reside) or transferring worms with a wire pick. Long-term observation may help uncover novel spontaneous behaviors that have never been observed due to animal stimulation.

It remains to be determined whether reduced spontaneous movement of insulin-signaling mutants is required for lifespan extension. Reduced movement in insulin-signaling mutants has been likened to hibernation in mammals, a prolonged behavior state that requires reduced movement and exhibits reduced insulin signaling (O. L. Nelson et al. 2014; Andrews 2007; Carey, Andrews, and Martin 2003; Gaglia and Kenyon 2009). Furthermore, insulin-signaling mutants exhibit increased fat stores, another hallmark of mammalian hibernation (Mullaney and Ashrafi 2009; Ackerman and Gems 2012; Carey, Andrews, and Martin 2003). Because insulin-signaling exhibit reduced food intake, especially at older ages at which they are behaviorally quiescent, it is feasible that reduced spontaneous movement is required in order to maintain their high fat stores. Therefore, it remains plausible that spontaneous movement reductions are required for increased longevity in insulin-signaling mutants.

While ODR-10 mutations did not decouple spontaneous movement from *daf-2* longevity, other genes may be able to do so. The WorMotel is a useful tool with which to perform a reverse genetic screen for genes that rescue *daf-2* spontaneous locomotion.

Another approach toward decoupling reduced movement and longevity is to perform more frequent stimulation. My experiments utilized a blue light to stimulate animals twice per day for 10 seconds. More frequent stimulus periods might enable a significant increase in the fraction of an animal's life spent moving. However, blue light toxicity effects would need to be taken into account. Another option is the use of mechanical vibration as an aversive stimulus. Again, however, the effects of mechanical damage

would need to be accounted for. However, the WorMotel is an appropriate tool to test any of these approaches.

QUANTITATIVE ANALYSIS OF BEHAVIOR STATES

Using the WorMotel, I elucidated a neural circuit that regulates fasting and feeding locomotion behavior states (Chapter 3). To quantify behavior, I used image processing to generate longitudinal activity measurements for worms over 16 hours. I then fit individual activity histograms to the sum of an exponential and Gaussian curve, and I then showed that these mathematical fits corresponded to manually scored behavior states. This approach allowed me to quantitatively describe the fraction of time animals spend in quiescent, dwelling, and roaming behavior states.

Measurement of locomotion behavior is often performed in a qualitative fashion (Sawin and Horvitz 2000; Flavell et al. 2013a). While much has been learned from this type of analysis, faster computing power and data processing capabilities enable more quantitative analysis. Such approaches can help uncover subtle or highly variable behavior phenotypes, and will ultimately lead to a more complete description of animal behavior and how neural circuits govern behavior.

ANTAGONISTIC BIOGENIC AMINES REGULATE LOCOMOTION IN RELATION TO FOOD LEVELS

I found that serotonin and octopamine regulate locomotion in response to food levels. I found that serotonin suppresses roaming and quiescent behavior and promotes dwelling to produce a "feeding-like" behavioral profile. As has been previously reported, I found that the serotonin-gated chloride channel MOD-1 acted to suppress movement and promote dwelling in response to serotonin (Ranganathan, Cannon, and Horvitz 2000; Flavell et al. 2013a), and that MOD-1 likely acts in AIY to mediate this effect (Flavell et al. 2013a). By contrast, I found that the GPCR SER-5 acts to increase movement in response to serotonin. Surprisingly, I found that SER-5 acts in both muscle and neurons to mediate its effect on behavior. Future work will need to uncover which neurons SER-5 functions in to mediate its role in locomotion, as well as how SER-5 in the muscle regulates locomotion.

I found that octopamine signaling suppresses quiescence and increases roaming to generate a "fasting-like" behavioral profile. As was previously reported for another octopamine-dependent phenotype, I found that the receptors SER-3 and SER-6 are both required for octopamine's behavioral effect (Yoshida et al. 2014). SER-3 and SER-6 act in the SIA neurons to increase CREB levels in response to octopamine (Yoshida et al. 2014; Suo, Kimura, and Tol 2006). Similarly, I found that SER-3 and SER-6 act in the SIA neurons to mediate octopamine's behavioral effect. Therefore, octopamine elicits both metabolic and behavioral effects by acting through SER-3 and SER-6, and both effects are mediated by the SIA neurons. Future work should aim to identify

octopamine's effectors downstream of SER-3 and SER-6 within the SIA neurons, as well as the neurons or other tissues downstream to which the SIA neurons signal.

APPENDIX I: An Imaging System for *C. elegans* Behavior

Matthew A. Churgin[1] and Christopher Fang-Yen[1,2]

[1]Department of Bioengineering, University of Pennsylvania, Philadelphia, PA 19104
[2]Department of Neuroscience, University of Pennsylvania, Philadelphia, PA 19104

This appendix is a slightly modified version of an article published in *Methods in Molecular Biology* (Churgin et al. 2015). Chris Fang-Yen helped with drafting and revision of the manuscript.

SUMMARY

Many experiments in *C. elegans* neurobiology and development benefit from automated imaging of worm behavior. Here we describe procedures for building a flexible and inexpensive imaging system using standard optical and mechanical components.

INTRODUCTION

The nematode *C. elegans* is a powerful model for investigating the neural and genetic bases of behavior, owing to its easily manipulable genome and well-mapped nervous system (White et al. 1986). Much of our understanding of *C. elegans* neurobiology including synaptic function (Richmond 2005) , sensory systems (Goodman 2006; Bargmann 2006), motor systems (Von Stetina, Treinin, and Miller 2006), and feeding (Leon Avery and You 2012) have hinged on well-designed measurements of behavior.

Many behavioral assays can be conducted by visual observation (A. Hart 2006). Others, such as those requiring observations over long time scales (hours to weeks), or those involving subtle details of behavior are only practical with tools for automated imaging (Husson et al. 2012).

The simplest method for digital imaging is to add a digital camera to the trinocular port on an existing stereo microscope. However, this approach may not be desirable when long-term imaging and/or simultaneous imaging on multiple setups are required. In the course of our experiments to monitor behavior during development (Yu, Raizen, and Fang-Yen 2014) and aging (Churgin et al., n.d.), we have developed a table-top imaging

system using commercially available cameras, optics, light sources, and mechanical components. Since the system is relatively modest in cost ($500-800 not including the computer) we have been able to construct several of these systems for various uses in our laboratory.

MATERIALS

1. Aluminum bottom plate 12” x 12” x ½” (e.g. McMaster-Carr 8975K135)
2. Acrylic top plate 12” x 12” x ¼” (e.g. McMaster-Carr 8505K91)
3. 1.5” post clamp (Thorlabs C1501), qty. 2
4. 1.5” diameter stainless steel mounting post, 14” long (Thorlabs P14)
5. 1.5” diameter stainless steel mounting post, 6” long (Thorlabs P6)
6. 0.5” diameter stainless steel post (Thorlabs TR2)
7. Post holder (Thorlabs PH2)
8. Post holder base (Thorlabs BA1 or BA2)
9. Flexible red LED strip, 4.7” long, qty. 4 (Oznium Inc.)
10. 3-12V power supply (e.g. Marlin P. Jones and Associates 9902PS)
11. CMOS or CCD camera (e.g. Imaging Source DMK 23GP031, 2592x1944 pixel sensor, up to 15 images/s)
12. Power supply for camera, if needed (e.g. Imaging Source GigE23/PWR/Trig 1)
13. Data cable for camera
14. Imaging software (e.g. Imaging Source Image Capture 2.1)
15. C-mount camera lens (e.g. Fujinon HF12.5SA-1 2/3", 12.5mm focal length, f/1.4)
16. C-mount extension rings (Imaging Source LAex5, LAex1)

17. Borosilicate glass sheet 8” x 8” x ¼” (McMaster-Carr 8476K18)
18. Aluminum 2-hole inside corner bracket (80/20 part #4302)
19. 5-minute epoxy adhesive (Devcon)
20. ¼”-20 stainless steel cap head screws (qty 5), set screw (qty 1), and 1/4” washer (qty 4) (e.g. Thorlabs HW-KIT1)
21. Black gaffer’s tape, 1” wide (McMaster-Carr 7612A82)
22. Binder clips (Office Depot, 5/8” capacity)
23. Blackout fabric (Thorlabs BK5)
24. Self-adhesive bumpers (McMaster-Carr 95495K62, Polyurethane, 7/8" Wide, 13/32" high), qty. 4
25. 3/16” hex screwdriver (e.g. Thorlabs BD-3/16)
26. *Tools required if machining top and bottom plates yourself:*
    a. Drill press or handheld electric drill
    b. 1/8” diameter drill bit
    c. 5/16” diameter drill bit

METHODS

Designing the imaging system

1. Decide what field of view (FOV) and resolution are needed for your experiment. The field of view FOV is related to the sensor size SS, working distance WD (distance between the lens and object being imaged), and lens focal length f by the formula FOV = SS * WD / f. (see Notes A1.1, A1.2)

The field of view can be adjusted by moving the camera up or down. The setup detailed in Materials will accommodate a field of view ranging from approximately 2.7 cm x 2.0 cm to 11.1 cm x 8.3 cm.

2. Select the lens. Considerations include the focal length, aperture size, and compatibility with the camera sensor size. A zoom or varifocal lens provides adjustable focal length, but may be slightly less sharp and provide slightly lower contrast than a fixed focal length lens.

3. Select the camera. Considerations include the desired pixel resolution, sensor size, and maximum frame rate. In our experience, data transfer from Gigabit Ethernet cameras is more reliable over the long term than using USB cameras.

Constructing the mechanical components

1. Drill 5/16" diameter holes at the points indicated on the top (acrylic) and bottom (aluminum) plates as indicated in Fig. A1.1. A tolerance of ±1/8" is acceptable. See Notes A1.3 and A1.4.

2. Wrap a 14" x 14" piece of blackout fabric tightly around base plate and tape to bottom of plate using gaffer's tape (Fig. A1.2).

3. Feel for the hole on the top of the plate previously made in the base plate. Using a razor blade, cut the blackout fabric at an approximately 1" square around this hole and tape the fabric to the plate, leaving the hole clear (Fig. A1.2).

4. Attach 4 self-adhesive rubber feet to the bottom of the aluminum plate near the corners (Fig. A1.2).

5. Use a ¼”-20 hex head cap screw and 3/16” hex screwdriver to attach the 1.5” diameter x 14” long stainless steel rod to the base plate (Fig. A1.2).

6. Using a ¼”-20 set screw, connect the two 1.5” diameter stainless steel rods.

7. Place the first and second mounting carriers on the 1.5” diameter rod such that the side with the tapped holes faces the front of the apparatus. To set the height, tighten the clamp using a 3/16” hex screwdriver. When loosening either 1.5” post carrier clamp, support the carrier with your other hand, otherwise the carrier may fall and cause damage.

8. Attach the L-bracket to the edge of the glass plate using epoxy adhesive (Fig. A1.3). The adhesive will harden within minutes. Allow to cure overnight for full strength.

9. Mount the glass stage onto the lower post carrier using a ¼”-20 screw with washer. Adjust so that the plate is level (Fig. A1.3).

10. Attach the top plate (black acrylic) to the top of the 1.5” diameter post using a ¼”-20 screw and washer. Rotate the plate so that it is positioned directly above the base plate, then tighten the screw using the 3/16” hex screwdriver.

11. To minimize stray light from outside the imaging system, cut a piece of blackout cloth to cover the left, right, and back sides of the imaging system, and tape to the top plate. Add another piece to cover the front of the system.

Assembling the camera, lens, and light source:

1. Screw the lens onto the camera, separated by 5mm and 1mm extension rings. These rings allow the imaging system to focus on objects located closer than the

normal minimum distance. Depending on your application, the extension distance may need to be increased or decreased. See Note A1.5.

2. Mount a base plate to a post holder using a 1/4"-20 socket head cap screw. Attach a 1/2" diameter post (Thorlabs TR2) to the camera tripod mount using a 1/4"-20 set screw. Mount the post to the post holder by loosening the adjustment knob (Fig. A1.4).

3. Mount the camera with post and base onto the 1.5" post carrier using at least two ¼-20 cap screws (Fig. A1.4).

4. Attach the power supply and Ethernet cable to the camera. Install the camera software according to the manufacturer's directions.

5. Use a wire cutter to strip 1/2" of the insulation off the LED wires, if needed. Connect the bare leads of the LED to the positive and negative terminals of the power supply by loosening the terminal screws, placing the bare wire behind the terminals, and retightening the terminals.

6. Place the LED strip in a ring on the base plate. Alternatively, place four shorter LED strips in a square configuration with LEDs facing inward (Fig. A1.5). The LEDs should be wired in parallel (each pair of leads connected to the terminals of the power supply), not in series. See Notes A1.6 and A1.7.

7. Test the LEDs by turning on the power supply. The brightness can be adjusted by varying the voltage. See Note A1.8.

Alignment and Optimization

1. The lens has rings for adjustment of focus and aperture size. Set the lens focus near the middle of its range. Set the aperture near the middle of its range.

2. Turn on the power supply for the LEDs. Open the camera software, select the camera, and set to preview mode. You should see an image, which may be out of focus or uniformly black or grey.

3. Place a worm plate, or any sample with height equivalent to what you will use during experiments, onto the glass stage. Adjust the height of the upper carrier to bring the object into focus (Fig. A1.6). Make fine adjustments using the lens focus. Familiarize yourself with the gain and exposure time settings. To minimize noise, set the gain to the minimum value and provide more light if necessary.

4. Set the lens aperture size. Opening the aperture will increase the amount of light collected and decrease the depth of field. The sharpness of the image is usually poor at the extremes of aperture (wide open or nearly closed) and best somewhere in the middle.

5. Set exposure time. Exposure should be set to collect an adequate amount of light without blurring due to movement. The optimum exposure is usually such that the brightest spots in the important part of the image represent about 75% of the dynamic range of the camera. If the exposure is too low, the signal-to-noise ratio will be poor. If the exposure is too high, parts of the image will be saturated (i.e. reach the maximum pixel value). The pixel values can be assayed within the IC Capture application by moving the cursor over the image.

Acquiring image data

1. Acquire time lapse image sequences using the in IC Capture using the Sequence Timer dialog (Fig. A1.6). Save images in BMP format in a new folder devoted to the image sequence. Using JPEG format results in smaller files, but the lossy compression algorithm increases image noise.

2. To block all ambient light, close openings in the black curtains using binder clips.

3. The temperature inside the rig can be monitored by a thermometer. We use a RT100 thermistor probe and handheld meter (Omega). Note the LEDs may increase the temperature inside the rig; the voltage can be lowered to reduce LED heating. See Note A1.9.

4. Fogging of the plate lid can be a problem, particularly when the temperature drops. We prepare the lids with an anti-fog coating as follows: We pour a sterile-filtered solution of 20% Tween 20 in water onto the inner surface of the lid, pour off the excess, and allow the lid to dry in a sterile hood.

5. Preparing plates in a clean hood minimizes the chances of media contamination.

6. Data can be acquired from multiple cameras using a single computer. To use multiple Gigabit Ethernet cameras, first install an Ethernet hub. Next, run a separate instance of IC Capture for each camera and configure them individually.

7. We analyze data using custom MATLAB scripts modified for each experiment. Image data acquired using this imaging system can be analyzed using worm tracking codes described elsewhere (Husson et al. 2012).

NOTES

A1.1 This formula is approximately valid for WD much greater than f.

A1.2 The sensor size can be found in the camera specifications; the sensor of the Imaging Source DMK 23GP031 camera is 5.70mm(H) x 4.28mm(V).

A1.3 When working with aluminum, drilling a 1/8" pilot hole, and use of a cutting lubricant will make machining easier. While a drill press is preferred, a hand drill can also be used. Be sure to properly secure the workpiece during drilling and include backing material if needed to avoid damaging the surface underneath.

A1.4 For any use of power tools, wear eye protection and consult personnel trainied in their use.

A1.5 A CS-mount camera may come supplied with one 5 mm extension ring for C-mount compatibility; an additional ring should be added.

A1.6 For bright field imaging, a single LED source can be placed under the plate, with a diffuser made from a round piece of paper added to improve image quality.

A1.7 The use of red LEDs reduces the behavioral effects of the illumination compared with green, blue, or white light. Infrared LEDs can also be used.

A1.8 If you accidentally attach the LEDs in reverse, the LEDs will not light, but nothing else bad will happen.

A1.9 In one of our setups, we placed multiple imaging rigs inside a 4' x 4' x 4' temperature-controlled chamber built using 80/20 framing and covered with black

curtains. We installed a small, digital window-style air conditioner (Frigidaire Energy Star) to control the temperature inside the chamber to better than ±0.5C. Similarly, an electric heater with a temperature controller can be used to maintain temperature at a fixed value above the ambient.

FIGURES

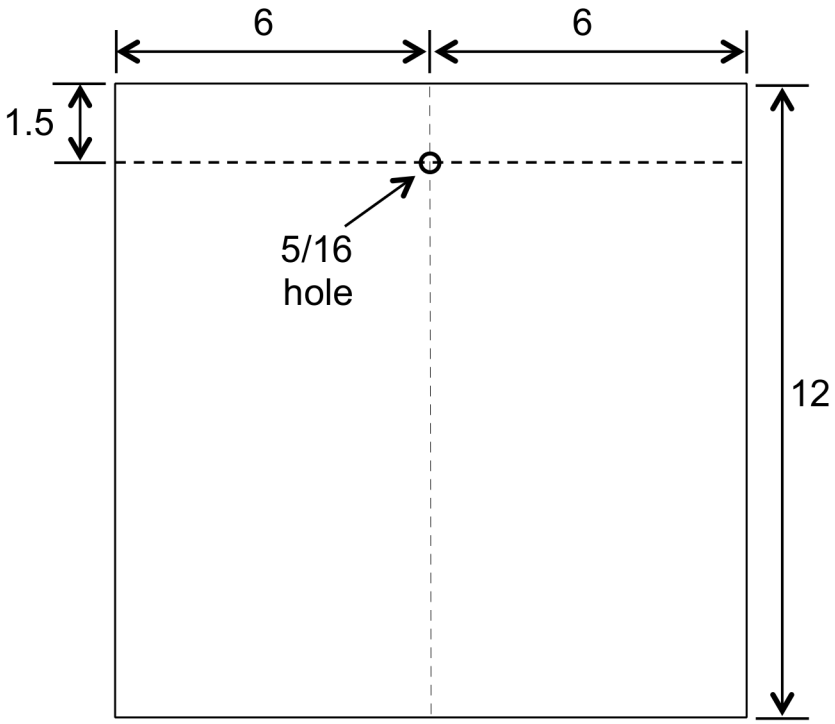

Figure A1.1 Location of holes in top and bottom plates for mounting to support rod.

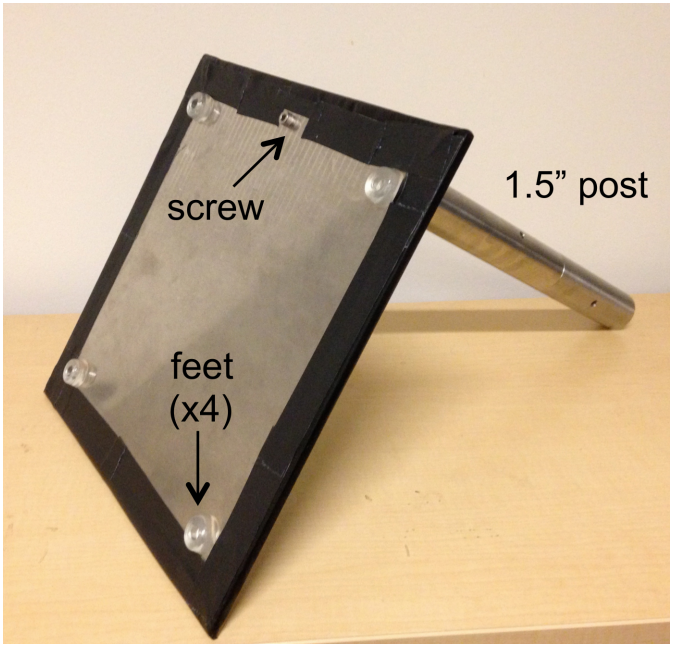

Figure A1.2 Bottom view of bottom plate with blackout fabric, mounted 1.5” diameter support rod, and feet.

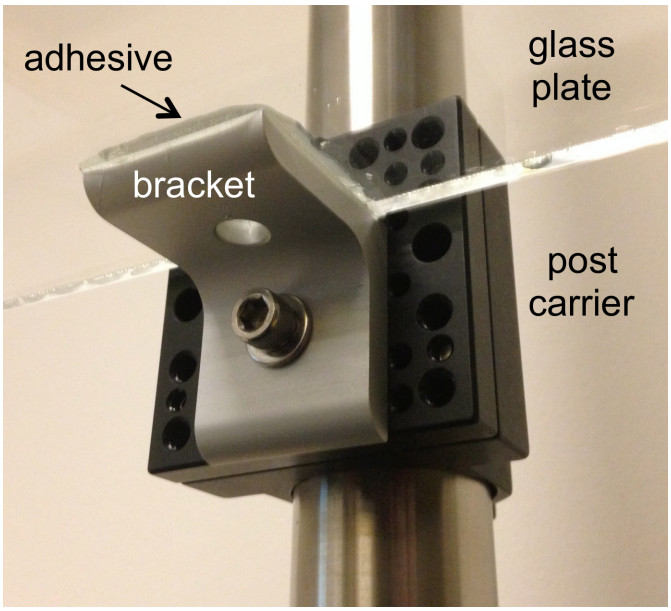

Figure A1.3 View from below of post carrier mounted on 1.5” post, 2-hole bracket, and glass platform.

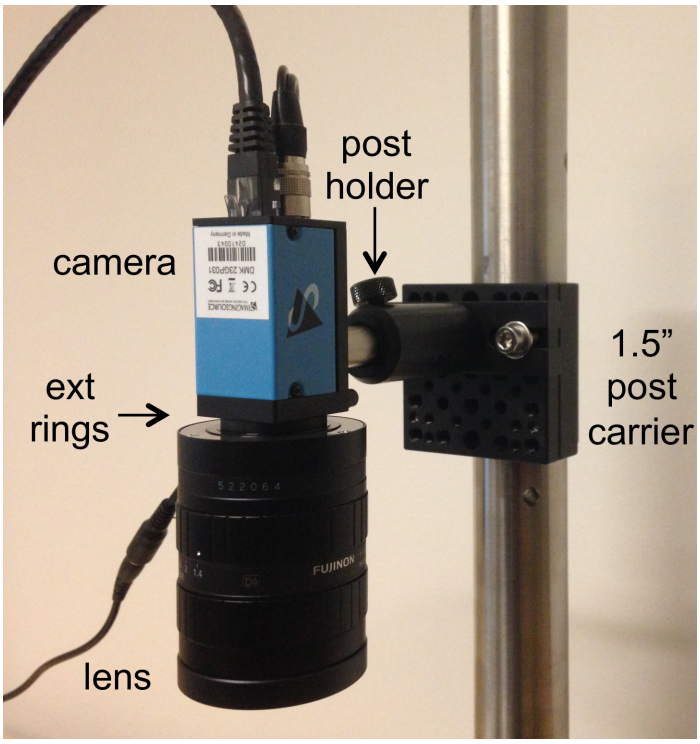

Figure A1.4 Camera assembly containing camera, lens, cables, ½" post, post holder, base, 1.5" post carrier, and 1.5" post.

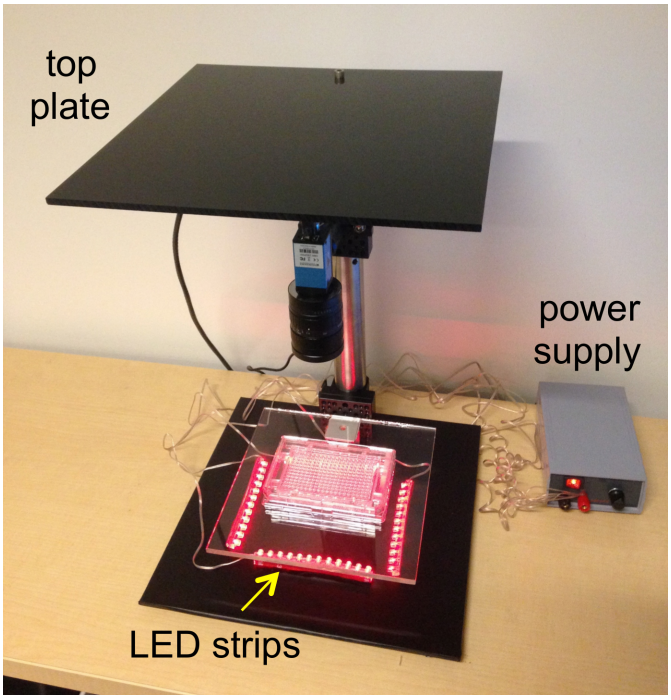

Figure A1.5 Completed imaging system including LED strips, power supply, and sample to be imaged. During data acquisition, system should be completely covered by blackout curtains (not shown).

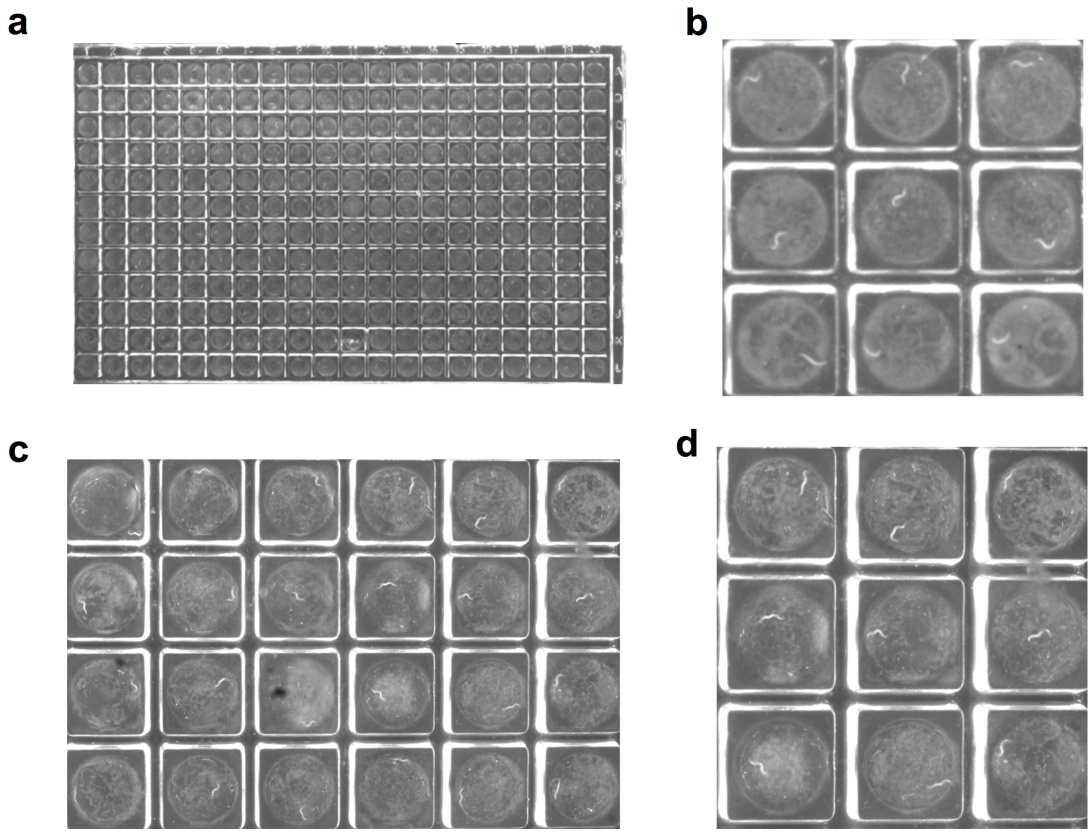

Figure A1.6 A. Image of a 240-well microfabricated 'WorMotel' device containing one worm per well (Churgin et al., 2017b). B. Detail of 9 wells from A. C. Image of 24 wells. D. Detail of 9 wells from C. Note higher spatial resolution with smaller field of view. In all images, center-to-center spacing between wells is 4.5 mm. This imaging system also works well with glass wells (Yu, Raizen, and Fang-Yen 2014), hanging droplets (Clark et al. 2007), and standard NGM plates.

APPENDIX II: Efficient single-cell transgene induction in *Caenorhabditis elegans* using a pulsed infrared laser

Matthew A. Churgin[*], Liping He[*], John I. Murray[§], and Christopher Fang-Yen[*]

*Department of Bioengineering, School of Engineering and Applied Sciences, University of Pennsylvania, Philadelphia PA 19104, USA.

§ Department of Genetics, Perelman School of Medicine, University of Pennsylvania, Philadelphia PA 19104, USA

This appendix is a slightly modified version of an article that was originally published in *G3* (Churgin et al. 2013). Liping He performed FLP rescue experiments and embryo heat shock experiments. John Murray helped with conceiving the project, analyzing data, drafting and revising the manuscript. Chris Fang-Yen helped with conceiving the project, planning experiments, constructing the custom microscope, analyzing data, drafting and revising the manuscript.

ABSTRACT

The coupling of transgenes to heat shock promoters is a widely applied method for regulating gene expression. In *C. elegans* gene induction can be controlled temporally through timing of heat shock, and spatially via targeted rescue in heat shock mutants. Here we present a method for evoking gene expression in arbitrary cells, with single-cell resolution. We use a focused pulsed infrared laser to locally induce a heat shock response in specific cells. Our method builds on and extends a previously reported method using a continuous-wave laser. In our technique the pulsed laser illumination enables a much higher degree of spatial selectivity due to diffusion of heat between pulses. We apply our method to induce transient and long-term transgene expression in embryonic, larval, and adult cells. Our method allows highly selective spatiotemporal control of transgene expression and is a powerful tool for model organism biology.

INTRODUCTION

Methods for inducing transgene expression in a tissue-specific or cell-specific manner are important for investigating the roles of genes and cells in development, physiology, and behavior. Cell-specific expression has been achieved by use of cell-specific promoters, intersectional promoters, and inducible strategies (Bacaj and Shaham 2007; Wei et al. 2012) some of which also enable *temporal* control of transgene activity. However, these methods depend on cell-specific promoters or promoter combinations, which are not available in many cases. Moreover, these strategies need to be developed for every cell under study, making them impractical for application in many different cell types.

A truly general method would be capable of inducing transgene expression in arbitrary cells. A method introduced by Kamei *et al* called infrared-laser evoked gene operator (IR-LEGO) (Kamei et al. 2009) made progress toward this goal. In this technique, a focused continuous-wave (CW) infrared laser beam was used to heat a small volume in the organism. This heating was coupled to transgene expression by using a heat shock inducible promoter. While shown to be effective for some cases, this method has two important limitations which have limited its adoption: (1) it causes substantial diffusion of heat to neighboring cells, such that off-target transgene induction was difficult or impossible to avoid for small cells, and (2) the efficiency of transgene induction was low (20%) for many cell types. Here we present an improved method for laser-induced heat shock that overcomes these two limitations. First, we employed a pulsed rather than CW infrared laser beam to heat targeted cells with dramatically reduced off-target heating. Second, we have optimized conditions to improve the efficiency of transgene induction to as high as 95% depending on cell type in diverse embryonic and postembryonic cell types.

Theory suggests that pulsed illumination could reduce the size of the heated region as illustrated in Fig. A2.1a. During CW illumination, the temperature rapidly reaches an approximately steady-state (time-independent) distribution. For a small source of heat in an infinite homogenous medium, the steady-state laser-induced temperature increase outside the source decreases as the inverse of the distance to the source. By contrast, a brief pulse of heating at a small source will induce a Gaussian temperature profile that

decreases sharply with distance (Supplementary Text A2.S1). Therefore given equal peak temperatures at the laser focus, the peak temperature at a distance r from the laser focus should be smaller for pulsed laser heating than for CW heating.

We implemented pulsed heating using an inexpensive, thermoelectrically-cooled, fiber-coupled diode laser with 1480 nm wavelength, which is absorbed efficiently by water. The beam emerging from the fiber end was collimated by a lens, reflected from a short-pass dichroic beam splitter, then entered a 100X, NA 1.3, oil-immersion objective which focused the beam onto the sample of an inverted microscope (Fig. A2.1b).

RESULTS

We compared the temperature distributions for CW and pulsed infrared irradiation by using GFP-expressing *E. coli* as a temperature sensor. GFP fluorescence intensity decreases linearly with temperature by approximately 1%/°C over the range 20 – 60 °C (Kamei et al. 2009) (Supplementary Fig. A2.S1). We measured the CW laser spatial temperature profile by measuring the spatial patterns of laser-induced change in fluorescence intensity, and we measured the temperature changes during pulsed irradiation by using pulsed blue LED illumination to selectively excite GFP at specific times relative to the infrared laser pulse (Fig. A2.2a). The temperature decays to a nearly uniform distribution when the laser is in the off state, preventing heat buildup away from the laser focus. Modulating the laser power, repetition frequency, and duty cycle (fraction of time on) allowed us to tune the peak temperature and extent of spatial heating

(Supplementary Fig. A2.S2- A2.S3).

Because the laser heating profile is sharply peaked at the laser focus, reducing the overall temperature of the sample served to minimize the size of the region experiencing a heat shock. To reduce baseline temperature, we cooled the sample from 23 °C to 18 °C by passing cooled water through flexible plastic tubing wrapped around the objective lens, which is in thermal contact with the sample via the immersion oil. We measured the temperature at the sample using a microthermocouple placed inside an agar pad and confirmed that it was equal to the objective temperature to within ±0.1 °C.

Given a hypothetical peak temperature of 50 °C, we sought to determine over how large a region the laser-induced temperature exceeded 35 °C, a common threshold used for whole body heat shock in worms, using CW illumination, pulsed illumination (PIR), and pulsed illumination with objective cooling. The radius of the region heated above 35 °C decreased from 12 μm under CW illumination, to 5 μm under PIR, to 3 μm under PIR with objective cooling (Fig. A2.2b). Previous work established that the extent of axial heating was approximately twice that of lateral heating (Kamei et al. 2009), suggesting that the axial resolution of pulsed illumination with cooling is approximately 6 μm. The four-fold reduction in lateral and axial heated radius corresponds to a 64-fold reduction in heated volume compared to CW illumination.

We confirmed that results from E. coli accurately represented temperature shifts in *C. elegans* by measuring temperature changes in single GFP-expressing mechanosensory

neurons in intact worms (Supplementary Fig. A2.S4).

We sought to determine whether the reduced spatial extent of pulsed laser-induced heating translated to more selective transgene induction, compared with continuous-wave illumination. We compared the performance of a pulsed and continuous (Kamei et al. 2009) IR laser in inducing a HS response in seam cells in L4 larvae. Seam cells are specialized hypodermal cells 20 μm in length located beneath the worm's cuticle (skin). We identified these cells with a GFP-tagged adherens junction marker *ajm-1::GFP*. Heat shock activation was assayed by scoring fluorescence three hours after laser heating of worms expressing GFP under the control of the *hsp16.2* promoter (Fig. A2.3b-c). Our irradiation protocol consisted of a pulse repetition frequency of 30 Hz, pulse length of 1 ms, and duration of 6 minutes. The objective was cooled from room temperature of 24 °C to 20 °C. We found that laser powers between 220 and 260 mW induced GFP expression in 75% of targeted single cells in L4 worms with no expression visible in untargeted neighbor cells (n = 40).

To test the limits of spatial selectivity of our method we targeted head neurons in L2 larvae. The cell bodies of these neurons are among the smallest in the animal, about 3-5 μm in diameter. To assist in cell identification, we used the red fluorescent lipophilic dye DiI to stain cell membranes of the amphid (sensory) neurons (Shaham 2006). We then applied the same laser heating protocol as applied to seam cells, and assayed cells for GFP expression three hours after heat shock. We observed GFP in the targeted neuron, ADL, 30% of the time, with no visible expression in neighboring cells or pharyngeal

muscle (Fig. A2.3d-f). We were also able to induce gene expression in the amphid neuron AWB (30% induction rate, n=30) and mechanosensory neuron ALM (90% induction rate, n=10) without observing any off-target expression. These results indicate that our method f can be used to induce gene expression in a highly selective manner in the *C. elegans* nervous system.

Next, we used single-cell heat shock to induce transgene modifications through the site-specific recombinase FLP. In contrast to direct heat shock activation, which induces transient expression, expression of FLP, when combined with the appropriate FRT-flanked transgene, is capable of inducing changes such as permanent induction of transgene expression or selective knockout of a rescuing transgene (Davis et al. 2008). To test this concept, we expressed FLP under a heat shock promoter and used it to excise a termination cassette upstream of the GFP coding sequence. Single intestinal cells targeted by our pulsed laser displayed robust and permanent GFP expression within 12h (66.7% induction, n=21, Fig. A2.3g-j), whereas non-targeted cells did not. Therefore our method is capable of engineering permanent genetic changes in single cells.

Finally, we tested our method's ability to induce gene expression in embryonic cells. During early embryonic development, tissue-specific promoters are not active because cell types have not yet been specified. However the positions and cell types produced by each early embryonic blastomere are predictable because *C. elegans* develops through an invariant lineage (Sulston et al. 1983). Induction of transgenes in individual targeted embryonic cells will be useful for tracing cell positions in mutants or for lineage-specific

rescue experiments. We individually targeted each of the cells in 4-cell stage embryos in P*hsp-16.2::GFP* worms. With a modified heating protocol, we could both maximize hatch rate (>74%) , and observe efficient induction of GFP expression (>80%) in the descendants of ABp, ABa, and EMS (Supplementary Table A2.S1). The frequency of GFP induction in P2 was lower, perhaps due to this cell's transcriptional quiescence during the 4-cell stage (Leatherman and Jongens 2003), but we still observed expression in this lineage in 26% of embryos. We confirmed that expression was limited to the targeted cell and its progeny by comparing the observed fluorescence pattern three hours after heat-shock (Fig. A2.4b, f, j, n) with an AceTree computer simulation of the expected positions at that stage (Boyle et al. 2006) (Fig. A2.4d, h, l, p). Our finding that single cell heat shock is capable of inducing gene expression in the daughters of individual cells during development points to its potential usefulness in genetically manipulating developing embryos with fine spatiotemporal control.

DISCUSSION

In summary, we have developed a robust, efficient and specific method for transgene induction in single cells. Our method can evoke gene expression in a variety of cell types while avoiding gene induction in neighbors only about 5 μm from the laser focus. This represents a vast improvement in spatial selectivity compared with existing methods. We have optimized irradiation protocols for efficiently inducing expression without visible damage in both developing embryos and larvae. Our method is inexpensive and similar in technical complexity to laser ablation systems, which are used widely in studies of *C.*

elegans (Fang-Yen et al. 2011), and therefore should extend readily to other transparent organisms such as embryos and larvae of *Drosophila* and zebrafish. We expect our method will be particularly useful in studying development, where expression of transgenes with fine spatiotemporal control can help elucidate the cellular and molecular mechanisms governing cell fate decisions (Abdus-Saboor et al. 2011), body patterning (Pearson, Lemons, and McGinnis 2005), and organogenesis (Mango 2009) .

METHODS

Laser and microscope. We combined a fiber-coupled infrared diode laser (Fitel FOL1425RUZ-317, wavelength 1480 nm, up to 400 mW) with an inverted microscope (Nikon Eclipse TE2000-S) equipped with DIC and fluorescence optics and with sample stage raised using a height adjustment kit (T-BSUK). The laser was controlled by a diode laser driver (Opto Power OPC-PS03-A) and a thermoelectric cooler (Thorlabs TEC2000). The emission from the fiber tip was collimated with a plano-convex lens (focal length f=75 mm). A shortpass dichroic mirror (Thorlabs DMSP1000R) positioned between the objective lens and the fluorescence turret reflected the collimated laser beam into the back of the objective lens (Nikon Plan Fluor 100x, NA 1.3). A pulse generator (Stanford Research Systems DG535) connected to the laser driver was used to control the frequency, duration, and number of laser pulses. We recorded images using a CCD camera (Photometrics Cascade 1k) and Micro-Manager software. Data analysis was performed using MATLAB (Mathworks Corp.).

The infrared beam is not detectable directly using our CCD. To determine the location of

the laser focus, we used laser trapping of 1 μm diameter polystyrene beads(E. Kim et al. 2013). On each day, prior to experiments with worms, we used our setup to illuminate a 0.25% suspension of 1 μm polystyrene beads (Polysciences) in an acqueous solution. We marked the location of a trapped bead on the computer monitor; this mark was used as a guide to perform laser heating of cells.

To lower the temperature of the sample, we wrapped plastic tubing (Tygon) around the microscope objective. Cool water at 5 °C was run through the tubing by a temperature-controlled water circulator (Brookfield). The circulator was turned on at least one hour before laser heat shock to allow the temperature of the objective to stabilize. We periodically monitored the temperature of the objective using a thermocouple.

Temperature Calibration of GFP. GFP-expressing *E. coli* were spread onto a 10% agarose pad using a platinum wire pick and the microscope slide carrying the pad was placed on a thermo-controllable microscope stage. The temperature was controlled with a water circulator. We inserted a microthermocouple (Physitemp) into the agarose pad to monitor the temperature of the pad. Fluorescence images of the same field of view were taken periodically as the temperature was shifted. Fluorescent illumination was only applied during image acquisition and the exposure time per image was less than 5 s. Images were corrected for photobleaching. The mean value of the same ROI was plotted versus temperature as measured by the microthermocouple (Supplementary Fig. A2.S1).

Temperature Measurement using GFP. GFP-expressing *E. coli* were spread onto a 10% agarose pad using a platinum wire pick and the microscope slide carrying the pad was placed on to a standard microscope stage. For continuous wave temperature measurements, the laser power was adjusted to the desired setting and two fluorescence images of the same field of view were acquired; the first image was acquired with the CW laser disabled and the second image was acquired with CW laser enabled. The exposure time was the same for both images but varied day to day from 0.5 to 2 s. The laser spatial heating profile was calculated by dividing the pixel intensity values between the two images and converting the decrease in fluorescence intensity during laser heating into temperature change using the calibration curve described above (Supplementary Figure A2.S1).

For pulsed laser temperature measurements we used a 10W blue LED (center wavelength 445 nm). The LED light was collimated with a 40 mm focal length aspheric condenser lens (diameter = 50 mm) and directed through the fluorescence port of the modified inverted microscope. The same pulse generator that controlled the laser also controlled the LED driver via a solid-state relay (Grayhill 70-ODC5).

To measure the temperature changes as the laser pulsed at 1 kHz with 0.2 ms pulse length (Fig. A2.2a), the blue LED was set to illuminate from 0.1 to 0.2 ms during the pulse cycle (Fig. A2.2a inset). In this case, pulsing the LED in phase with the pulsed laser effectively sensitized the camera to the GFP signal during the laser on state. As with CW temperature measurements, two images were taken; one with the pulsed laser disabled

and one with the pulsed laser enabled. Both images were acquired with the same exposure time which varied day to day from 1 to 10 s. Next, the LED was set to illuminate during 0.8 to 0.9 ms of the pulse cycle and two images were acquired in the same manner as before. In this case, pulsing the LED out of phase with the pulsed laser effectively sensitized the camera to the GFP signal during the laser off state (Fig. A2.2a). The pulsed laser spatial heating profile during the laser on and off states was determined in the same way as for CW temperature measurements using the GFP temperature calibration to convert fluorescence decrease into temperature shift (Supplementary Figure A2.S1).

We sought to confirm that the *in vitro* scenario accurately described *in vivo* temperature shifts. We conducted an experiment using live, immobilized worms expressing GFP in mechanosensory neurons as a temperature sensor, analogous to the *E. coli* experiments. We targeted the cell body of one of the bilateral ALM neurons and measured peak temperature as a function of IR laser power. We found no difference in peak temperature between *E. coli* and the ALM cell body proximal to the coverslip (Supplementary Fig. A2.S4). However, targeting ALM distal to the coverslip generated a slightly higher peak temperature, possibly due to removal of a heat-sinking effect of the glass coverslip. Our results indicate that the *in vitro* model of laser heating accurately describes *in vivo* temperature shifts.

Strains. Worms were cultured on NGM agar seeded with OP50 bacteria using standard methods (Sulston, J, and Hodgkin, J 1988). Larval and adult worms were handled with a

platinum wire pick. Embryos were handled with a mouth pipette. Worms used for larvae and adult experiments were grown at 20 °C. Worms used for embryo experiments were grown at 15 °C. All heat shock experiments were carried out using the strain ST66 (*ncIs17* [P*hsp16.2::EGFP*]). We occasionally observed GFP expression in single cells prior to heat shock. All GFP induction experiments were carried out using cells in which GFP expression was not observed prior to heat shock. To monitor *in vivo* temperature shifts in adult worms, we used strain *muIs32* (P*mec-7::gfp*). To identify and target seam cells for heat shock we constructed the strain YX40 by crossing *ncIs17* and *ncIs13*. The transgene *ncIs13* contained P*ajm-1::gfp*, an adherens junction marker which delineated seam cells in larval worms. GFP was never visible in seam cells prior to heat shock. Experiments in which the neuron ALM was targeted for heat shock were carried out using the strain containing *ncIs18; muIs32*. *ncIs18* [P*hsp16.2::mRFP]*. RFP expression was never visible in ALM prior to heat shock. All experiments involving amphid neurons and all experiments involving embryos were carried out using the strain containing transgene *ncIs17*. GFP expression was never visible in amphid neurons or embryos prior to heat shock. For experiments using FLP, we constructed the strain YX29 (qhEx15 [*hsp16.48p*::FLP; *his-72p*::FRT*mCherry*FRT_GFP::*unc-54* 3'UTR]. One of four of the first intestinal ring cells in L3 or L4 worms were heated with 25% duty cycle at 100 Hz for 3 minutes. GFP expression was scored 18-24 hours later after heat shock.

For seam cell heat shock experiments, L4 animals were removed from food for one day prior to experiments After heat shock, animals were recovered to a new seeded OP50 plate. We found that this process increased the efficiency of single cell heat shock

activation four-fold in addition to raising the damage threshold (Fig. A2.3a, Supplementary Fig. A2.S5). Animals were only starved for use in experiments in which seam cells were targeted.

To label the cell membranes of amphid neurons (Fig. A2.3d-e), we used DiI staining (Shaham 2006).

Larvae Laser Heat Shock and Mounting. During imaging and heating, 5-10 worms were immobilized using 10% agarose pads and 0.1 μm polystyrene beads as described by Kim et al (E. Kim et al. 2013). Worms underwent the pulsed laser heat shock and recovered to a seeded NGM agar plate within one hour of mounting.

To activate FLP-coupled heat shock-mediated gene expression in L3 and L4 animals (Fig. A2.3g-j), intestinal cells were targeted with the IR laser for 3 minutes with pulse repetition frequency of 100 Hz and pulse length of 2.5 ms. GFP induction was scored >12 hours after heat shock.

Embryo Laser Heat Shock and Mounting. For embryo experiments, 4-cell stage embryos were mounted according to the protocol described by Bao and Murray (Bao and Murray 2011). All slides contained control embryos not subjected to laser illumination. Embryos were imaged and heat shocked within 20 minutes of mounting. Cell were targeted during the four-cell stage for 15 s with pulse repetition frequency of 100 Hz and pulse length of 2.5 ms. 2-3 hours after laser irradiation, we scored GFP induction using a

Leica DM2500 fluorescence microscope. Embryos remained mounted overnight in a humidified chamber to score hatching the following morning (Supplemental Table A2.S1). The hatch rate for control animals was 100%.

Computer Simulation. We used AceTree (Boyle et al. 2006) to generate 3D images of the expected positions for each 4-cell blastomere's progeny after 3 hours based on a reference model of embryogenesis (Richards et al. 2013) (Figs. A2.4d, h, l, p).

ACKNOWLEDGMENTS

We thank Shin Takagi and Erik Jorgensen for providing strains and plasmids. Some strains were provided by the Caenorhabditis Genetics Center, which is funded by NIH Office of Research Infrastructure Programs (P40 OD010440). We thank David Raizen and Meera Sundaram for helpful discussions. This work was supported by a Penn Comprehensive Neuroscience Center pilot grant. C. F.-Y. was supported by an Alfred P. Sloan Research Fellowship. J.I.M. was supported by the NIH (GM083145), by the Penn Genome Frontiers Institute, and by a Grant from the Pennsylvania Department of Health, which disclaims responsibility for any analyses, interpretations or conclusions.

FIGURES

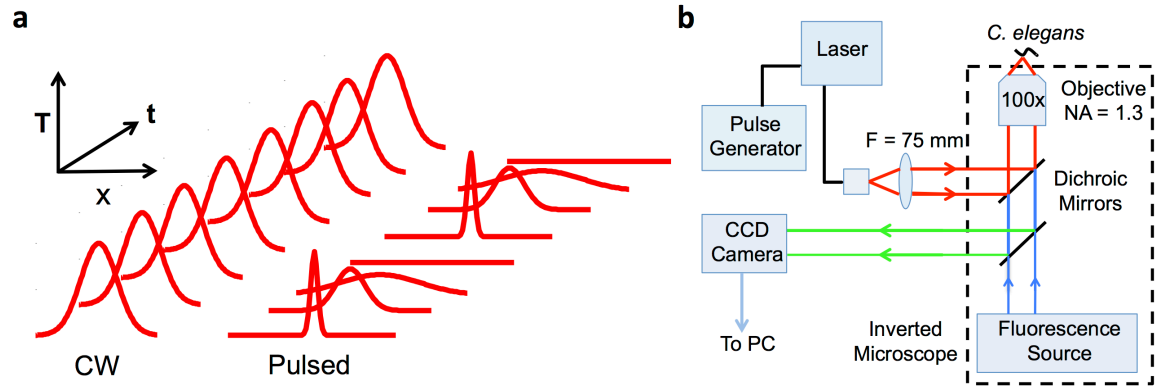

Figure A2.1 Pulsed and CW laser heating. (a) Principle of pulsed-laser-induced gene expression. By allowing time for heat to dissipate after each pulse, a pulsed laser heats a smaller volume than continuous wave illumination, avoids heating neighboring cells, and confines gene induction to the targeted cell. (b) Experimental setup.

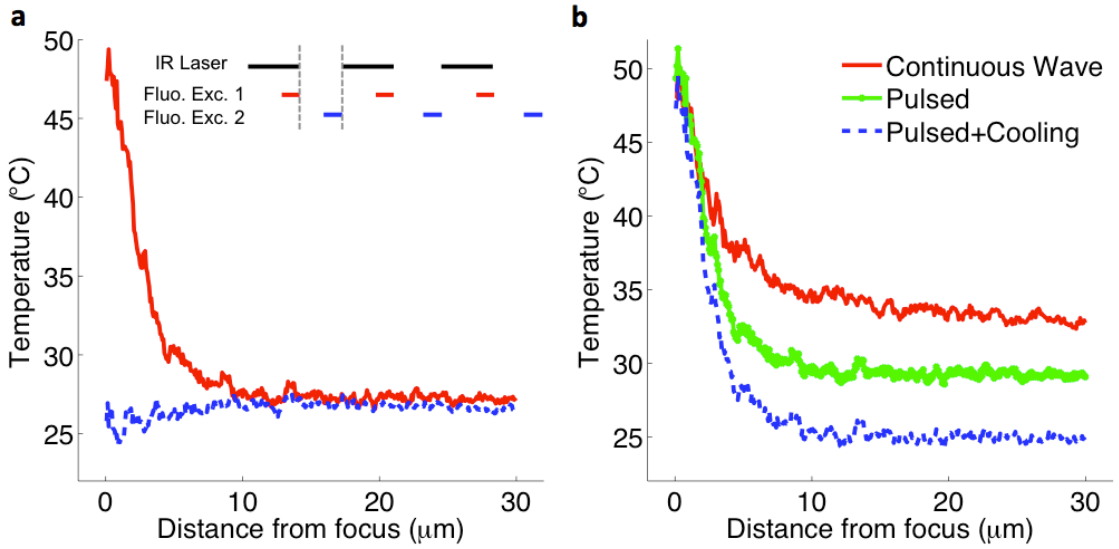

Figure A2.2 Pulsed Laser Temperature Profile (a) Spatial heating profile for IR laser pulsed at 1 kHz repetition frequency and 0.2 ms pulse length, as measured using the temperature dependence of GFP. The temperature profile during the IR laser pulse (red) peaks at the laser focus and decays sharply away from the focus. The temperature profile between pulses (blue) is nearly uniform. Inset (not to scale): fluorescence blue LED excitation pulses applied during (red) or after (blue) the pulsed IR laser (black). (b) Comparison of spatial heating profiles for CW laser (solid red), pulsed laser (dotted green), and pulsed laser with cooled objective (dashed blue).

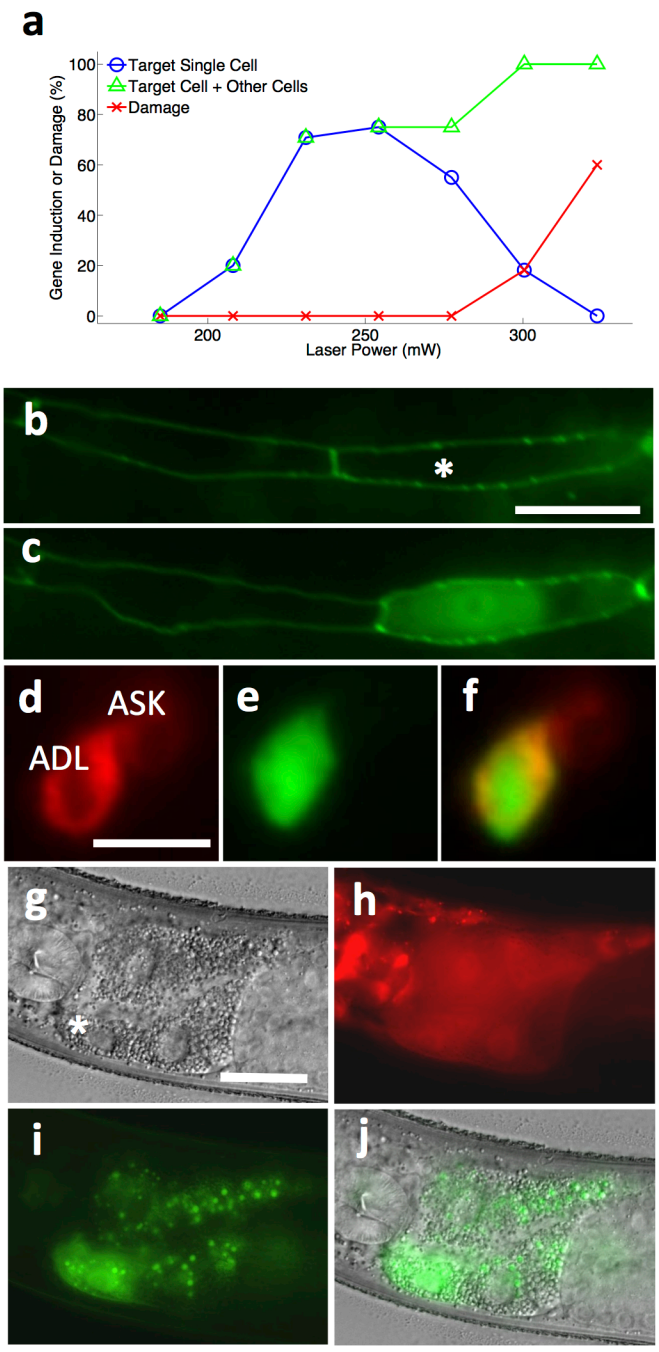

Figure A2.3 Efficient pulsed laser-induced gene expression in *C. elegans* (a) Gene induction and damage rate plotted against laser power for seam cells in L4 animals. Blue circles represent gene expression in only the targeted cell. Green triangles indicate expression in the target cell and other cells. Red crosses indicate cell damage. n > 10 for each point (b) Two seam cells in an L4 animal prior to laser heat shock. White asterisk indicates the targeted cell. Scale bar, 10 µm. (c) The same two seam cells 3 hours after heat shock. Cytoplasmic GFP is visible in only the targeted cell. (d) Single cell GFP expression in neurons of L2 larvae. Red lipophilic DiI stains the cell membranes of amphid neurons. ADL was targeted for heat shock. Scale bar, 5 µm. (e) Cytoplasmic GFP is visible in only ADL 3 hours after HS. (f) Merge of d and e. (g) FLP-coupled gene

expression in a single intestinal cell (white asterisk). Scale bar, 20 μm (h) FRT-flanked mCherry expression (i) GFP induction in the targeted cell (j) Merge of k and m.

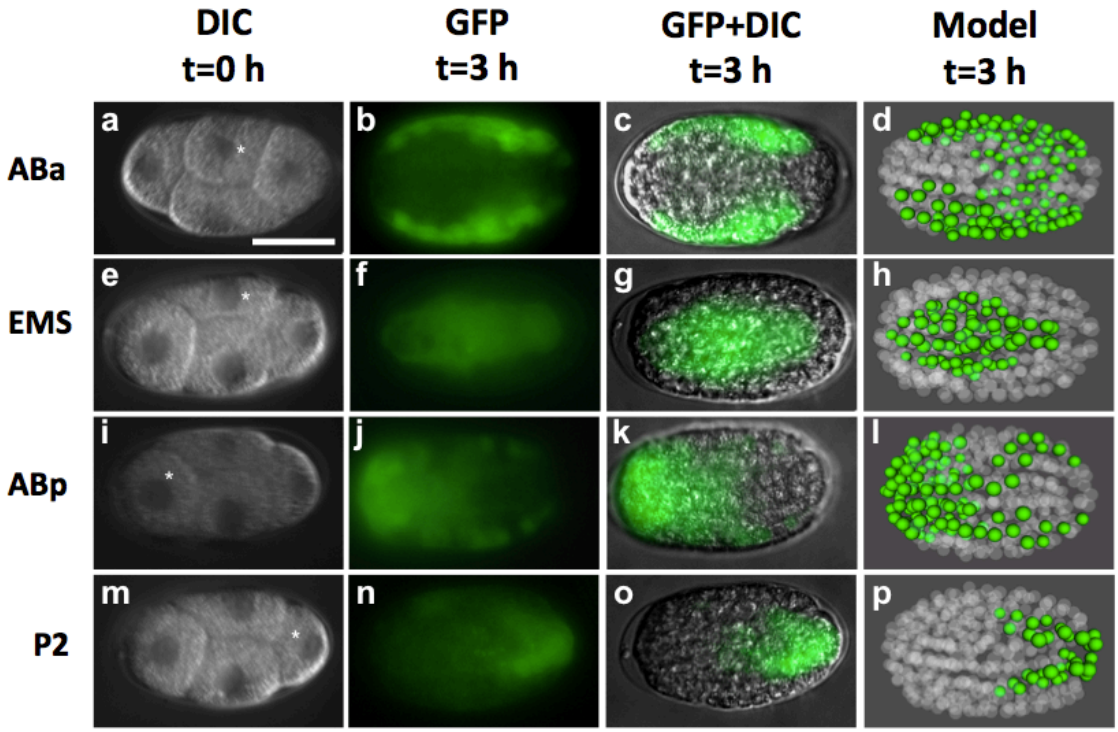

Figure A2.4 Efficient pulsed laser-induced gene expression in the daughters of individual cells in *C. elegans* embryos (a) Four cell stage embryo just prior to laser heat shock with ABp denoted by a white asterisk (b) Cytoplasmic GFP seen in only the descendants of ABp 3 hours after heat shock. (c) Brightfield microscopy image merged with b to show embryo stage. (d) AceTree simulation of an embryo 3 hours after four-cell stage showing the descendants of ABp labeled green. The fluorescence pattern in b and c agree, suggesting only ABp was heat shocked. The same results as for ABp are shown for targeting EMS (e-h), ABa (i-l), and P2 (m-p). White asterisks label the cell targeted for heat shock. All cells were targeted during the four-cell stage for 15 s with pulse repetition frequency of 100 Hz and pulse length of 2.5 ms. The microscope objective was not cooled during these experiments. Scale bar, 20 μm.

SUPPLEMENTARY INFORMATION

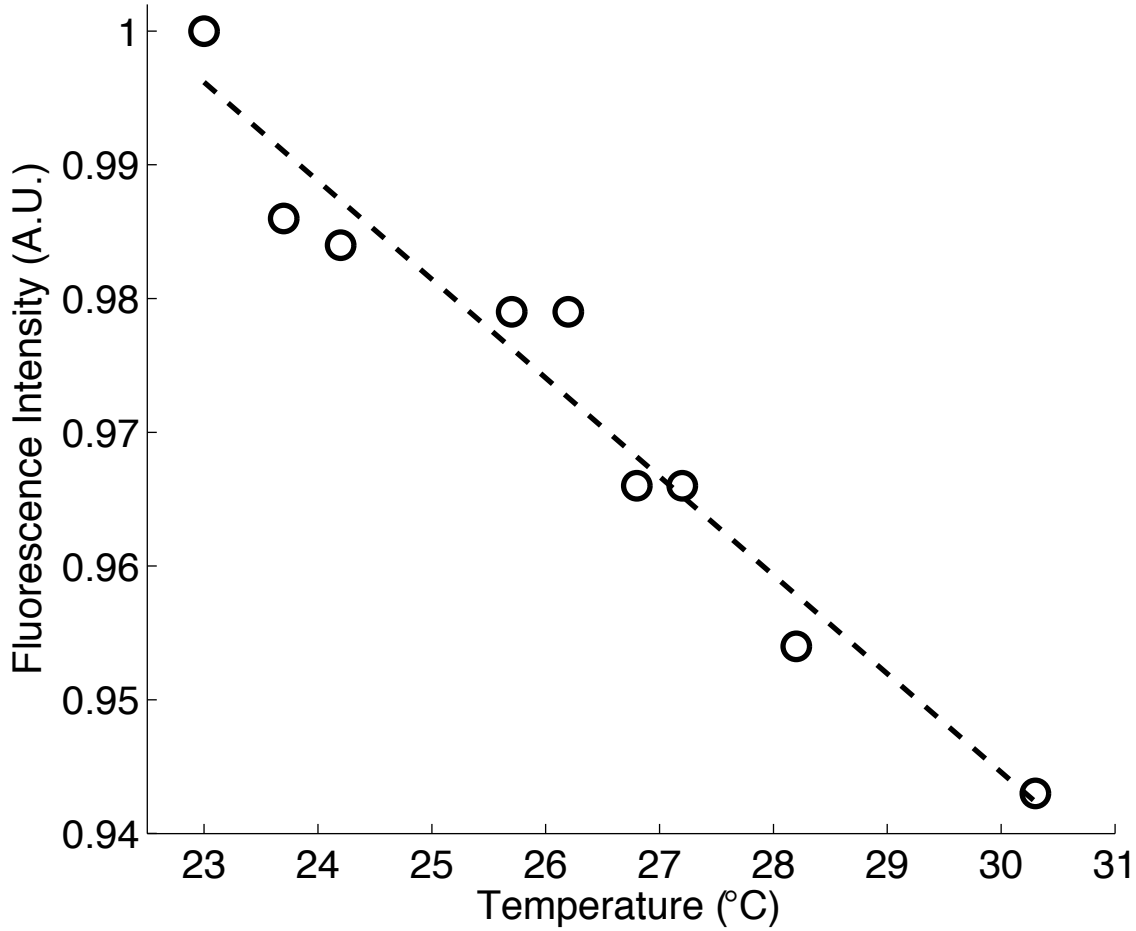

Supplementary Figure A2.S1 Temperature Dependence of GFP-expressing *E. coli*. Fluorescence intensity of GFP (solid black curve) expressed in *E. coli* measured on a thermo-controllable stage decreases linearly. In all calibration experiments we used the fit line, F, to convert changes in fluorescence intensity into temperature changes. The fit (dashed black curve) obeys f = -0.0079t + 1.18, where t is the temperature in °C and f is the fluorescence intensity relative to the fluorescence intensity at 23 °C. The fluorescence temperature dependence measured here is comparable to that previously described[3].

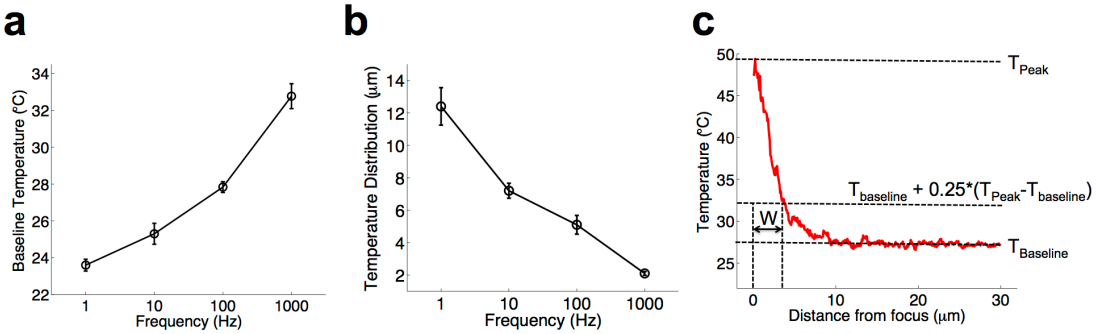

Supplementary Figure A2.S2 Frequency Modulates Baseline Temperature and Width of Spatial Temperature Distribution

The pulse repetition frequency and pulse length modulate the baseline temperature and width of the spatial temperature distribution, with higher repetition frequencies raising the temperature throughout the field of view and shorter pulses narrowing the temperature distribution.

(**a**) Temperature at the laser focus during the laser off state increases with frequency. For a given duty cycle (10%) and laser power, the temperature at the laser focus during the laser off state increased with the pulse repetition frequency. Error bars represent SEM for 3 measurements.

(**b**) Spatial width of temperature decay curve decreases with frequency. We measured the radial distance from the laser focus (peak of the temperature distribution) to the points where the temperature equaled the baseline temperature plus 25% of the difference between the peak and baseline temperatures. This distance decreased with frequency. Error bars represent SEM for 3 measurements.

(**c**) Illustration of how the temperature distribution width W plotted in **b** was calculated.

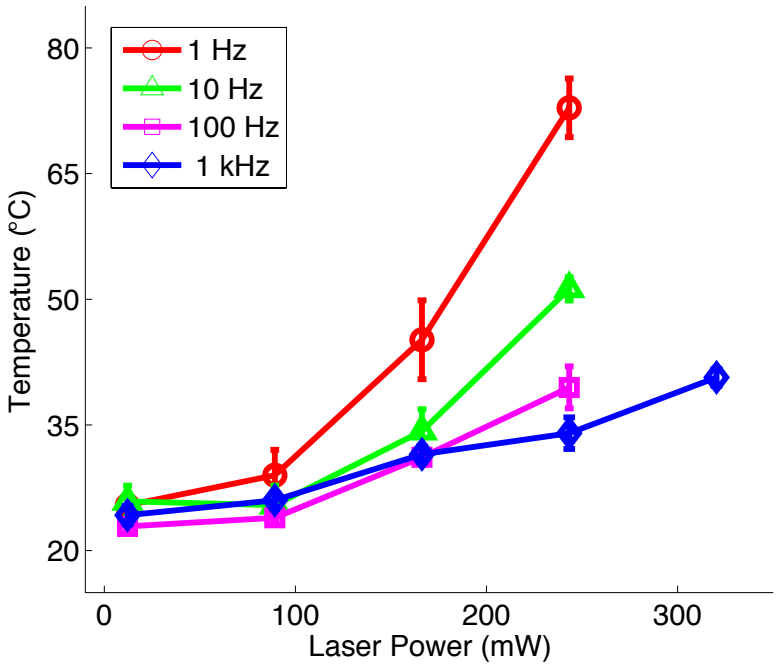

Supplementary Figure A2.S3 Laser Power and Frequency Influence Peak Temperature

The temperature at the laser focus during the pulsed laser on state was measured for a range of laser powers and repetition frequencies while holding the duty cycle at 10%. Temperature curves increase approximately linearly with laser power. As expected, higher frequencies have shallower slopes than lower frequencies, owing to the fact that as frequency increases the laser is on for less continuous time and as a result lower peak temperatures are generated. Error bars represent SEM for 3 measurements.

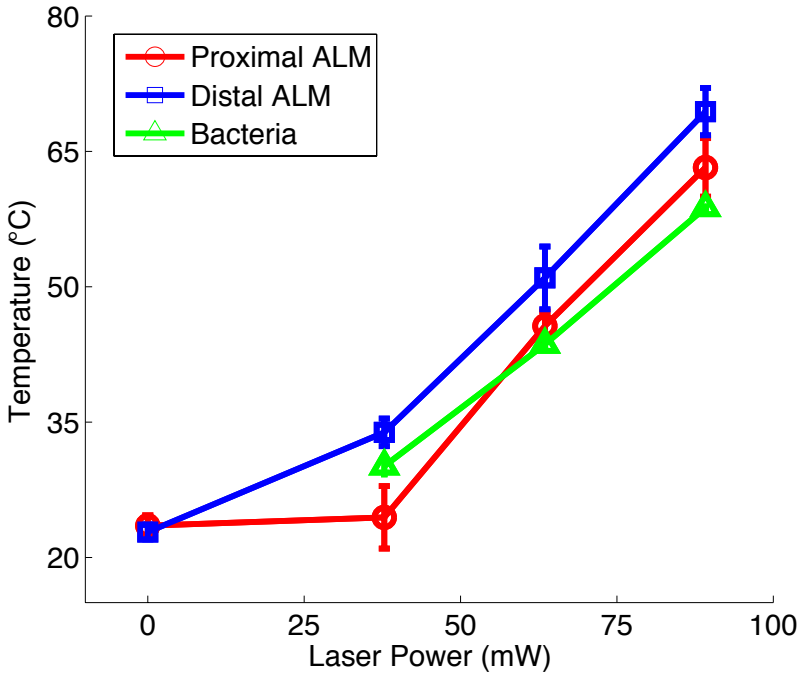

Supplementary Figure A2.S4 Comparison of *in vitro* and *in vivo* temperature shift. The temperature shift was calculated for a continuous wave laser in GFP-expressing *E. coli* (green). *In vivo* temperature shifts were measured using the transgene *mec-7::gfp* which is expressed in the bilateral ALM neurons. Adult hermaphrodites were immobilized and the ALM neurons were targeted with the CW laser. When immobilized, the ALM neurons lie either adjacent (proximal) to the coverslip or adjacent to the mounting pad (distal to the coverslip). Targeting the proximal ALM cell body generated a similar temperature curve as targeting GFP-expressing *E. coli*. Targeting the distal ALM generated slightly higher (5 °C) temperature shifts that we attribute to a heat sinking effect of the glass coverslip. Error bars represent SEM for 3 measurements.

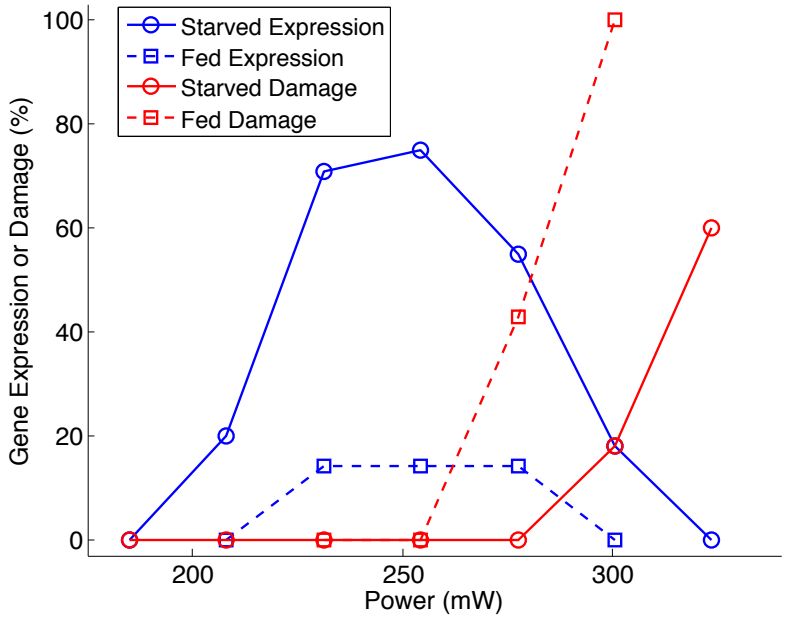

Supplementary Figure A2.S5 Starvation Increases Probability of Single Cell Gene Expression and Increases Damage Threshold

For a range of laser powers we measured GFP induction in seam cells for starved (solid blue curve) and well-fed (dashed blue curve) L4 animals. Starved animals exhibited a much higher rate of GFP induction. Additionally, the rate at which we observed damage seam cells after heat shock was different between starved (solid red curve) and well-fed (dashed red curve) L4 animals. The threshold at which damage became apparent was higher for starved animals then for well-fed animals.

Supplementary Table A2.S1 Gene expression and hatch rate for single cells targeted during four-cell stage

Cell Targeted	GFP induction rate	Hatch rate
Abp	30/31 (96.8%)	23/31 (74.2%)
EMS	20/25 (80.0%)	23/25 (92.0%)
Aba	21/26 (80.8%)	20/26 (76.9%)
P2	7/27 (25.9%)	23/27 (85.2%)

SUPPLEMENTARY TEXT A2.S1

Heat transport during continuous-wave and pulsed laser illumination
The dynamics of the temperature distribution is described by the heat equation with external input:

$$\rho c_p \frac{\partial T}{\partial t} = \kappa \nabla^2 T + P$$

Where ϱ is the density, c_p is the specific heat, $\varkappa$ is the thermal conductivity, and $P(\mathbf{r},t)$ is the heat power deposited by the laser. Suppose $P=0$ outside a small radius r_0.
For **continuous-wave illumination** P is constant. At steady-state (time derivative of temperature is zero) we have

$$T(r,t) = T_0 + \frac{P}{4\pi\kappa r}$$

for $r > r_0$. Therefore the laser-induced temperature shift decreases as the inverse of the radius from the center of the heated region.
For **pulsed illumination**, an infinitely small and short pulse of heat creates a thermal distribution described by the fundamental solution

$$T(r,t) = T_0 + \frac{E}{4\pi\rho c_p (\alpha t)^{3/2}} e^{-r^2/4\alpha t}$$

where

$$\alpha = \frac{\kappa}{\rho c_p}$$

is the thermal diffusivity and E is the total energy deposited by the pulse:

$$E = \int_{\text{pulse}} P dt$$

Therefore in pulsed illumination the laser-induced temperature shift decreases exponentially with the square of the distance to the heat source.

APPENDIX III: Construction of a system for single-cell transgene induction in *Caenorhabditis elegans* using a pulsed infrared laser

Matthew A. Churgin[*], Liping He[*], John I. Murray[†], and Christopher Fang-Yen[*‡]

*Department of Bioengineering, School of Engineering and Applied Sciences, University of Pennsylvania, Philadelphia, Pennsylvania 19104

[†]Department of Genetics, Perelman School of Medicine, University of Pennsylvania, Philadelphia, Pennsylvania 19104

[‡]Department of Physics, Korea University, Anam-dong, Seongbuk-gu, Seoul 136-701, South Korea

This appendix is a slightly modified version of an article that was originally published in *Methods* (Churgin et al. 2014). Liping He performed FLP rescue experiments and embryo heat shock experiments. John Murray helped with conceiving the project, analyzing data, drafting and revising the manuscript. Chris Fang-Yen helped with conceiving the project, planning experiments, constructing the custom microscope, analyzing data, drafting and revising the manuscript.

ABSTRACT

The spatial and temporal control of transgene expression is an important tool in *C. elegans* biology. We previously described a method for evoking gene expression in arbitrary cells by using a focused pulsed infrared laser to induce a heat shock response (Churgin *et al* 2013). Here we describe detailed methods for building and testing a system for performing single-cell heat shock. Steps include setting up the laser and associated components, coupling the laser beam to a microscope, and testing heat shock protocols. All steps can be carried out using readily available off-the-shelf components.

Highlights

1. **We describe methods for construction of a system for single-cell transgene induction in *C. elegans***
2. **We use a pulsed infrared diode laser to heat a single cell**
3. **The system is built from only off-the-shelf components**

Keywords

***C. elegans*, transgenes, heat shock, lasers**

INTRODUCTION

The goal of this protocol is to modify a microscope so that an external infrared laser is coupled through the microscope objective for the purpose of inducing heat shock in single cells of embryonic, larval, or adult *C. elegans*. The basic design of the system is

shown in Fig. A3.1. A fiber-coupled infrared diode laser is operated in a pulsed laser mode using a laser driver and pulse generator. The laser beam exits the fiber, is collimated by a lens, and enters through the rear of the objective lens of a microscope after reflecting from a dichroic filter. The objective focuses the laser beam to a sub-micron-sized focused spot at the sample plane. Some of the laser light is absorbed by water or other molecules in the targeted cell, causing the local temperature to rise. The use of a pulsed laser allows targeting with higher spatial resolution than possible with continuous-wave illumination, as described previously (Churgin et al. 2013).

First, we discuss the laser, microscope, and components and procedures necessary to align the two with respect to one another. Next, we describe calibration of the laser beam and steps for optimizing the laser heating protocol for specific cell types. Optional modifications, such as objective or sample cooling, can also be made to optimize spatial resolution.

Before beginning work with any lasers, ensure that users have completed all appropriate laser safety training and that any relevant safety equipment including protective eyewear and/or laser curtains has been obtained. Invisible infrared laser radiation poses a particular hazard. Infrared viewing cards (e.g. Thorlabs VRC2) can be used to visualize laser beam position and size. Use of an optical power meter (e.g. Coherent LaserMate) is recommended to measure laser power propagating at different locations in the optical setup.

CONSTRUCTION OF THE APPARATUS

Selection and modification of the microscope

The primary considerations when selecting a microscope for single-cell heat shock are (1) compatibility with imaging methods for targeting the appropriate cell(s), and (2) access to the back aperture of the microscope objective. The laser beam will enter from outside the microscope itself and the collimated beam will be directed into the back aperture of the objective via a dichroic mirror. We used a Nikon TE2000 inverted microscope in which the sample stage and objective turret was raised by 60 mm using a Nikon T-BSUK stage height adjustment kit. The dichroic mirror was positioned at a 45° angle under the microscope objective using Thorlabs posts and positioners. Alternatively, the dichroic can be mounted within a fluorescence filter cube and placed within a filter cube turret (either a previously existing one or another mounted above or below the first).

To couple a laser into Leica microscopes including the DMI and DM series, custom filter cubes are available (W. Nuhsbaum Inc., McHenry IL) for coupling lasers into the objective from a direction 90 degrees from the fluorescence illumination pathway. For other types of microscopes, consult manufacturer representatives to discuss strategies for laser coupling. The considerations discussed here are nearly identical to those which appear when designing a system for laser surgery (Fang-Yen et al. 2012) or optical trapping (Neuman and Block 2004). Optical configurations for coupling to older finite tube length microscopes are also available (Bargmann and Avery 1995).

Regardless of strategy for coupling the laser into the microscope, ensure that the dichroic is mounted in a stable manner and that the reflective side of the dichroic is facing the objective. The microscope should be safely secured to an optical table or breadboard before attempting to align the laser. This can be done by surrounding the feet of the microscope by optical bases (e.g. Thorlabs BA series) and mounting them to the breadboard.

It is important that the laser fiber mount, lens, dichroic mirror, and microscope are fixed in position with respect to one another. Shifting of the optical components, even by a very small amount, will require time-consuming realignment.

Laser selection and setup

Infrared light generates heat in biological tissue primarily through absorption by water in the tissue. Therefore, to maximize the temperature increase attainable for a given laser power the wavelength of the infrared laser should be chosen to be efficiently absorbed by water. We used a laser with 1465 nm wavelength, at which the absorption coefficient of water (Kou, Labrie, and Chylek 1993) is approximately α=31.6 cm^{-1}. That is, radiation at this wavelength will be attenuated by factor of 1/e upon propagation through water over the absorption length $1/\alpha = 316\ \mu m$. (By comparison, the absorption length of water is 0.44 m at λ=800 nm and 3.75 m at λ =600 nm.)

We used a Fitel FOL1425RUZ-317 fiber-coupled diode laser module with 1465 nm wavelength, maximum drive current 1750 mA, and maximum power 400 mW. This laser diode module, which was designed as a pump laser for fiber amplifiers, was purchased from Lightwavestore (Ottawa, Ontario, Canada) with an FC/PC fiber optic connector and a short length of SMF-28 optical fiber (Corning) attached via fusion splice to the fiber end. Great care must be taken to avoid contact of any object with the fiber end, which is easily fouled or damaged. The fiber end can be cleaned with ethanol and lens tissue. The laser module contains an integrated thermoelectric cooler (TEC) and thermometer for temperature control. We installed the laser module into a 14-pin butterfly laser diode mount (Thorlabs LM14S2) according to the manufacturer's instructions.

The laser diode mount contains two connectors, one for a laser diode driver and one for a temperature controller. We connected the diode mount to a laser diode driver (Opto Power OPC-PS03-A) and connected the temperature controller mount to a temperature controller (Thorlabs TEC2000), both via cables with DB9 connectors on both ends. Nearly any other laser diode driver and/or thermoelectric controller capable of supplying sufficient currents would also suffice. The laser diode temperature should be set according to manufacturer recommendations. The laser power can be adjusted by controlling the output current. If an optical power meter is available, calibrate the power vs. current curve and compare with the specifications. To maximize lifespan of the laser diode, use only the minimum current necessary to achieve optical trapping and/or the desired level of heating.

To control the pulse repetition rate (frequency) and pulse duration of the laser, we used a pulse generator (Stanford Research Systems DG535). We set the trigger frequency to be the pulse frequency, "A delay" to be 0 ms, "B delay" to be the pulse duration, and then used the "AB" output configured to produce 5V high outputs to control the laser diode driver through the external input BNC connector. Pulse outputs can be monitored on an oscilloscope (optional). For applications where larger heated regions (>3μm) are acceptable the laser can be driven continuously (continuous wave, CW) in which case the pulse generator is not required. In addition, use the laser in CW mode during alignment procedures.

Coupling the laser beam to the microscope

We attached the FC connector at the fiber end to a Thorlabs SM1FC adapter which was mounted on an X-Y translatable stage to aid beam alignment (Thorlabs ST1XY-S). All optical components should be mounted on optical posts, post holders, and bases (e.g. Thorlabs TR4, PH4, BA2) secured to an optical table or optical breadboard (e.g. Thorlabs).

Turn the laser on with low power and use an infrared reader card to visualize the beam by placing the card near (but not touching) the fiber tip. You should see the beam profile on the card. As you move the IR card away from the fiber tip the beam profile should expand because the beam diverges upon exiting the fiber.

If the microscope is an infinity-corrected system, the laser beam needs to be nearly collimated (neither diverging nor converging) when it enters the microscope objective in order to produce a focus coincident with the image plane. Therefore, a collimating lens should be inserted between the output of the fiber-coupled laser and the dichroic mirror. The focal length of the required lens is given by $f = r/\tan(\theta)$, where r is the radius of the objective's back aperture and θ is the beam divergence angle. The beam divergence angle is specified by the numerical aperture of the optical fiber NA = sin θ, equal to 0.13 for SMF-28 fiber; this corresponds to the angle from the optical axis at which the beam's power is 5% of the maximum. We used a plano-convex lens with f = 75 mm (Thorlabs). The back aperture of the objective was 1 cm wide.

The collimating lens should be mounted on a linear translation stage (e.g. Thorlabs) oriented in the Z direction so that fine adjustments can be made to the beam collimation. Secure the linear translation stage to the table/breadboard so that the collimating lens is approximately one focal length away from the fiber tip. Align the lens and the fiber tip to be at the same height. Turn the laser on at low power and visualize the beam with the IR card at various distances. The beam should not diverge after passing through the collimating lens. Adjust the Z-translation stage so that the beam diameter remains constant as the IR card moves away or toward the lens.

Before entering the microscope, the laser beam can be routed to the appropriate position using one or more mirrors (e.g. Thorlabs BB1-E04) mounted on mirror mounts (e.g.

Thorlabs KM100). The use of such mirrors provides easily manipulated degrees of freedom which can aid in alignment of the beam with respect to the microscope.

The dichroic mirror which couples the laser beam into the objective needs to efficiently reflect the infrared laser wavelength while passing visible wavelengths to allow for simultaneous laser heating and imaging of the sample by brightfield, DIC, or fluorescence microscopy. We used a shortpass dichroic mirror (Thorlabs DMSP1000R) positioned under the microscope objective and oriented at a 45 degree angle with respect to the incoming beam.

Optimal focus of the infrared beam requires a high numerical aperture objective (NA>1). We used an oil-immersion Nikon CFI 100X Plan Fluor (NA 1.3) objective.

For initial alignment of the laser into the microscope, remove the objective and use an IR viewing card to position the laser beam at the center of the objective mount. Adjust the beam position and direction using adjustment knobs on the optomechanical components between the laser and objective.

Next, switch to a low magnification objective (e.g. 5-10X). Attach the IR card to the front of the objective using tape. Adjust the X-Y translators on the fiber mount and collimating lens to maximize the amount of IR light transmitted through the objective. Periodically move the IR card away from the objective to ensure the light is not exiting the objective at an angle relative to the objective axis. If light is not exiting

perpendicularly from the objective axis, ensure that (i) The dichroic mirror is oriented at 45° and (ii) The fiber mount and/or collimating lens are directed along the axis toward the dichroic mirror. If either requirement is not met it may be difficult to achieve optical trapping and thus visualize the laser beam focus. Repeat this alignment procedure with the higher magnification, high NA objective until the light transmitted is maximized through the desired objective.

Location of the laser focus

Precise location of the focused laser beam is critical for aligning the laser and for accurate targeting of single cells. Since infrared radiation at 1.45 μm is invisible both to the human eye and to nearly all imaging sensors, another method of visualizing the focused beam is needed. We used optical trapping to locate the position of the infrared laser focus and thus test how well the laser is coupled into the objective. Briefly, optical trapping is a method whereby a tightly focused laser beam generates forces that can trap small objects located at the focus of the laser (Neuman and Block 2004). A weakly focused laser beam cannot generate sufficient forces for optical trapping, so the ability to trap small objects, such as 1 μm diameter polystyrene beads, is a good metric to judge the quality of laser coupling.

To create a suspension of polystyrene beads for visualization of optical trapping, dilute a 2.5% solution of 1 μm beads (Polysciences 07310-15) by a factor of 10 in water. 1 mL of this stock solution should last for at least one month when kept at 4°C. Mount the

bead suspension on the microscope on a slide outfitted with a coverslip using plastic shim stock (McMaster-Carr 9513K57) or glass coverslips as spacers. When the laser is off the beads will undergo rapid random Brownian motion due to thermal fluctuations. When the laser is turned on (in continuous-wave mode) and properly aligned, beads away from the focus should begin moving more rapidly due to heat-driven convection, while a single bead near the laser focus will become trapped and nearly stationary at the laser focus (Fig. A3.5).

Starting with the laser at zero current, slowly increase the current until you can see the polystyrene beads moving faster due to the laser-induced temperature increase. Slowly move the sample stage. Most beads will move along with the stage. Look for a bead that remains fixed in the field of view as the sample stage moves. This bead is trapped at the laser focus. If you cannot find a trapped bead, adjust the collimating lens Z-translation stage by 5-10 microns and repeat. If the laser beam is not sufficiently collimated, either (i) the beam focused by the objective may not be tight enough to trap the beads or (ii) the beam may be focused at a plane away from the objective's focal plane.

Monitor the laser current and/or power required to achieve optical trapping. This gives an indirect measure of laser transmission through the objective: if the beam is poorly aligned with the objective back aperture, some fraction will be lost and a greater total power will be required for trapping.

Adjust the laser beam lateral position to bring the focus near the center of the field of view. If the trapped bead does not appear to be in focus, the collimation of the laser beam can be adjusted to bring it into the focal plane. Note that adjusting the microscope focus knob cannot be used to focus on the trapped bead, since the optical trap location moves with the objective.

Once optical trapping is observed, capture an image on the camera attached to the microscope. Record the pixel location of the trapped bead to represent the location of the laser focus. This can be done by marking a position via the camera software, or by using a fine permanent marker to mark the bead's position on the computer screen displaying the image. For the latter, do not move or resize the image window. The mark can be removed using ethanol.

Optional sample cooling

Cooling the sample by 5-10º C improves the spatial selectivity of the heat shock induction (Churgin et al. 2013). Commercial sample cooling devices are available from several vendors including Physitemp, Microptik, and Instec. We used a simple method in which cool water was circulated through flexible plastic laboratory tubing (Tygon, 1/4" diameter) wrapped around the objective lens (Fig. A3.4), which is thermally coupled to the sample via the immersion oil. Cool water was provided by a digital temperature-controlled water circulator (Brookfield).

CALIBRATION AND TESTING OF LASER HEAT SHOCK

Calibrating the laser-induced temperature increase

In order to choose the appropriate laser power for a given application it is important to determine the relationship between laser current and/or power and the induced temperature change. The decrease in GFP fluorescence with temperature can be used to measure the laser-induced temperature shift (Kamei et al. 2008). GFP-expressing *E. coli* (available from the Caenorhabditis Genetics Center) can be used to generate a uniform layer of GFP for quantification of fluorescence changes.

Smear a clump of GFP-expressing *E. coli* with a platinum wire pick onto an agarose pad. Let the pad air dry for 10-15 minutes. When the coverslip is placed on the pad, it should stick firmly and not slide around. Place the microscope slide containing the pad and *E. coli* on the microscope and locate a region of relatively uniform bacterial density using a GFP filter. Capture a fluorescence image with the laser off. Turn the laser on and record a second image, being sure not to move the field of view or change any image acquisition parameters. Using an image analysis program (we use MATLAB) quantify the fluorescence in a small region of interest (~1 μm x 1 μm) at the laser focus by summing up the intensity values in the ROI. Divide the measured quantity attained during the laser-on image by that attained during the laser-off image, and the resulting ratio will be a measure of the decrease in fluorescence intensity. The fluorescence relative to baseline should approximately obey the relationship f=-0.0079T + 1.18, where T is the temperature in degrees Celsius (Churgin et al. 2013). This equation can be used to

convert relative fluorescence decrease into temperature shift. This calculation can be repeated for multiple laser powers to generate a curve for peak temperature vs. laser power and/or current.

It is also possible to measure temperature changes during pulsed laser illumination. This requires a blue LED (for GFP illumination) to be pulsed at different phases with respect to the pulsed infrared illumination. This can be done by configuring the pulse generator to generate two pulse trains, with the first pulse train governing the infrared illumination and the second pulse train governing the blue LED illumination via the LED drive electronics. Shifting the delay of blue LED illumination relative to pulsed infrared heating enables measurements of temperature while the laser is in the on or off state.

Performing laser heat shock in larval or adult C. elegans

To assess heat shock in single cells, we used the strain ST66 (hsp-16.2::GFP (Kamei et al. 2008)). Immobilize up to 10 worms on a 1 mm-thick 10% agarose pad and 0.05-0.1μm diameter polystyrene beads (E. Kim et al. 2013). Do not allow worms to remain immobilized on the pad for longer than necessary; about an hour should be the limit. During experiments, all slides should contain control (mock-treated) worms.

Mount the slide on the microscope. For each worm, center the target at the laser focus and turn the laser on for the duration required. During experiments, the pulsed laser was turned on or off by enabling and disabling the laser driver. We used laser heat shock

times in the range of 1-5 minutes for larvae and adult worms. Recover the worms to seeded NGM plates. Check gene induction after 3 hours or as needed. We find GFP fluoresence is usually visible within 3 hours and is maximum between 8 and 12 hours after heat shock. Note any reduced viability in experiment and control animals.

Laser heat shock of C. elegans embryos

Mount embryos according to the protocol described by Bao and Murray (Bao and Murray 2011). Mount embryos slightly younger than the stage at which you would like to heat shock. All slides should contain control (mock-treated) embryos. For each embryo, center the target at the laser focus and turn the laser on for the duration required. We used laser heat shock times in the range of 10-20 seconds for embryos. We noticed that heating for longer durations, even at very low laser power, resulted in a high probability of embryos arresting. Onset of gene induction will depend on the stage at which embryos are heated. Check for gene induction after 1 hour. Note any embryonic arrests or reduced viability in experiment and control animals.

Optimization of laser heat shock protocols

Several parameters can be varied to optimize heat shock response in the targeted cells: (i) laser power, (ii) pulse duration, (iii) frequency of laser pulses, and (iii) total duration of pulsed laser illumination. Modulating these parameters provides some flexibility in the characteristics of heat shock experienced by the targeted cell.

Increasing laser power will increase the peak temperature at the laser focus. Decreasing the pulse duration will yield finer spatial resolution of heat shock as more time is introduced between pulses for thermal energy to dissipate. Increasing the laser frequency will raise the baseline temperature but enable the use of shorter pulse durations.

If laser heat shock yields no observable gene induction, we recommend first increasing the laser power in 10% increments. If gene expression is not confined to the desired region we recommend then taking steps to limit the spatial extent of heating, such as decreasing the pulse duration or employing sample cooling. Once these steps are taken it may be necessary to then increase the laser power and/or heat shock duration, as shorter pulses or sample cooling will reduce the peak temperature at the laser focus. Through iteration one can achieve a range of peak temperatures with a range of spatial resolutions. For larvae or adult worms we recommend starting with heat shock durations in the range of 3-5 minutes. For embryos we recommend starting with heat shock durations in the range of 10-20 seconds.

SUMMARY

We have presented a protocol for adapting a microscope for pulsed laser heat shock, and for using it to induce transgene expression in single *C. elegans* cells. We have tested these methods for turning on GFP expression in several cell types including neurons, seam cells, and intestinal cells (Churgin et al. 2013). However, we expect that researchers will adapt the methods for expressing arbitrary constructs within arbitrary

cell(s) of interest. We also anticipate that our method will be readily extensible to other model systems including *Drosophila*, zebrafish, and cultured cells.

ACKNOWLEDGMENTS

Some strains were provided by the Caenorhabditis Genetics Center, which is funded by NIH Office of Research Infrastructure Programs (P40 OD010440). C. F.-Y. was supported by NIH, Ellison Medical Foundation, and the Alfred P. Sloan Research Foundation. J.I.M. was supported by the NIH (GM083145), by the Penn Genome Frontiers Institute, and by a grant from the Pennsylvania Department of Health, which disclaims responsibility for any analyses, interpretations, or conclusions.

FIGURES

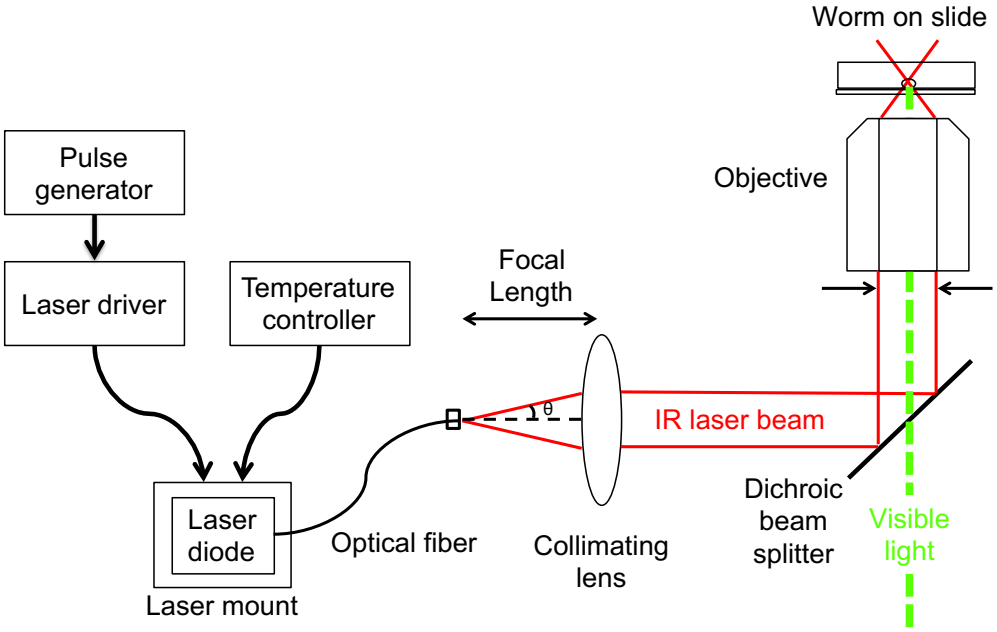

Figure A3.1 Experimental Setup. An infrared laser controlled by a laser driver and pulse generator is directed into the back aperture of a microscope objective and induces local heating in *C. elegans*.

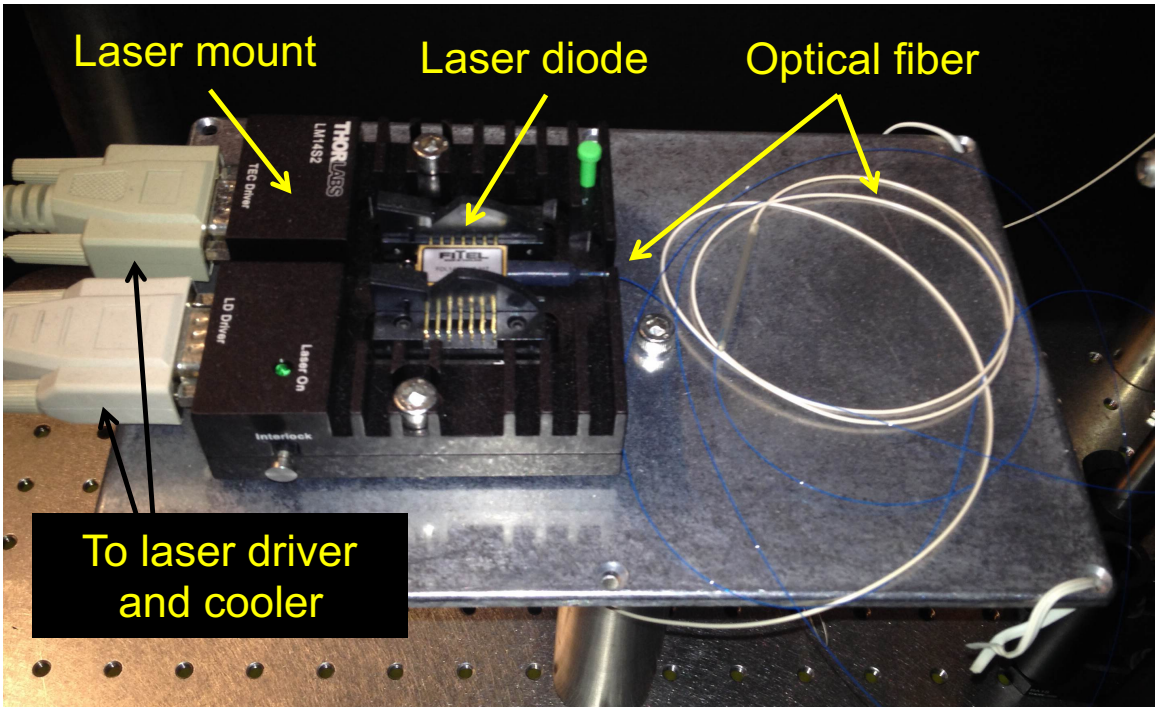

Figure A3.2 Laser setup**.** A fiber-coupled infrared diode laser with 1465 nm wavelength and integrated thermoelectric cooler.

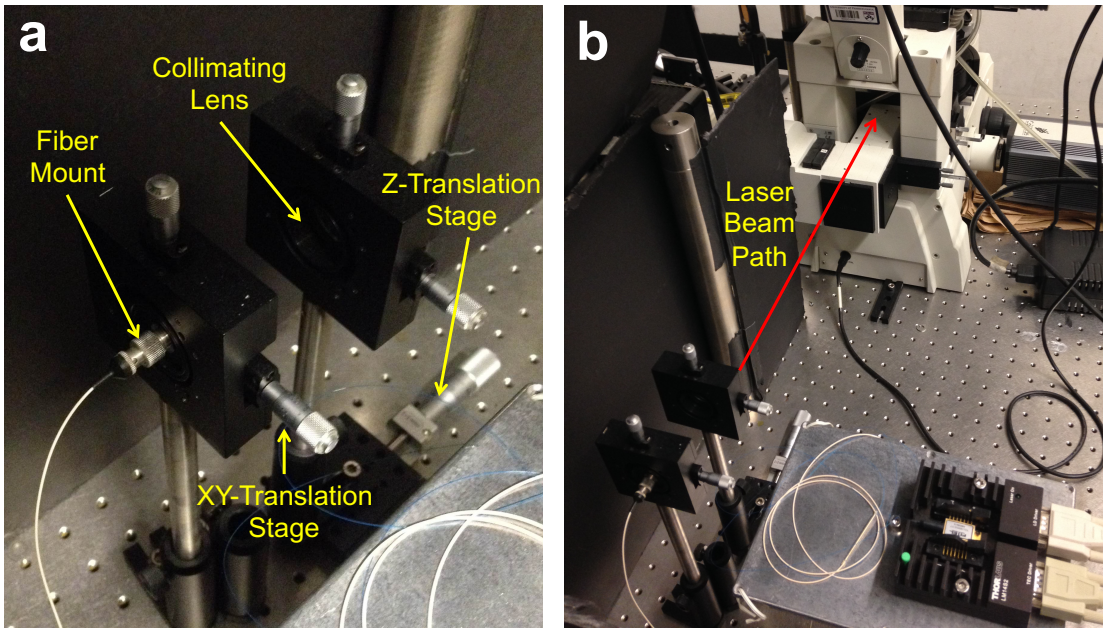

Figure A3.3 a. Fiber-to-free space launch setup including translation stages for fine adjustments. b. Beam path showing back of microscope.

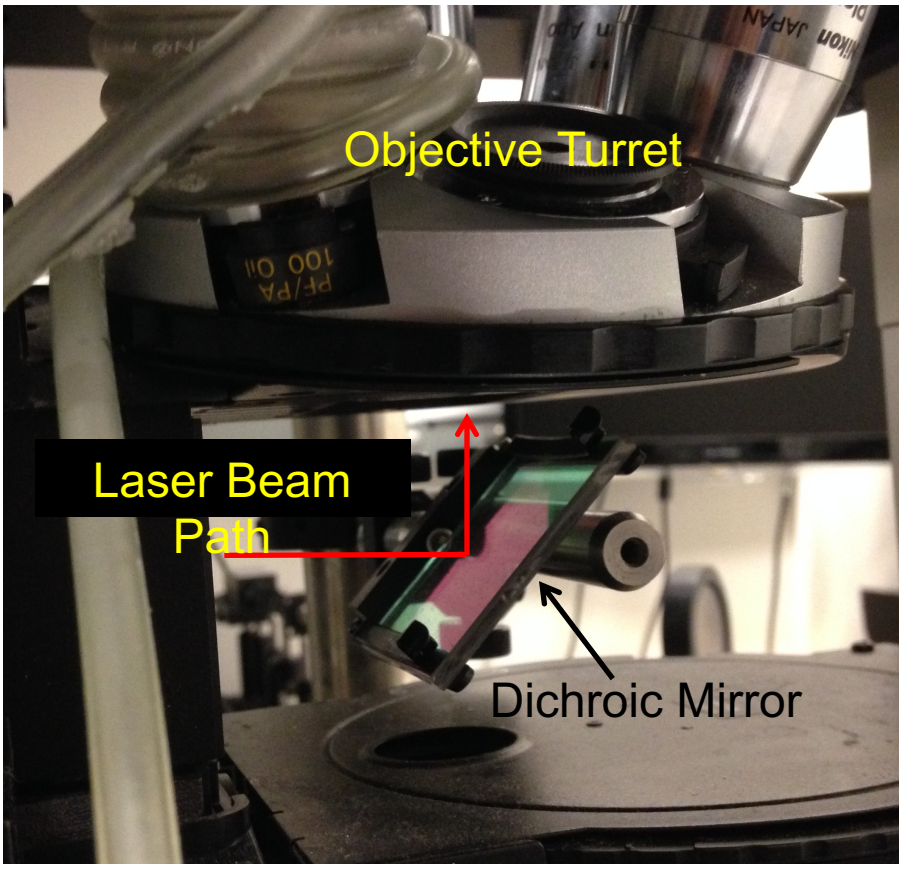

Figure A3.4 Dichroic mirror positioned under raised objective lens reflects IR laser into objective and transmits visible light.

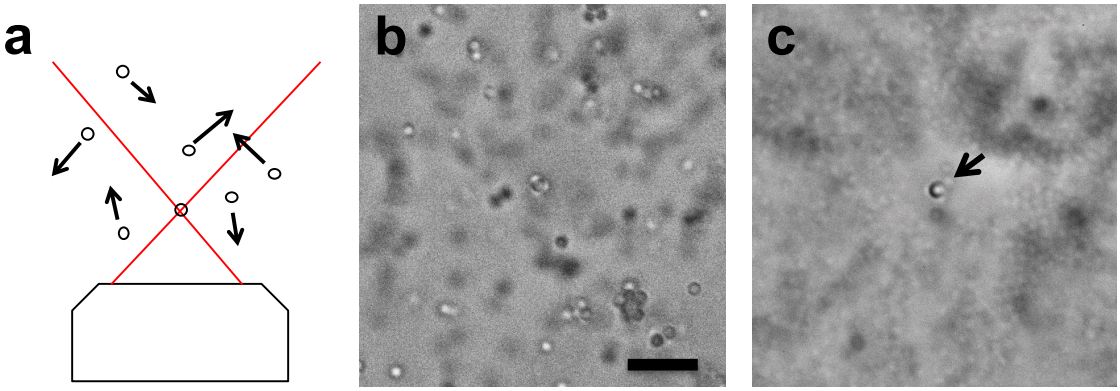

Figure A3.5 Visualizing the laser focus using optical trapping. a) Optical trapping of one bead. Untrapped beads undergo random Brownian movement. b) Bright field image of 1 μm diameter polystyrene beads. Scale Bar: 5 μm c) Long exposure image of the same beads with the infrared laser enabled. A single bead is trapped at the laser focus (arrow). Untrapped beads are blurred due to long exposure time.

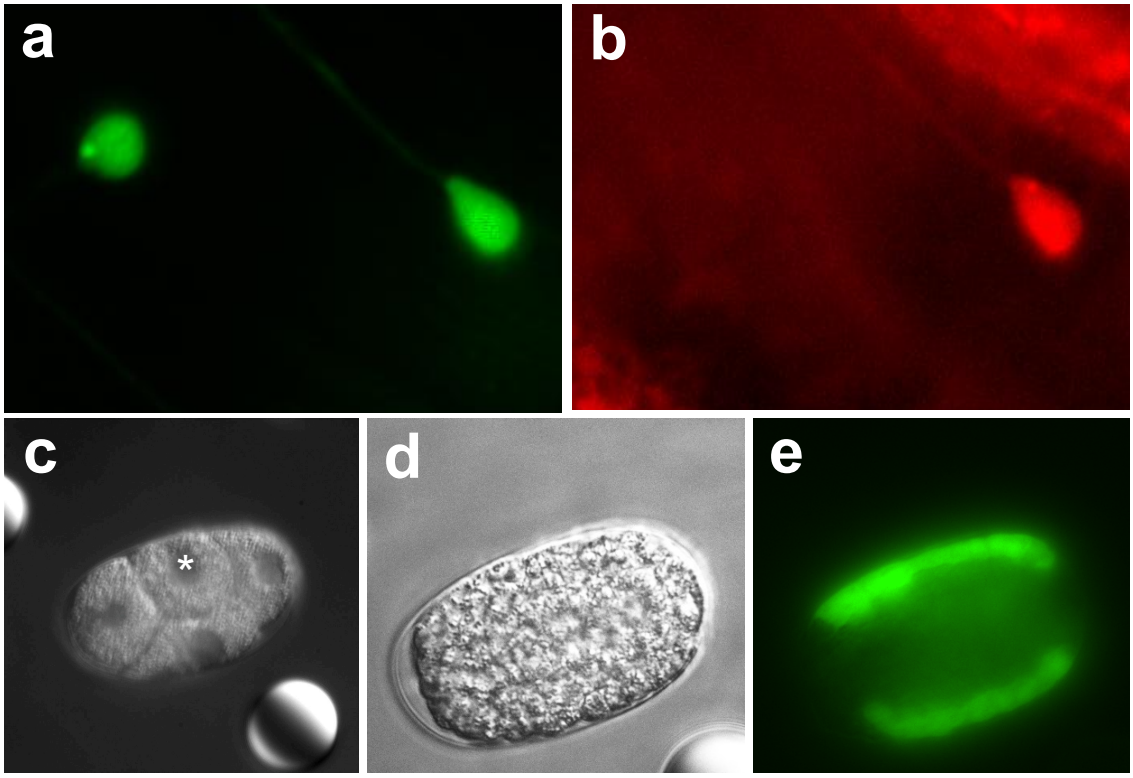

Figure A3.6 Single-cell gene induction using pulsed laser heat shock. a) Mechanosensory neurons ALM and AVM expressing GFP. Scale bar: 10 μm b) Heat shock induction of RFP in ALM only (same field of view as panel a). c) f) DIC image of a 4-cell stage embryo before heat shock to ABp (asterisk). d) Same embryo 2-3 h later. e) GFP induced in the daughters of ABp.

REFERENCES

Abdus-Saboor, Ishmail, Vincent P Mancuso, John I Murray, Katherine Palozola, Carolyn Norris, David H Hall, Kelly Howell, Kai Huang, and Meera V Sundaram. 2011. "Notch and Ras Promote Sequential Steps of Excretory Tube Development in C. Elegans." *Development (Cambridge, England)* 138 (16): 3545–55. doi:10.1242/dev.068148.

Ackerman, Daniel, and David Gems. 2012. "The Mystery of C. Elegans Aging: An Emerging Role for Fat: Distant Parallels between C. Elegans Aging and Metabolic Syndrome?" *BioEssays* 34 (6): 466–71. doi:10.1002/bies.201100189.

Aguzzi, Adriano, and Tracy O'Connor. 2010. "Protein Aggregation Diseases: Pathogenicity and Therapeutic Perspectives." *Nature Reviews. Drug Discovery* 9 (3). Nature Publishing Group: 237–48. doi:10.1038/nrd3050.

Ailion, M, T Inoue, C I Weaver, R W Holdcraft, and J H Thomas. 1999. "Neurosecretory Control of Aging in Caenorhabditis Elegans." *Proceedings of the National Academy of Sciences* 96 (June): 7394–97. doi:10.1073/pnas.96.13.7394.

Alkema, Mark J., Melissa Hunter-Ensor, Niels Ringstad, and H. Robert Horvitz. 2005. "Tyramine Functions Independently of Octopamine in the Caenorhabditis Elegans Nervous System." *Neuron* 46 (2): 247–60. doi:10.1016/j.neuron.2005.02.024.

An, Jae Hyung, and T Keith Blackwell. 2003. "SKN-1 Links C. Elegans Mesendodermal Specification to a Conserved Oxidative Stress R Esponse." *Genes & Development* 17: 1882–93. doi:10.1101/gad.1107803.Maduro.

Andrews, Matthew T. 2007. "Advances in Molecular Biology of Hibernation in Mammals." *BioEssays* 29 (5): 431–40. doi:10.1002/bies.20560.

Apfeld, J, and C Kenyon. 1999. “Regulation of Lifespan by Sensory Perception in Caenorhabditis Elegans.” *Nature* 402 (6763): 804–9. doi:10.1038/45544.

Apfeld, Javier, Greg O’Connor, Tom McDonagh, Peter S DiStefano, and Rory Curtis. 2004. “The AMP-Activated Protein Kinase AAK-2 Links Energy Levels and Insulin-like Signals to Lifespan in C. Elegans.” *Genes & Development* 18 (24): 3004–9. doi:10.1101/gad.1255404.

Avery, L. 1993. “The Genetics of Feeding in Caenorhabditis Elegans.” *Genetics* 133 (4): 897–917.

Avery, Leon, and Young-Jai You. 2012. “C. Elegans Feeding.” *WormBook: The Online Review of C. Elegans Biology*, 1–23. doi:10.1895/wormbook.1.150.1.

Bacaj, Taulant, and Shai Shaham. 2007. “Temporal Control of Cell-Specific Transgene Expression in Caenorhabditis Elegans.” *Genetics* 176 (4): 2651–55. doi:10.1534/genetics.107.074369.

Bais, Swarna, Matthew A. Churgin, Christopher Fang-Yen, and Robert M. Greenberg. 2015. “Evidence for Novel Pharmacological Sensitivities of Transient Receptor Potential (TRP) Channels in Schistosoma Mansoni.” *PLOS Neglected Tropical Diseases* 9 (12): e0004295. doi:10.1371/journal.pntd.0004295.

Bansal, Ankita, Lihua J. Zhu, Kelvin Yen, and Heidi A. Tissenbaum. 2015. “Uncoupling Lifespan and Healthspan in Caenorhabditis Elegans Longevity Mutants.” *Proceedings of the National Academy of Sciences* 112: E277–86. doi:10.1073/pnas.1412192112.

Bao, Zhirong, and John I Murray. 2011. “Mounting Caenorhabditis Elegans Embryos for Live Imaging of Embryogenesis.” *Cold Spring Harbor Protocols* 2011 (9).

doi:10.1101/pdb.prot065599.

Bargmann, Cornelia I. 2006. “Chemosensation in C. Elegans.” *WormBook: The Online Review of C. Elegans Biology*, 1–29. doi:10.1895/wormbook.1.123.1.

Bargmann, Cornelia I, and Leon Avery. 1995. “Laser Killing of Cells in Caenorhabditis Elegans.” In *C Elegans: Modern Biological Analysis of an Organism*, 225–50. Academic Press.

Bargmann, Cornelia I, and H Robert Horvitz. 1991. “Chemosensory Neurons with Overlapping Functions Direct Chemotaxis to Multiple Chemicalsin C. Elegans,” *Neuron* 7:729-742.

Barzilai, Nir, Derek M Huffman, Radhika H Muzumdar, and Andrzej Bartke. 2012. “The Critical Role of Metabolic Pathways in Aging.” *Diabetes* 61 (6): 1315–22. doi:10.2337/db11-1300.

Baur, Joseph a, Kevin J Pearson, Nathan L Price, Hamish a Jamieson, Carles Lerin, Avash Kalra, Vinayakumar V Prabhu, et al. 2006. “Resveratrol Improves Health and Survival of Mice on a High-Calorie Diet.” *Nature* 444 (7117): 337–42. doi:10.1038/nature05354.

Baur, Joseph A, Zoltan Ungvari, Robin K Minor, David G Le Couteur, and Rafael de Cabo. 2012. “Are Sirtuins Viable Targets for Improving Healthspan and Lifespan?” Nature Publishing Group, 1–19. http://dx.doi.org/10.1038/nrd3738.

Belfer, Samuel J, Han-Sheng Chuang, Benjamin L Freedman, Jinzhou Yuan, Michael Norton, Haim H Bau, and David M Raizen. 2013. “Caenorhabditis-in-Drop Array for Monitoring C. Elegans Quiescent Behavior.” *Sleep* 36 (5).

Bousquet, P, J Feldman, and J Schwartz. 1984. “Central Cardiovascular Effects of Alpha

Adrenergic Drugs: Differences between Catecholamines and Imidazolines." *The Journal of Pharmacology and Experimental Therapeutics* 230: 232–36.

Boyle, Thomas J, Zhirong Bao, John I Murray, Carlos L Araya, and Robert H Waterston. 2006. "AceTree: A Tool for Visual Analysis of Caenorhabditis Elegans Embryogenesis." *BMC Bioinformatics* 7: 275. doi:10.1186/1471-2105-7-275.

Brenner, S. 1974. "The Genetics of C Elegans." *Genetics* 77: 71–94.

Brenner, Sydney. 2003. "Sydney Brenner - Nobel Lecture: Nature's Gift to Science," 1–9.

Bringmann, Henrik. 2011. "Agarose Hydrogel Microcompartments for Imaging Sleep- and Wake-like Behavior and Nervous System Development in Caenorhabditis Elegans Larvae." *Journal of Neuroscience Methods* 201 (1). Elsevier B.V.: 78–88. doi:10.1016/j.jneumeth.2011.07.013.

Calhoun, Adam J., Ada Tong, Navin Pokala, James A.J. Fitzpatrick, Tatyana O. Sharpee, and Sreekanth H. Chalasani. 2015. "Neural Mechanisms for Evaluating Environmental Variability in Caenorhabditis Elegans." *Neuron* 86 (2). Elsevier Inc.: 428–41. doi:10.1016/j.neuron.2015.03.026.

Calhoun, Adam J, and Benjamin Y Hayden. 2015. "The Foraging Brain." *Current Opinion in Behavioral Sciences* 5. Elsevier Ltd: 24–31. doi:10.1016/j.cobeha.2015.07.003.

Canguilhem, B, J L Miro, E Kempf, and P Schmitt. 1986. "Does Serotonin Play a Role in Entrance into Hibernation?" *The American Journal of Physiology* 251 (4 Pt 2): R755–61.

Carey, Hannah V, Matthew T Andrews, and Sandra L Martin. 2003. "Mammalian

Hibernation: Cellular and Molecular Responses to Depressed Metabolism and Low Temperature." *Physiological Reviews* 83 (4): 1153–81. doi:10.1152/physrev.00008.2003.

Carre-Pierrat, Maïté, David Baillie, Robert Johnsen, Rhonda Hyde, Anne Hart, Laure Granger, and Laurent Ségalat. 2006. "Characterization of the Caenorhabditis Elegans G Protein-Coupled Serotonin Receptors." *Invertebrate Neuroscience* 6 (4): 189–205. doi:10.1007/s10158-006-0033-z.

Chalfie, Martin, J Sulston, J White, E Southgate, J. Nichol Thomson and S Brenner. 1985. "The Neural Circuit for Touch Sensitivity in Caenorhabditis Elegans'," *The Journal of Neuroscience* 5(4): 956-964.

Chalfie, M, Y Tu, G Euskirchen, W W Ward, and D C Prasher. 1994. "Green Fluorescent Protein as a Marker for Gene Expression." *Science* 263 (5148): 802–5. doi:10.1126/science.8303295.

Chase, Daniel L, and Michael R. Koelle. 2007. "Biogenic Amine Neurotransmitters in C. Elegans." *WormBook*. ed. The *C. elegans* Research Community, WormBook, doi/10.1895/wormbook.1.132.1

Christensen, Kaare, Gabriele Doblhammer, Roland Rau, and James W Vaupel. 2010. "Ageing Populations : The Challenges Ahead" 374 (9696): 1196–1208. doi:10.1016/S0140-6736(09)61460-4.Ageing.

Churgin, Matthew A., and Christopher Fang-Yen. 2015. "An Imaging System for *C. elegans* Behavior." *Methods in Molecular Biology* 1327: 199–207. doi:10.1007/978-1-4939-2842-2_14.

Churgin, Matthew A, Liping He, John I Murray, and Christopher Fang-Yen. 2013.

"Efficient Single-Cell Transgene Induction in *Caenorhabditis elegans* Using a Pulsed Infrared Laser." *G3 (Bethesda, Md.)* 3 (10): 1827–32. doi:10.1534/g3.113.007682.

Churgin, Matthew A, Liping He, John I Murray, and Christopher Fang-Yen. 2014. "Construction of a system for single-cell transgene induction in *Caenorhabditis elegans* using a pulsed infrared laser." *Methods*. 63(3):431-6. doi:10.1016/j.ymeth.2014.05.001.

Churgin, Matthew A, Richard McCloskey, Emily Peters, and Christopher Fang-Yen. 2017. "Antagonistic serotonergic and octopaminergic neural circuits mediate food-dependent locomotory behavior in *Caenorhabditis elegans*." *The Journal of Neuroscience*. (Accepted)

Churgin, Matthew A, Sangkyu Jung, Chih-Chieh Yu, Xiangmei Chen, David M Raizen, and Christopher Fang-Yen. 2017. "Longitudinal imaging of *Caenorhabditis elegans* in a microfabricated device reveals variation in behavioral decline during aging." *eLife* 2017 6:e26652. doi: 10.7554/eLife.26652

Cirelli, C, and G Tononi. 2008. "Is Sleep Essential?," *Plos Biology* 6(8):1605-1611.

Clark, Damon A., Christopher V. Gabel, Timothy M. Lee, and Aravinthan D. T. Samuel. 2007. "Short-Term Adaptation and Temporal Processing in the Cryophilic Response of Caenorhabditis Elegans." *Journal of Neurophysiology* 97 (3): 1903–10. doi:10.1152/jn.00892.2006.

Colman, Ricki J., T. Mark Beasley, Joseph W. Kemnitz, Sterling C. Johnson, Richard Weindruch, and Rozalyn M. Anderson. 2014. "Caloric Restriction Reduces Age-Related and All-Cause Mortality in Rhesus Monkeys." *Nature Communications* 5:

1–5. doi:10.1038/ncomms4557.

Crocker, A., and A. Sehgal. 2008. "Octopamine Regulates Sleep in Drosophila through Protein Kinase A-Dependent Mechanisms." *Journal of Neuroscience* 28 (38): 9377–85. doi:10.1523/JNEUROSCI.3072-08a.2008.

Crocker, A, and A Sehgal. 2010. "Genetic Analysis of Sleep." *Genes & Development* 24 (12): 1220–35.

Cunningham, Katherine A, Zhaolin Hua, Supriya Srinivasan, Jason Liu, Brian H Lee, Robert H Edwards, and Kaveh Ashrafi. 2012. "AMP-Activated Kinase Links Serotonergic Signaling to Glutamate Release for Regulation of Feeding Behavior in *C. elegans*." *Cell Metabolism* 16 (1). Elsevier Ltd: 113–21. http://dx.doi.org/10.1016/j.cmet.2012.05.014.

Curran, Kevin P., and Sreekanth H. Chalasani. 2012. "Serotonin Circuits and Anxiety: What Can Invertebrates Teach Us?" *Invertebrate Neuroscience* 12 (2): 81–92. doi:10.1007/s10158-012-0140-y.

Dauer, W, and S Przedborski. 2003. "Parkinson's Disease: Mechanisms and Models," *Neuron* 39:889-909.

Davis, M Wayne, J Jason Morton, Dana Carroll, and Erik M Jorgensen. 2008. "Gene Activation Using FLP Recombinase in C. Elegans." *PLoS Genetics* 4 (3): e1000028. doi:10.1371/journal.pgen.1000028.

Deelen, Joris, Hae-Won Uh, Ramin Monajemi, Diana van Heemst, Peter E Thijssen, Stefan Böhringer, Erik B van den Akker, et al. 2013. "Gene Set Analysis of GWAS Data for Human Longevity Highlights the Relevance of the insulin/IGF-1 Signaling and Telomere Maintenance Pathways." *Age (Dordrecht, Netherlands)* 35 (1): 235–

49. doi:10.1007/s11357-011-9340-3.

DiLoreto, Race, and Coleen T. Murphy. 2010. “The Cell Biology of Aging.” *Molecular Biology of the Cell* 190 (3): 285–96. doi:10.1083/jcb.201003144.

Driver, Robert J, Annesia L Lamb, Abraham J Wyner, and David M Raizen. 2013. “DAF-16/FOXO Regulates Homeostasis of Essential Sleep-like Behavior during Larval Transitions in C. elegans.” *Current Biology* 23 (6): 501–6.

Edwards, Stacey L, Nicole K Charlie, Marie C Milfort, Brandon S Brown, Christen N Gravlin, Jamie E Knecht, and Kenneth G Miller. 2008. “A Novel Molecular Solution for Ultraviolet Light Detection in Caenorhabditis Elegans.” Edited by Mario de Bono. *PLoS Biology* 6 (8): e198.

Eijkelenboom, Astrid, and Boudewijn M T Burgering. 2013. “FOXOs: Signalling Integrators for Homeostasis Maintenance.” *Nature Reviews Molecular Cell Biology* 14 (2). Nature Publishing Group: 83–97. http://dx.doi.org/10.1038/nrm3507.

Estevez, Annette O., Robin H. Cowie, Kathy L. Gardner, and Miguel Estevez. 2006. “Both Insulin and Calcium Channel Signaling Are Required for Developmental Regulation of Serotonin Synthesis in the Chemosensory ADF Neurons of Caenorhabditis Elegans.” *Developmental Biology* 298 (1): 32–44. doi:10.1016/j.ydbio.2006.06.005.

Fang-Yen, Christopher, Christopher Gabel, Cornelia I Bargmann, Aravinthan D T Samuel, and Leon Avery. 2011. “Laser Microsurgery in C. Elegans.” In *Caenorhabditis Elegans: Modern Biological Analysis of an Organism*. Methods in Cell Biology. Elsevier Academic Press.

Fang-Yen, Christopher, Christopher V Gabel, Aravinthan D T Samuel, Cornelia I

Bargmann, and Leon Avery. 2012. *Laser Microsurgery in Caenorhabditis Elegans*. *Methods in Cell Biology*. Second Edi. Vol. 107. Elsevier Inc. doi:10.1016/B978-0-12-394620-1.00006-0.

Finch, C E, and D M Cohen. 1997. "Aging, Metabolism, and Alzheimer Disease: Review and Hypotheses." *Exp Neurol* 143 (1): 82–102. doi:10.1006/exnr.1996.6339.

Flavell, Steven W., Navin Pokala, Evan Z. Macosko, Dirk R. Albrecht, Johannes Larsch, and Cornelia I. Bargmann. 2013a. "Serotonin and the Neuropeptide PDF Initiate and Extend Opposing Behavioral States in C. Elegans." *Cell* 154 (5). Elsevier Inc.: 1023–35. doi:10.1016/j.cell.2013.08.001.

Flavell, Steven W, Navin Pokala, Evan Z Macosko, Dirk R Albrecht, Johannes Larsch, and Cornelia I Bargmann. 2013b. "Serotonin and the Neuropeptide PDF Initiate and Extend Opposing Behavioral States in C. Elegans." *Cell* 154 (5). Elsevier Inc.: 1023–35. doi:10.1016/j.cell.2013.08.001.

Fontana, L, L Partridge, and V D Longo. 2010. "Extending Healthy Life Span--From Yeast to Humans." *Science* 328 (5976): 321–26.

Friedman, David B, and Thomas E Johnson. 1988. "A Mutation in the Age-1 Gene in C Aenorhabditis Elegans Lengthens Life and Reduces Hermaphrodite Fertility." *Genetics* 86 (Martin 1978): 75–86.

Gaglia, M M, and C Kenyon. 2009. "Stimulation of Movement in a Quiescent, Hibernation-Like Form of Caenorhabditis Elegans by Dopamine Signaling." *Journal of Neuroscience* 29 (22): 7302–14.

Gallagher, Thomas, Theresa Bjorness, Robert Greene, Young-jai You, and Leon Avery. 2013. "The Geometry of Locomotive Behavioral States in C. Elegans." Edited by

Aravinthan Samuel. *PLoS ONE* 8 (3): e59865.

Gallagher, Thomas, Jeongho Kim, Marieke Oldenbroek, Rex Kerr, and Young-jai You. 2013. "ASI Regulates Satiety Quiescence in C. Elegans." *The Journal of Neuroscience* 33 (23): 1–10.

Garrity, P A, M B Goodman, A D Samuel, and P Sengupta. 2010. "Running Hot and Cold: Behavioral Strategies, Neural Circuits, and the Molecular Machinery for Thermotaxis in C. Elegans and Drosophila." *Genes & Development* 24 (21): 2365–82.

Gems, David, and Linda Partridge. 2013. "Genetics of Longevity in Model Organisms: Debates and Paradigm Shifts." *Annual Review of Physiology* 75 (1): 621–44.

Gems, David, Amy J Sutton, Mark L Sundermeyer, Patrice S Albert, Kevin V King, Mark L Edgley, Pamela L Larsen, and Donald L Riddle. 1998. "Two Pleiotropic Classes of Daf-2 Mutation Affect Larval Arrest, Adult Behavior, Reproduction and Longevity in Caenorhabditis Elegans." *Genetics* 150: 129–55.

Gerstner, Jason R, Isaac J Perron, and Allan I Pack. 2012. "The Nexus of Aβ , Aging , and Sleep," *Science Translational Medicine* 4 (150): 4–6.

Ghosh, R, and S W Emmons. 2008. "Episodic Swimming Behavior in the Nematode C. Elegans." *Journal of Experimental Biology* 211 (23): 3703–11.

Goodman, Miriam B. 2006. "Mechanosensation." *WormBook: The Online Review of C. Elegans Biology*, 1–14. doi:10.1895/wormbook.1.62.1.

Gray, Jesse M, Joseph J Hill, and Cornelia I Bargmann. 2005. "A Circuit for Navigation in Caenorhabditis Elegans," *Proceeding of the National Academy of Sciences* 102(9): 3184-3191.

Greer, E L, and A Brunet. 2007. “FOXO Transcription Factors in Ageing and Cancer.” *Acta Physiologica* 192 (1): 19–28.

Greer, Elisabeth R., Carissa L. Pérez, Marc R. Van Gilst, Brian H. Lee, and Kaveh Ashrafi. 2008. “Neural and Molecular Dissection of a C. Elegans Sensory Circuit That Regulates Fat and Feeding.” *Cell Metabolism* 8 (2). Elsevier Inc.: 118–31. doi:10.1016/j.cmet.2008.06.005.

Greer, Eric L, and Anne Brunet. 2009. “Different Dietary Restriction Regimens Extend Lifespan by Both Independent and Overlapping Genetic Pathways in C. Elegans.” *Aging Cell* 8 (2): 113–27. doi:10.1111/j.1474-9726.2009.00459.x.

Grotewiel, Michael S., Ian Martin, Poonam Bhandari, and Eric Cook-Wiens. 2005. “Functional Senescence in Drosophila Melanogaster.” *Ageing Research Reviews* 4 (3): 372–97. doi:10.1016/j.arr.2005.04.001.

Guo, Min, Tai-Hong Wu, Yan-Xue Song, Ming-Hai Ge, Chun-Ming Su, Wei-Pin Niu, Lan-Lan Li, et al. 2015. “Reciprocal Inhibition between Sensory ASH and ASI Neurons Modulates Nociception and Avoidance in Caenorhabditis Elegans.” *Nature Communications* 6. Nature Publishing Group. doi:10.1038/ncomms6655.

Gürel, Güliz, Megan a. Gustafson, Judy S. Pepper, H. Robert Horvitz, and Michael R. Koelle. 2012. “Receptors and Other Signaling Proteins Required for Serotonin Control of Locomotion in Caenorhabditis Elegans.” *Genetics* 192 (4): 1359–71. doi:10.1534/genetics.112.142125.

Hahm, Jeong-Hoon, Sunhee Kim, Race DiLoreto, Cheng Shi, Seung-Jae V. Lee, Coleen T. Murphy, and Hong Gil Nam. 2015. “C. Elegans Maximum Velocity Correlates with Healthspan and Is Maintained in Worms with an Insulin Receptor Mutation.”

Nature Communications 6. Nature Publishing Group: 8919. doi:10.1038/ncomms9919.

Haider, S, and D J Haleem. 2000. "Decreases of Brain Serotonin Following a Food Restriction Schedule of 4 Weeks in Male and Female Rats." *Medical Science Monitor : International Medical Journal of Experimental and Clinical Research* 6 (6): 1061–67.

Hansen, Malene, and Brian K. Kennedy. 2016. "Does Longer Lifespan Mean Longer Healthspan?" *Trends in Cell Biology*. doi:10.1016/j.tcb.2016.05.002.

Hapiak, Vera M., Robert J. Hobson, Lindsay Hughes, Katherine Smith, Gareth Harris, Christina Condon, Patricia Komuniecki, and Richard W. Komuniecki. 2009. "Dual Excitatory and Inhibitory Serotonergic Inputs Modulate Egg Laying in Caenorhabditis Elegans." *Genetics* 181 (1): 153–63. doi:10.1534/genetics.108.096891.

Harris, Gareth P, Vera M Hapiak, Rachel T Wragg, Sarah B Miller, Lindsay J Hughes, Robert J Hobson, Robert Steven, Bruce Bamber, and Richard W Komuniecki. 2009. "Three Distinct Amine Receptors Operating at Different Levels within the Locomotory Circuit Are Each Essential for the Serotonergic Modulation of Chemosensation in Caenorhabditis Elegans." *The Journal of Neuroscience* 29 (5): 1446–56. doi:10.1523/JNEUROSCI.4585-08.2009.

Hart, Anne. 2006. "Behavior." *WormBook*, 1–67. doi:10.1895/wormbook.1.87.1.

Hausdorff, J M, S L Mitchell, R Firtion, C K Peng, M E Cudkowicz, J Y Wei, and a L Goldberger. 1997. "Altered Fractal Dynamics of Gait: Reduced Stride-Interval Correlations with Aging and Huntington's Disease." *Journal of Applied Physiology*

(Bethesda, Md. : 1985) 82 (1): 262–69. doi:10.1016/j.measurement.2012.04.013.

Hedgecock, E M, and R L Russell. 1975. "Normal and Mutant Thermotaxis in the Nematode C. Elegans," *Proceeding of the National Academy of Sciences* 72(10): 4061-4065.

Helmstaedter, Moritz, Kevin L Briggman, Srinivas C Turaga, Viren Jain, H Sebastian Seung, and Winfried Denk. 2014. "Connectomic Reconstruction of the Inner Plexiform Layer in the Mouse Retina." *Nature* 500 (7461). Nature Publishing Group: 168–74. http://dx.doi.org/10.1038/nature12346.

Herndon, L A, Schmeissner, P J, Dudaronek, J M, Brown, P A, Listner, K M, Sakano, Y, Paupard, M C, Hall, D H, and M Driscoll. 2002. "Stochastic and Genetic Factors Influence Tissue-Specific Decline in Ageing C. Elegans." *Nature* 419: 808-814.

Hobson, Robert J., Vera M. Hapiak, Hong Xiao, Kara L. Buehrer, Patricia R. Komuniecki, and Richard W. Komuniecki. 2006. "SER-7, a Caenorhabditis Elegans 5-HT7-like Receptor, Is Essential for the 5-HT Stimulation of Pharyngeal Pumping and Egg Laying." *Genetics* 172 (1): 159–69. doi:10.1534/genetics.105.044495.

Hoffman, B J, S R Hansson, E Mezey, and M Palkovits. 1998. "Localization and Dynamic Regulation of Biogenic Amine Transporters in the Mammalian Central Nervous System." *Frontiers in Neuroendocrinology* 19 (3): 187–231. doi:10.1006/frne.1998.0168.

Hsu, Ao-Lin, Murphy, Coleen T. and Cynthia Kenyon 2003. "Regulation of Aging and Age-Related Disease by DAF-16 and Heat-Shock Factor." *Science* 300 (5622): 1142–45.

Hsu, Ao-Lin, Zhaoyang Feng, Meng-Yin Hsieh, and X Z Shawn Xu. 2009.

"Identification by Machine Vision of the Rate of Motor Activity Decline as a Lifespan Predictor in C. Elegans." *Neurobiology of Aging* 30 (9): 1498–1503. doi:10.1016/j.neurobiolaging.2007.12.007.

Huang, Cheng, Chengjie Xiong, and Kerry Kornfeld. 2004. "Measurements of Age-Related Changes of Physiological Processes That Predict Lifespan of Caenorhabditis Elegans." *Proceedings of the National Academy of Sciences* 101 (21).

Hulme, S Elizabeth, Sergey S Shevkoplyas, Alison P McGuigan, Javier Apfeld, Walter Fontana, and George M Whitesides. 2010a. "Lifespan-on-a-Chip: Microfluidic Chambers for Performing Lifelong Observation of C. Elegans." *Lab on a Chip* 10 (5): 589-597.

Husson, Steven J, Wagner Steuer Costa, Cornelia Schmitt, and Alexander Gottschalk. 2012. "Keeping Track of Worm Trackers," 1–17. doi:10.1895/wormbook.1.15.

Iannacone, Michael J, Isabel Beets, Lindsey E Lopes, Matthew A Churgin, Christopher Fang-Yen, Matthew D Nelson, Liliane Schoofs, and David M Raizen. 2017. "The RFamide Receptor DMSR-1 Regulates Stress-Induced Sleep in *C. Elegans*." *eLife* 6: 1–20. doi:10.7554/eLife.19837.

Iino, Y, and K Yoshida. 2009. "Parallel Use of Two Behavioral Mechanisms for Chemotaxis in Caenorhabditis Elegans." *Journal of Neuroscience* 29 (17): 5370–80.

Iwanir, Shachar, Nora Tramm, Stanislav Nagy, Charles Wright, Daniel Ish, and David Biron. 2013. "The Microarchitecture of C. Elegans Behavior during Lethargus: Homeostatic Bout Dynamics, a Typical Body Posture, and Regulation by a Central Neuron." *SLEEP* 36 (3): 385–95.

Iwasa, Hiroaki, Simon Yu, Jian Xue, and Monica Driscoll. 2010. "Novel EGF Pathway Regulators Modulate C. Elegans Healthspan and Lifespan via EGF Receptor, PLC-Γ, and IP3R Activation." *Aging Cell* 9 (4): 490–505.

Jarrell, T A, Y Wang, A E Bloniarz, C A Brittin, M Xu, J N Thomson, D G Albertson, D H Hall, and S W Emmons. 2012. "The Connectome of a Decision-Making Neural Network." *Science* 337 (6093): 437–44.

Kaern, Mads, Timothy C Elston, William J Blake, and James J Collins. 2005. "Stochasticity in Gene Expression: From Theories to Phenotypes." *Nature Reviews Genetics* 6 (6): 451–64. doi:10.1038/nrg1615.

Kamei, Yasuhiro, Motoshi Suzuki, Kenjiro Watanabe, Kazuhiro Fujimori, Takashi Kawasaki, Tomonori Deguchi, Yoshihiro Yoneda, et al. 2008. "Infrared Laser–mediated Gene Induction in Targeted Single Cells in Vivo." *Nature Methods* 6 (1): 79–81. doi:10.1038/nmeth.1278.

Kawano, Taizo, Po, Michelle D., Gao, Shangbang, Leung, George, Ryu, William S. and Mei Zhen. 2011. "An Imbalancing Act: Gap Junctions Reduce the Backward Motor Circuit Activity to Bias C. Elegans for Forward Locomotion Exp Proc," *Neuron* 72: 572-586.

Kaye, Walter H, Harry E Gwirtsman, David T George, and Michael H Ebert. 1991. "Altered Serotonin Activity in Anorexia." *Archives General Psychiatry* 48 (6): 556–62. doi:10.1001/archpsyc.1991.01810300068010.

Kenyon, Cynthia, Jean Chang, Erin Gensch, Adam Rudner, and Ramon Tabtiang. 1993. "A C. Elegans Mutant That Lives Twice as Long as Wild Type." *Nature* 366 (2): 1–4.

Kenyon, Cynthia J. 2010. "The Genetics of Ageing." *Nature* 464 (7288).

Kim, Dennis H. 2013. "Bacteria and the Aging and Longevity of Caenorhabditis Elegans." *Annual Review of Genetics* 47 (1): 233–46.

Kim, Eric, Lin Sun, Christopher V Gabel, and Christopher Fang-Yen. 2013. "Long-Term Imaging of Caenorhabditis Elegans Using Nanoparticle-Mediated Immobilization." *PLoS ONE* 8 (1): e53419.

Kimura, K. D., D. L. Riddle, and G. Ruvkun. 2011. "The C. Elegans DAF-2 Insulin-like Receptor Is Abundantly Expressed in the Nervous System and Regulated by Nutritional Status." *Cold Spring Harbor Symposia on Quantitative Biology* 76: 113–20. doi:10.1101/sqb.2011.76.010660.

Kirkwood, Thomas B L, Martin Feder, Caleb E Finch, Claudio Franceschi, Amiela Globerson, Christian Peter Klingenberg, Kelly LaMarco, Stig Omholt, and Rudi G J Westendorp. 2005. "What Accounts for the Wide Variation in Life Span of Genetically Identical Organisms Reared in a Constant Environment?" *Mechanisms of Ageing and Development* 126 (3): 439–43. doi:10.1016/j.mad.2004.09.008.

Komuniecki, Richard W, Robert J Hobson, Elizabeth B Rex, Vera M Hapiak, and Patricia R Komuniecki. 2004. "Biogenic Amine Receptors in Parasitic Nematodes : What Can Be Learned from Caenorhabditis Elegans ?" *Molecular and Biochemical Parastology* 137: 1–11. doi:10.1016/j.molbiopara.2004.05.010.

Komuniecki, Rick, Gareth Harris, Vera Hapiak, Rachel Wragg, and Bruce Bamber. 2012. "Monoamines Activate Neuropeptide Signaling Cascades to Modulate Nociception in C. Elegans: A Useful Model for the Modulation of Chronic Pain?" *Invertebrate Neuroscience* 12 (1): 53–61. doi:10.1007/s10158-011-0127-0.

Kou, L, D Labrie, and P Chylek. 1993. “Refractive Indices of Water and Ice in the 0.65- to 2.5-Mm Spectral Range.” *Applied Optics* 32 (19): 3531–40.

Kuwahara, T, and T Iwatsubo. 2005. “Familial Parkinson Mutant -Synuclein Causes Dopamine Neuron Dysfunction in Transgenic Caenorhabditis Elegans,” *The Journal of Biological Chemistry* 281(1): 334-340.

Lakhina, Vanisha, and Coleen T Murphy. 2015. “For Longevity, Perception Is Everything.” *Cell* 160 (5). Elsevier Inc.: 807–9. doi:10.1016/j.cell.2015.02.027.

Lakowski, Bernard, and Siegfried Hekimi. 1998. “The Genetics of Caloric Restriction in Caenorhabditis Elegans.” *Proceedings of the National Academy of Sciences* 95: 13091-13096.

Lam, Daniel, Daniel D Lam, and Lora K Heisler. 2007. “Serotonin and Energy Balance : Molecular Mechanisms and Implications for Type 2 Diabetes Serotonin and Energy Balance : Molecular Mechanisms and Implications for Type 2 Diabetes.” *Expert Rev Mol Med* 9 (5). doi:10.1017/S1462399407000245.

Lam, R. V. 2006. “Sleep Disturbances and Depression: A Challenge for Antidepressants.” *International Clinical Psychopharmacology* 21: 75–78. doi:10.1097/01.yic.0000195658.91524.61.

Leatherman, Judith L, and Thomas A Jongens. 2003. “Transcriptional Silencing and Translational Control: Key Features of Early Germline Development.” *BioEssays: News and Reviews in Molecular, Cellular and Developmental Biology* 25 (4): 326–35. doi:10.1002/bies.10247.

Lee, Shin-Hae, and Kyung-Jin Min. 2013. “Caloric Restriction and Its Mimetics.” *BMB Reports* 46 (4): 181–87. http://www.ncbi.nlm.nih.gov/pubmed/24316687.

Lehner, Ben. 2013. “Genotype to Phenotype: Lessons from Model Organisms for Human Genetics.” *Nature Reviews Genetics* 14 (3). Nature Publishing Group: 168–78. doi:10.1038/nrg3404.

Liang, Bin, Mustapha Moussaif, Chih-jen Kuan, J Jay Gargus, and Ji Ying Sze. 2006a. “Serotonin Targets the DAF-16 / FOXO Signaling Pathway to Modulate Stress Responses.” *Cell Metabolism* 4 (December): 429–40. doi:10.1016/j.cmet.2006.11.004.

Liang, Bin, Mustapha Moussaif, Chih-Jen Kuan, J Jay Gargus, and Ji Ying Sze. 2006b. “Serotonin Targets the DAF-16/FOXO Signaling Pathway to Modulate Stress Responses.” *Cell Metabolism* 4 (6): 429–40. doi:10.1016/j.cmet.2006.11.004.

Liu, Katharine S, and Paul W Sternberg. 1995. “Sensory Regulation of Male Mating Behavior in Caenorhabditiselegans,” *Neuron* 14: 79-89.

Lockery, S R, K J Lawton, J C Doll, S Faumont, S M Coulthard, T R Thiele, N Chronis, K E McCormick, M B Goodman, and B L Pruitt. 2008. “Artificial Dirt: Microfluidic Substrates for Nematode Neurobiology and Behavior.” *Journal of Neurophysiology* 99 (6): 3136–43. doi:10.1152/jn.91327.2007.

Longo, Valter D., Adam Antebi, Andrzej Bartke, Nir Barzilai, Holly M. Brown-Borg, Calogero Caruso, Tyler J. Curiel, Rafael De Cabo, et al. 2015. “Interventions to Slow Aging in Humans: Are We Ready?” *Aging Cell* 14 (4): 497–510. doi:10.1111/acel.12338.

Lopez-Otin, Carlos, Maria A. Blasco, Linda Partridge, Manuel Serrano, and Guido Kroemer. 2013. “The Hallmarks of Aging.” *Cell* 153 (6). doi:10.1016/j.cell.2013.05.039.

Lund, James, Patricia Tedesco, Kyle Duke, John Wang, Stuart K. Kim, and Thomas E. Johnson. 2002. "Transcriptional Profile of Aging in C. Elegans." *Current Biology* 12 (18): 1566–73. doi:10.1016/S0960-9822(02)01146-6.

Luo, Linjiao, Quan Wen, Jing Ren, Michael Hendricks, Marc Gershow, Yuqi Qin, Joel Greenwood, et al. 2014. "Dynamic Encoding of Perception, Memory, and Movement in a C. Elegans Chemotaxis Circuit." *Neuron* 82 (5): 1115–28. doi:10.1016/j.neuron.2014.05.010.

Mango, Susan E. 2009. "The Molecular Basis of Organ Formation: Insights from the C. Elegans Foregut." *Annual Review of Cell and Developmental Biology* 25: 597–628. doi:10.1146/annurev.cellbio.24.110707.175411.

Martin, George M. 2011. "The Biology of Aging: 1985-2010 and Beyond." *FASEB Journal : Official Publication of the Federation of American Societies for Experimental Biology* 25 (11): 3756–62. doi:10.1096/fj.11-1102.ufm.

Martin, Sandra L. 2008. "Mammalian Hibernation: A Naturally Reversible Model for Insulin Resistance in Man?" *Diabetes & Vascular Disease Research : Official Journal of the International Society of Diabetes and Vascular Disease* 5 (2): 76–81. doi:10.3132/dvdr.2008.013.

McCloskey, Richard J, Anthony D Fouad, Matthew A Churgin, and Christopher Fang-Yen. 2017. "Food Responsiveness Regulates Episodic Behavioral States in *Caenorhabditis Elegans*." *Journal of Neurophysiology* 19104: jn.00555.2016. doi:10.1152/jn.00555.2016.

McCormick, Mark, Kan Chen, Priya Ramaswamy, and Cynthia Kenyon. 2011. "New Genes That Extend Caenorhabditis Elegans' Lifespan in Response to Reproductive

Signals." *Aging Cell* 11 (2): 192–202. http://doi.wiley.com/10.1111/j.1474-9726.2011.00768.x.

McElwee, Joshua J, Eugene Schuster, Eric Blanc, James H Thomas, and David Gems. 2004. "Shared Transcriptional Signature in Caenorhabditis Elegans Dauer Larvae and Long-Lived Daf-2 Mutants Implicates Detoxification System in Longevity Assurance." *Journal of Biological Chemistry* 279 (43): 44533–43.

Meltzer, Carolyn Cidis, Gwenn Smith, Steven T DeKosky, Bruce G Pollock, Chester a Mathis, Robert Y Moore, David J Kupfer, Charles F Reynolds, and Charles F Reynolds. 1998. "Serotonin in Aging , Late-Life Depression , and Alzheimer ' S Disease : The Emerging Role of Functional Imaging." *Neuropsychopharmacology* 18 (6): 407–30. doi:10.1016/S0893-133X(97)00194-2.

Metaxakis, Athanasios, Luke S Tain, Sebastian Grönke, Oliver Hendrich, Yvonne Hinze, Ulrike Birras, and Linda Partridge. 2014. "Lowered Insulin Signalling Ameliorates Age-Related Sleep Fragmentation in Drosophila." *PLoS Biology* 12 (4): e1001824. doi:10.1371/journal.pbio.1001824.

Mills, Holly, Rachel Wragg, Vera Hapiak, Michelle Castelletto, Jeffrey Zahratka, Gareth Harris, Philip Summers, et al. 2011. "Monoamines and Neuropeptides Interact to Inhibit Aversive Behaviour in Caenorhabditis Elegans." *The EMBO Journal* 31 (3). Nature Publishing Group: 667–78. doi:10.1038/emboj.2011.422.

Mirzaei, Hamed, Jorge a. Suarez, and Valter D. Longo. 2014. "Protein and Amino Acid Restriction, Aging and Disease: From Yeast to Humans." *Trends in Endocrinology & Metabolism*, August. Elsevier Ltd, 1–9. doi:10.1016/j.tem.2014.07.002.

Moon, Minho, Jin Gyu Choi, Dong Woo Nam, Hyun Seok Hong, Young Ju Choi,

Myung Sook Oh, and Inhee Mook-Jung. 2011. “Ghrelin Ameliorates Cognitive Dysfunction and Neurodegeneration in Intrahippocampal Amyloid-β1-42 Oligomer-Injected Mice.” *Journal of Alzheimer’s Disease* 23 (1): 147–59. doi:10.3233/JAD-2010-101263.

Mullaney, Brendan C., and Kaveh Ashrafi. 2009. “C. Elegans Fat Storage and Metabolic Regulation.” *Biochimica et Biophysica Acta - Molecular and Cell Biology of Lipids* 1791 (6): 474–78. doi:10.1016/j.bbalip.2008.12.013.

Murphy, Coleen T. 2006. “The Search for DAF-16/FOXO Transcriptional Targets: Approaches and Discoveries.” *Experimental Gerontology* 41 (10): 910–21. doi:10.1016/j.exger.2006.06.040.

Murphy, Coleen T, Seung-Jae Lee, and Cynthia Kenyon. 2007. “Tissue Entrainment by Feedback Regulation of Insulin Gene Expression in the Endoderm of Caenorhabditis Elegans.” *Proceedings of the National Academy of Sciences* 104 (48): 19046–50. doi:10.1073/pnas.0709613104.

Murphy, Coleen T, Steven A McCarroll, Cornelia I Bargmann, Andrew G Fraser, Ravi S. Kamath, Julie Ahringer, Hao Li, and C Kenyon. 2003. “Genes That Act Downstream of DAF-16 to Influence the Lifespan of Caenorhabditis Elegans.” *Nature* 424: 1–8.

Nagy, Stanislav, David M Raizen, and David Biron. 2014. “Measurements of Behavioral Quiescence in Caenorhabditis Elegans.” *Methods (San Diego, Calif.)* 68 (3). Elsevier Inc.: 500–507. doi:10.1016/j.ymeth.2014.03.009.

Nelken, Israel, Gal Chechik, Thomas D. Mrsic-Flogel, Andrew J. King, and Jan W H Schnupp. 2005. “Encoding Stimulus Information by Spike Numbers and Mean

Response Time in Primary Auditory Cortex." *Journal of Computational Neuroscience* 19 (2): 199–221. doi:10.1007/s10827-005-1739-3.

Nelson, M D, N F Trojanowski, J B George-Raizen, C J Smith, C-C Yu, C Fang-Yen, and D M Raizen. 2013. "The Neuropeptide NLP-22 Regulates a Sleep-like State in Caenorhabditis Elegans." *Nature Communications* 4 (January): 2846. doi:10.1038/ncomms3846.

Nelson, Matthew D., Kun He Lee, Matthew A. Churgin, Andrew J. Hill, Cheryl Van Buskirk, Christopher Fang-Yen, and David M. Raizen. 2014. "FMRFamide-like FLP-13 Neuropeptides Promote Quiescence Following Heat Stress in Caenorhabditis Elegans." *Current Biology* 24 (September). Elsevier Ltd: 1–5. doi:10.1016/j.cub.2014.08.037.

Nelson, O. Lynne, Heiko T. Jansen, Elizabeth Galbreath, Kurt Morgenstern, Jamie Lauren Gehring, Kimberly Scott Rigano, Jae Lee, et al. 2014. "Grizzly Bears Exhibit Augmented Insulin Sensitivity While Obese Prior to a Reversible Insulin Resistance during Hibernation." *Cell Metabolism* 20 (2). Elsevier Inc.: 376–82. doi:10.1016/j.cmet.2014.07.008.

Neuman, Keir C, and Steven M Block. 2004. "Optical Trapping." *The Review of Scientific Instruments* 75 (9): 2787–2809. doi:10.1063/1.1785844.

Noble, Tallie, Jonathan Stieglitz, and Supriya Srinivasan. 2013. "An Integrated Serotonin and Octopamine Neuronal Circuit Directs the Release of an Endocrine Signal to Control C. Elegans Body Fat." *Cell Metabolism* 18 (5). Elsevier Inc.: 672–84. doi:10.1016/j.cmet.2013.09.007.

Ogg, S, S Paradis, S Gottlieb, G I Patterson, L Lee, H A Tissenbaum, and G Ruvkun.

1997. “The Fork Head Transcription Factor DAF-16 Transduces Insulin-like Metabolic and Longevity Signals in C. Elegans.” *Nature* 389 (6654): 994–99. doi:10.1038/40194.

Oh, Seung Wook, Julie a. Harris, Lydia Ng, Brent Winslow, Nicholas Cain, Stefan Mihalas, Quanxin Wang, et al. 2014. “A Mesoscale Connectome of the Mouse Brain.” *Nature* 508 (7495). Nature Publishing Group: 207–14. doi:10.1038/nature13186.

Ohnishi, Noriyuki, Atsushi Kuhara, Fumiya Nakamura, Yoshifumi Okochi, and Ikue Mori. 2011. “Bidirectional Regulation of Thermotaxis by Glutamate Transmissions in Caenorhabditis Elegans.” *The EMBO Journal* 30 (7). Nature Publishing Group: 1376–88. http://dx.doi.org/10.1038/emboj.2011.13.

Onken, Brian, and Monica Driscoll. 2010. “Metformin Induces a Dietary Restriction–Like State and the Oxidative Stress Response to Extend C. Elegans Healthspan via AMPK, LKB1, and SKN-1.” *PLoS ONE* 5 (1): e8758.

Papatheodorou, Irene, Rudolfs Petrovs, and Janet M Thornton. 2014. “Comparison of the Mammalian Insulin Signalling Pathway to Invertebrates in the Context of FOXO-Mediated Ageing.” *Bioinformatics (Oxford, England)*, July. doi:10.1093/bioinformatics/btu493.

Partridge, Linda. 2014. “Intervening in Ageing to Prevent the Diseases of Ageing.” *Trends in Endocrinology and Metabolism: TEM*, August. Elsevier Ltd, 1–3. doi:10.1016/j.tem.2014.08.003.

Pearson, Joseph C, Derek Lemons, and William McGinnis. 2005. “Modulating Hox Gene Functions during Animal Body Patterning.” *Nature Reviews Genetics* 6 (12):

893–904. doi:10.1038/nrg1726.

Pierce-Shimomura, Jonathan T, Thomas M Morse, and Shawn R Lockery. 2012. "The Fundamental Role of Pirouettes in C Elegans Chemotaxis," *The Journal of Neuroscience* 19(21):9557-9569.

Pincus, Zachary, Thalyana Smith-Vikos, and Frank J Slack. 2011. "MicroRNA Predictors of Longevity in Caenorhabditis Elegans." *PLoS Genetics* 7 (9): 1–15.

Podshivalova, Katie, Rex A Kerr, and Cynthia Kenyon. 2017. "How a Mutation That Slows Aging Can Also Disproportionately Extend End-of-Life Decrepitude Report How a Mutation That Slows Aging Can Also Disproportionately Extend End-of-Life Decrepitude." *Cell Reports* 19 (3) 441–50. doi:10.1016/j.celrep.2017.03.062.

Richard Nass. 2010. "*C. elegans* genetic strategies to identify novel Parkinson's disease-associated therapeutic targets and leads," *Parkinson's Disease: molecular and therapeutic insights from model systems*. 361–368.

Raizen, David M, John E Zimmerman, Matthew H Maycock, Uyen D Ta, Young-jai You, Meera V Sundaram, and Allan I Pack. 2008. "Lethargus Is a Caenorhabditis Elegans Sleep-like State." *Nature* 451 (7178). Nature Publishing Group: 569–72.

Raj, Arjun, and Alexander van Oudenaarden. 2008. "Nature, Nurture, or Chance: Stochastic Gene Expression and Its Consequences." *Cell* 135 (2). Elsevier Inc.: 216–26.

Ramot, D, B L MacInnis, H C Lee, and M B Goodman. 2008. "Thermotaxis Is a Robust Mechanism for Thermoregulation in Caenorhabditis Elegans Nematodes." *Journal of Neuroscience* 28 (47): 12546–57. http://www.jneurosci.org/cgi/doi/10.1523/JNEUROSCI.2857-08.2008.

Ranganathan, R, S C Cannon, and H R Horvitz. 2000. "MOD-1 Is a Serotonin-Gated Chloride Channel That Modulates Locomotory Behaviour in C. Elegans." *Nature* 408 (6811): 470–75. doi:10.1038/35044083.

Rangaraju, Sunitha, Gregory M Solis, Ryan C Thompson, Rafael L Gomez-Amaro, Leo Kurian, Sandra E Encalada, Alexander B Niculescu, Daniel R Salomon, and Michael Petrascheck. 2015. "Suppression of Transcriptional Drift Extends *C. Elegans* Lifespan by Postponing the Onset of Mortality." *eLife* 4: 1–39. doi:10.7554/eLife.08833.

Reeder, DeeAnn M., Craig L. Frank, Gregory G. Turner, Carol U. Meteyer, Allen Kurta, Eric R. Britzke, Megan E. Vodzak, et al. 2012. "Frequent Arousal from Hibernation Linked to Severity of Infection and Mortality in Bats with White-Nose Syndrome." *PLoS ONE* 7 (6). doi:10.1371/journal.pone.0038920.

Rex, Elizabeth, and Richard W Komuniecki. 2002. "Characterization of a Tyramine Receptor from Caenorhabditis Elegans." *Journal of Neurochemistry* 82 (6): 1352–59. doi:10.1046/j.1471-4159.2002.01065.x.

Rex, Elizabeth, Scott C. Molitor, Vera Hapiak, Hong Xiao, Megan Henderson, and Richard Komuniecki. 2004. "Tyramine Receptor (SER-2) Isoforms Are Involved in the Regulation of Pharyngeal Pumping and Foraging Behavior in Caenorhabditis Elegans." *Journal of Neurochemistry* 91 (5): 1104–15. doi:10.1111/j.1471-4159.2004.02787.x.

Richards, Julia L, Amanda L Zacharias, Travis Walton, Joshua T Burdick, and John Isaac Murray. 2013. "A Quantitative Model of Normal Caenorhabditis Elegans Embryogenesis and Its Disruption after Stress." *Developmental Biology* 374 (1):

12–23. doi:10.1016/j.ydbio.2012.11.034.

Richmond, Janet. 2005. "Synaptic Function." *WormBook: The Online Review of C. Elegans Biology*, 1–14. doi:10.1895/wormbook.1.69.1.

Roeder, Thomas. 2005. "Tyramine and Octopamine: Ruling Behavior and Metabolism." *Annu. Rev. Entomol.*, no. 20. doi:10.1146/annurev.ento.50.071803.130404.

Roeder, Thomas, Mark Seifert, Christian Kahler, and Michael Gewecke. 2003. "Tyramine and Octopamine: Antagonistic Modulators of Behavior and Metabolism." *Archives of Insect Biochemistry and Physiology* 54 (1): 1–13. doi:10.1002/arch.10102.

Ross, C A, and M A Poirier. 2004. "Protein Aggregation and Neurodegenerative Disease." *Nature Medicine* 10 (7): S10–17. doi:10.1038/nm1066.

Sánchez-Blanco, Adolfo, and Stuart K Kim. 2011. "Variable Pathogenicity Determines Individual Lifespan in Caenorhabditis Elegans." *PLoS Genetics* 7 (4): e1002047.

Sawin, Elizabeth, and H Robert Horvitz. 2000. "*C. elegans* Locomotory Rate Is Modulated by the Environment through a Dopaminergic Pathway and by Experience through a Serotonergic Pathway." *Neuron* 26 (June): 1–13.

Ségalat, L, D a Elkes, and J M Kaplan. 1995. "Modulation of Serotonin-Controlled Behaviors by Go in Caenorhabditis Elegans." *Science (New York, N.Y.)* 267 (5204): 1648–51. doi:10.1126/science.7886454.

Sengupta, P., J. H. Chou, and C. I. Bargmann. 1996. "ODR-10 Encodes a Seven Transmembrane Domain Olfactory Receptor Required for Responses to the Odorant Diacetyl." *Cell* 84 (6): 899–909. doi:10.1016/S0092-8674(00)81068-5.

Sengupta, Piali. 2013. "The Belly Rules the Nose: Feeding State-Dependent Modulation

of Peripheral Chemosensory Responses." *Current Opinion in Neurobiology* 23 (1). Elsevier Ltd: 68–75. doi:10.1016/j.conb.2012.08.001.

Shaham, Shai. 2006. "Methods in Cell Biology." *WormBook*. doi:10.1895/wormbook.1.49.1.

Shepherd, Robert F, Filip Ilievski, Wonjae Choi, Stephen A Morin, Adam A Stokes, Aaron D Mazzeo, Xin Chen, Michael Wang, and George M Whitesides. 2011. "Multigait Soft Robot." *Proceedings of the National Academy of Sciences* 108 (51).

Singewald, Nicolas, and Athineos Philippu. 1996. "Involvement of Biogenic Amines and Amino Acids in the Central Regulation of Cardiovascular Homeostasis." *Trends in Pharmacological Sciences* 17 (10): 356–63. doi:10.1016/S0165-6147(96)10042-0.

Song, Bo Mi, Serge Faumont, Shawn Lockery, and Leon Avery. 2013. "Recognition of Familiar Food Activates Feeding via an Endocrine Serotonin Signal in Caenorhabditis Elegans." *eLife* 2013 (2): 1–27. doi:10.7554/eLife.00329.

Srinivasan, Supriya, Leila Sadegh, Ida C Elle, Anne G L Christensen, Nils J Faergeman, and Kaveh Ashrafi. 2008. "Serotonin Regulates C. Elegans Fat and Feeding through Independent Molecular Mechanisms." *Cell Metabolism* 7 (6). Elsevier Ltd: 533–44.

Stefani, Massimo, and Christopher M. Dobson. 2003. "Protein Aggregation and Aggregate Toxicity: New Insights into Protein Folding, Misfolding Diseases and Biological Evolution." *Journal of Molecular Medicine* 81 (11): 678–99. doi:10.1007/s00109-003-0464-5.

Stein, Geneva M, and Coleen T Murphy. 2012. "The Intersection of Aging, Longevity Pathways, and Learning and Memory in C. Elegans." *Frontiers in Genetics* 3: 1–13.

Stein, Geneva M, and Coleen T Murphy. 2014. "*C . elegans* Positive Olfactory

Associative Memory Is a Molecularly Conserved Behavioral Paradigm." *Neurobiology of Learning and Memory* 115. Elsevier Inc.: 86–94. doi:10.1016/j.nlm.2014.07.011.

Stiernagle, Theresa. 2006. "Maintenance of C. Elegans." *WormBook : The Online Review of C. Elegans Biology*, no. 1999(January): 1–11. doi:10.1895/wormbook.1.101.1.

Stroustrup, Nicholas, Winston E. Anthony, Zachary M. Nash, Vivek Gowda, Adam Gomez, Isaac F. López-Moyado, Javier Apfeld, and Walter Fontana. 2016. "The Temporal Scaling of Caenorhabditis Elegans Ageing." *Nature*. Nature Publishing Group. doi:10.1038/nature16550.

Stroustrup, Nicholas, Bryne E Ulmschneider, Zachary M Nash, Isaac F Lopez-Moyado, Javier Apfeld, and Walter Fontana. 2013. "The Caenorhabditis Elegans Lifespan Machine." *Nature Methods* 10. Nature Publishing Group: 665–70.

Sulston, J, and Hodgkin, J. 1988. "Methods." In *The Nematode C. Elegans*, 587–606. Cold Spring Harbor Press.

Sulston, J E, E Schierenberg, J G White, and J N Thomson. 1983. "The Embryonic Cell Lineage of the Nematode Caenorhabditis Elegans." *Developmental Biology* 100 (1): 64–119.

Sun, Jingru, Varsha Singh, Rie Kajino-Sakamoto, and Alejandro Aballay. 2011. "Neuronal GPCR Controls Innate Immunity by Regulating Noncanonical Unfolded Protein Response Genes." *Science (New York, N.Y.)* 332 (6030): 729–32. doi:10.1126/science.1203411.

Suo, Satoshi, Joseph G Culotti, and Hubert H M Van Tol. 2009. "Dopamine Counteracts Octopamine Signalling in a Neural Circuit Mediating Food Response in C.

Elegans." *The EMBO Journal* 28 (16). Nature Publishing Group: 2437–48. doi:10.1038/emboj.2009.194.

Suo, Satoshi, Yoshishige Kimura, and Hubert H M Van Tol. 2006. "Starvation Induces cAMP Response Element-Binding Protein-Dependent Gene Expression through Octopamine – G Q Signaling in Caenorhabditis Elegans." *Journal of Neuroscience* 26 (40): 10082–90. doi:10.1523/JNEUROSCI.0819-06.2006.

Swaab, Dick F., Ai Min Bao, and Paul J. Lucassen. 2005. "The Stress System in the Human Brain in Depression and Neurodegeneration." *Ageing Research Reviews* 4 (2): 141–94. doi:10.1016/j.arr.2005.03.003.

Swierczek, Nicholas A, Andrew C Giles, Catharine H Rankin, and Rex A Kerr. 2011. "High-Throughput Behavioral Analysis in C. Elegans." *Nature Methods* 8 (7). Nature Publishing Group: 592–98.

Sze, J Y, M Victor, C Loer, Y Shi, and G Ruvkun. 2000. "Food and Metabolic Signalling Defects in a Caenorhabditis Elegans Serotonin-Synthesis Mutant." *Nature* 403 (6769): 560–64. doi:10.1038/35000609.

Sze, Ji Ying, Shenyuan Zhang, Jie Li, and Gary Ruvkun. 2002. "The C. Elegans POU-Domain Transcription Factor UNC-86 Regulates the Tph-1 Tryptophan Hydroxylase Gene and Neurite Outgrowth in Specific Serotonergic Neurons." *Development (Cambridge, England)* 129 (16): 3901–11.

Tatar, M. 2009. "Can We Develop Genetically Tractable Models to Assess Healthspan (Rather Than Life Span) in Animal Models?" *The Journals of Gerontology Series A: Biological Sciences and Medical Sciences* 64A (2): 161–63.

Tecott, Laurence H. 2007. "Serotonin and the Orchestration of Energy Balance." *Cell*

Metabolism 6 (5): 352–61. doi:10.1016/j.cmet.2007.09.012.

Timmons, L, D L Court, and a Fire. 2001. "Ingestion of Bacterially Expressed dsRNAs Can Produce Specific and Potent Genetic Interference in Caenorhabditis Elegans." *Gene* 263 (1–2): 103–12.

Tøien, Øivind, John Blake, Dale M Edgar, Dennis a Grahn, H Craig Heller, and Brian M Barnes. 2011. "Hibernation in Black Bears: Independence of Metabolic Suppression from Body Temperature." *Science (New York, N.Y.)* 331 (6019): 906–9. doi:10.1126/science.1199435.

Trojanowski, N. F., M. D. Nelson, S. W. Flavell, C. Fang-Yen, and D. M. Raizen. 2015. "Distinct Mechanisms Underlie Quiescence during Two Caenorhabditis Elegans Sleep-Like States." *Journal of Neuroscience* 35 (43): 14571–84. doi:10.1523/JNEUROSCI.1369-15.2015.

Trojanowski, Nicholas F, Olivia Padovan-Merhar, David M Raizen, and Christopher Fang-Yen. 2014. "Neural and Genetic Degeneracy Underlies Caenorhabditis Elegans Feeding Behavior." *Journal of Neurophysiology* 112 (4): 951–61. doi:10.1152/jn.00150.2014.

Tu, Benjamin P, and Steven L McKnight. 2006. "Metabolic Cycles as an Underlying Basis of Biological Oscillations." *Nature Reviews. Molecular Cell Biology* 7 (9): 696–701. doi:10.1038/nrm1980.

Tullet, Jennifer M A, Maren Hertweck, Jae Hyung An, Joseph Baker, Ji Yun Hwang, Shu Liu, Riva P Oliveira, Ralf Baumeister, and T Keith Blackwell. 2008. "Direct Inhibition of the Longevity-Promoting Factor SKN-1 by Insulin-like Signaling in C. Elegans." *Cell* 132 (6). Elsevier Inc.: 1025–38.

Turlejski, Krzysztof. 1996. “Evolutionary Ancient Roles of Serotonin: Long-Lasting Regulation of Activity and Development.” *Acta Neurobiologiae Experimentalis* 56 (2): 619–36.

van Breukelen, Frank, and Sandra L. Martin. 2015. “The Hibernation Continuum: Physiological and Molecular Aspects of Metabolic Plasticity in Mammals.” *Physiology* 30 (4): 273–81. doi:10.1152/physiol.00010.2015.

Vaupel, James W. 2010. “Biodemography of Human Ageing” 464 (March). doi:10.1038/nature08984.

Vaupel, James W, James R Carey, Kaare Christensen, Thomas E Johnson, Anatoli I Yashin, Niels V Holm, Ivan A Iachine, et al. 1998. “Biodemographic Trajectories of Longevity.” *Science* 280 (5365): 855–60. doi:10.1126/science.280.5365.855.

Von Stetina, Stephen E, Millet Treinin, and David M Miller. 2006. “The Motor Circuit.” *International Review of Neurobiology* 69: 125–67. doi:10.1016/S0074-7742(05)69005-8.

Waggoner, Laura E., G. Tong Zhou, Ronald W. Schafer, and William R. Schafer. 1998. “Control of Alternative Behavioral States by Serotonin in Caenorhabditis Elegans.” *Neuron* 21 (1): 203–14. doi:10.1016/S0896-6273(00)80527-9.

Waggoner, Laura E, Laura Anne Hardaker, Steven Golik, and William R Schafer. 2000. “Effect of a Neuropeptide Gene on Behavioral States in C. Elegans Egg-Laying.” *Genetics* 154: 1181-1192.

Ward, Alex, Jie Liu, Zhaoyang Feng, and X Z Shawn Xu. 2008. “Light-Sensitive Neurons and Channels Mediate Phototaxis in C. Elegans.” *Nature Neuroscience* 11 (8): 916–22.

Wayne Davis, M, D Somerville, R Y N Lee, S Lockery, L Avery, and D M Fambrough. 1995. "Mutations in the Caenorhabditis Elegans Na, K-ATPase Gene, Alpha-Subunit Gene, Eat-6 , Disrupt Excitable Cell Function." *The Journal of Neuroscience* 15(12):8408-8418

Wei, Xing, Christopher J Potter, Liqun Luo, and Kang Shen. 2012. "Controlling Gene Expression with the Q Repressible Binary Expression System in Caenorhabditis Elegans." *Nature Methods* 9 (4): 391–95. doi:10.1038/nmeth.1929.

White, J.G., E. Southgate, J.N. Thomson, and S. Brenner. 1986. "The Structure of the Nervous System of the Nematode Caenorhabditis Elegans." *Phil. Trans. R. Soc. Lond. B* 314 (1165): 1–340.

Wilson, Sue, and Spilios Argyropoulos. 2005. "Antidepressants and Sleep: A Qualitative Review of the Literature." *Drugs* 65 (7): 927–47. doi:10.2165/00003495-200565070-00003.

Wimo, Anders, Linus J??nsson, John Bond, Martin Prince, and Bengt Winblad. 2013. "The Worldwide Economic Impact of Dementia 2010." *Alzheimer's and Dementia* 9 (1): 1–11. doi:10.1016/j.jalz.2012.11.006.

Wragg, Rachel T, Vera Hapiak, Sarah B Miller, Gareth P Harris, John Gray, Patricia R Komuniecki, and Richard W Komuniecki. 2007. "Tyramine and Octopamine Independently Inhibit Serotonin-Stimulated Aversive Behaviors in Caenorhabditis Elegans through Two Novel Amine Receptors." *Journal of Neuroscience* 27 (49): 13402–12. doi:10.1523/JNEUROSCI.3495-07.2007.

Xian, Bo, Jie Shen, Weiyang Chen, Na Sun, Nan Qiao, Dongqing Jiang, Tao Yu, et al. 2013. "WormFarm: A Quantitative Control and Measurement Device toward

Automated Caenorhabditis Elegans Aging Analysis." *Aging Cell* 12 (3): 398–409. doi:10.1111/acel.12063.

Yang, Zhe, Yue Yu, Vivian Zhang, Yinjun Tian, Wei Qi, and Liming Wang. 2015. "Octopamine Mediates Starvation-Induced Hyperactivity in Adult *Drosophila*." *Proceedings of the National Academy of Sciences* 112 (16): 5219–24. doi:10.1073/pnas.1417838112.

Ye, Xiaolan, James M Linton, Nicholas J Schork, Linda B Buck, and Michael Petrascheck. 2013. "A Pharmacological Network for Lifespan Extension in Caenorhabditis Elegans." *Aging Cell*, October, 1–10. doi:10.1111/acel.12163.

Yoshida, Midori, Eitaro Oami, Min Wang, Shoichi Ishiura, and Satoshi Suo. 2014. "Nonredundant Function of Two Highly Homologous Octopamine Receptors in Food-Deprivation-Mediated Signaling in Caenorhabditis Elegans." *Journal of Neuroscience Research* 92 (October 2013): 671–78. doi:10.1002/jnr.23345.

You, Young-jai, Jeongho Kim, David M Raizen, and Leon Avery. 2013. "Insulin, cGMP, and TGF-β Signals Regulate Food Intake and Quiescence in C. Elegans: A Model for Satiety." *Cell Metabolism* 7 (3). Elsevier Ltd: 249–57.

Yu, Chih-Chieh Jay, David M Raizen, and Christopher Fang-Yen. 2014. "Multi-Well Imaging of Development and Behavior in Caenorhabditis Elegans." *Journal of Neuroscience Methods* 223 (February). Elsevier B.V.: 35–39. doi:10.1016/j.jneumeth.2013.11.026.

Zariwala, H, S Faumont, and S R Lockery. 2003. "Step Response Analysis of Thermotaxis in C. Elegans," *Journal of Neuroscience* 23(10):4369-3477

Zhang, William B, Drew B Sinha, William E Pittman, Erik Hvatum, Nicholas Stroustrup,

and Zachary Pincus. 2016. “Extended Twilight among Isogenic C. Elegans Causes a Disproportionate Scaling between Lifespan and Health.” *Cell Systems* 3 (4). Elsevier Inc.: 333–45. doi:10.1016/j.cels.2016.09.003.

Zhang, Y, H Lu, and C I Bargmann. 2005. “Pathogenic Bacteria Induce Aversive Olfactory Learning in Caenorhabditis Elegans.” *Nature* 438 (7065): 179–84. doi:10.1038/nature04216.

Zhao, Yuan, Ann F. Gilliat, Matthias Ziehm, Mark Turmaine, Hongyuan Wang, Marina Ezcurra, Chenhao Yang, et al. 2017. “Two Forms of Death in Ageing Caenorhabditis Elegans.” *Nature Communications* 8 (May). Nature Publishing Group: 15458. doi:10.1038/ncomms15458.

Zheng, Xianwu, Shinjae Chung, Takahiro Tanabe, and Ji Ying Sze. 2005. “Cell-Type Specific Regulation of Serotonergic Identity by the C. Elegans LIM-Homeodomain Factor LIM-4.” *Developmental Biology* 286 (2): 618–28. doi:10.1016/j.ydbio.2005.08.013.